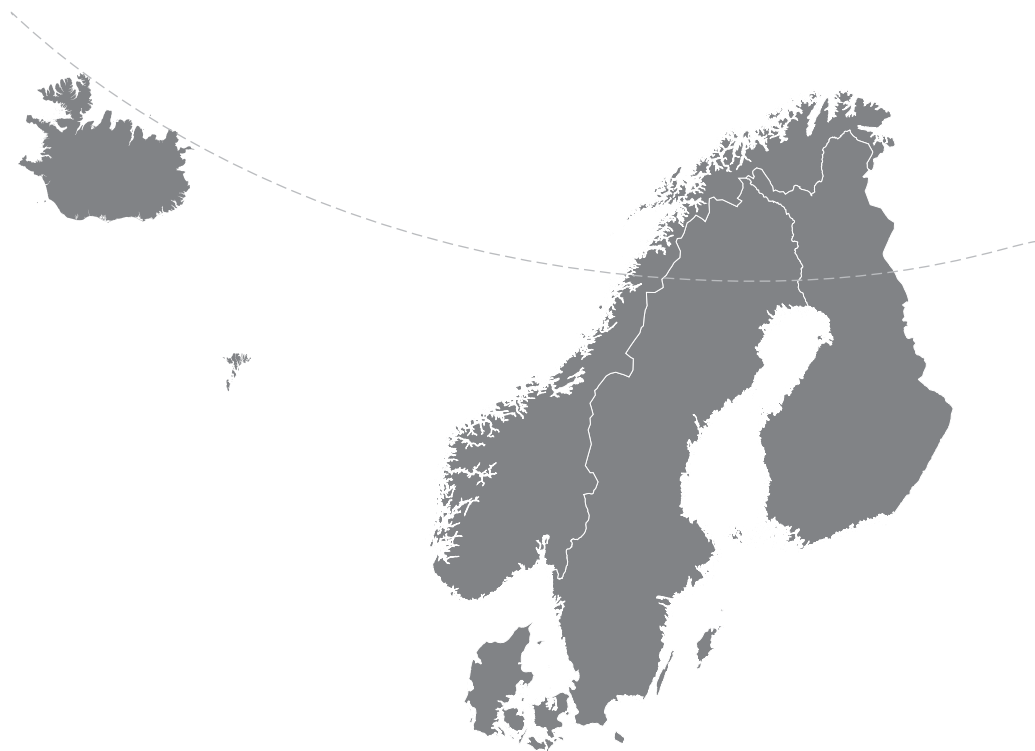


Nordic Concrete Research



Nordic
Concrete
Federation

NORDIC CONCRETE RESEARCH

**EDITED BY
THE NORDIC CONCRETE FEDERATION**

**CONCRETE ASSOCIATIONS OF: DENMARK
FINLAND
ICELAND
NORWAY
SWEDEN**

**PUBLISHER: NORSK BETONGFORENING
POSTBOKS 2312, SOLLI
N - 0201 OSLO
NORWAY**

STOCKHOLM/OSLO, JUNE 2017

Preface

Nordic Concrete Research (NCR) has during more than 35 years been an important publication for publishing scientific contributions on concrete research conducted in the Nordic countries, i.e., in Denmark, Finland, Iceland, Norway, and Sweden. After the 2nd World War, co-operation between the Nordic countries was strong in many areas. Politically, it could be seen as a peaceful alternative to the increasing polarity between Nato and the Warszawa Treaty Organization. Denmark, Iceland and Norway became members of Nato whereas Finland and Sweden stayed neutral. The concrete field was a successful arena for Nordic co-operation due to similarities in climate, society, industry, university system, tradition, and to some extent in language (DK, NO, SE) and geology (FI, NO, SE). In the 1950s, two conference series were started; Nordic Concrete Research Meeting (1953-) and Nordic Concrete Congress (1955-1995). This year (2017), the XXIII Nordic Concrete Research Meeting will be arranged in Aalborg in Denmark.

The Nordic concrete research has been very successful during the last 60 years and important and internationally recognized contributions on, e.g., durability, high performance concrete, and self-compacting concrete could be mentioned. The Nordic Concrete Federation – responsible for NCR – believes that there still is a need for a scientific publication devoted to Nordic concrete research. It ought to be an important alternative for concrete researchers in the Nordic countries searching for a journal to submit their papers. Simultaneously, it constitutes a window for Nordic concrete research exposing news and novelties from the five countries in northern Europe. For more information on the Nordic Concrete Federation, see www.nordicconcrete.net.

This spring, I accepted the role as Editor of NCR after Dr Terje Rønning who have edited the two latest issues of NCR and Dr Dirch Bager who was the Editor during many years but tragically passed away last year. I would like to thank them both for their great work with the journal. I had not accepted the role if I did not believe in the journal and its future. We have the ambition to make it scientifically recognized by the scientific society expressed as a so-called impact factor. Since we have a good number of good papers, excellent reviewers, and a well-working review system, we just need to guarantee a regular publication system with two issues a year (June and December). This will take some time but, please, be patient and continue to submit great papers. If you do so, I will do my very best to keep to the schedule.

Stockholm in June 2017

Johan Silfwerbrand
Editor of NCR

CONTENTS

1	Shayan Fahimi, Carlos Gil, Ignasi Fernandez Perez & Kamyab Zandi Replication of Crack Pattern in FE Analysis Based on Discretization of Tension Softening Curves	1
2	Arto Köliö, Jukka Lahdensivu & Matti Pentti The Role of the Active Corrosion Phase in the Service Life of Concrete Facades Exposed to Nordic Climate	11
3	Martta-Kaisa Olkkonen Feasibility Study of Moisture Measurement of a Concrete Pavement Tile Employing a 1.7 GHz Coaxial Surface Probe	25
4	Göran Fagerlund The Critical Flow Distance at Freezing of Concrete – Theory and Experiment	35
5	Jonny Nilimaa, Anders Hösthagen & Mats Emborg Thermal Crack Risk of Concrete Structures – Evaluation of Theoretical Models for Tunnels and Bridges	55
6	Harald Justnes Durable Aluminium Reinforced Environmentally-friendly Concrete Construction – DARE2C	71
7	Madumita Sadagopan, Katarina Malaga & Agnes Nagy RE:Concrete - Study on Recycling of Concrete in Sweden	83
	Research Council & Editorial Board of NCR	101

Replication of Crack Pattern in FE Analysis Based on Discretization of Tension Softening Curves



Shayan Fahimi, Master student at CBI Swedish Cement and Concrete Research Institute, Gothenburg, Sweden, sh.fahimi@ut.ac.ir



Carlos Gil, PhD candidate at Chalmers University of Technology, Gothenburg, Sweden, carlos.gil@chalmers.se



Ignasi Fernandez Perez, Postdoctoral researcher at Chalmers University of Technology, Gothenburg, Sweden, ignasi.fernandez@chalmers.se



Kamyab Zandi, Associate Professor at Chalmers University of Technology, Gothenburg, Sweden, Kamyab.Zandi@chalmers.se

ABSTRACT

Today, there is an increasing need for reliable methods for condition assessment and service-life evaluation of existing structures. Although advanced 3D Nonlinear Finite Element (3D NLFE) analysis has proven to be capable of describing the behavior of reinforced concrete in a comprehensive way, the analysis results are difficult to couple with visual inspection data such as cracking and spalling. Moreover, 3D NLFE programs are numerically expensive and incomprehensible for full-scale practical applications. Thus, the present study aims to couple 3D NLFE analysis with condition assessment data, and consequently to increase the accuracy, to optimize the computation time and to improve robustness of such analyses.

Key words: Nonlinear finite element analysis, condition assessment, crack pattern, corrosion, reinforced concrete, existing structures.

1. INTRODUCTION

Today, the anticipated environmental and economic cost of replacing the aging infrastructure stock is immense. Despite significant advances in structural health monitoring, infrastructure assessment practices still largely consist of intrusive, time-consuming and subjective measures which may compromise infrastructure accessibility and safety for users and inspectors. The current state-of-the-art solutions for a comprehensive assessment require partial or full closures of the infrastructure. This leads to extensive societal and environmental impacts and results in additional costs for the stakeholders. Thus, the present work is part of a framework, which is focused on innovating **Autonomous Automated Non-Intrusive Condition Assessment (UNICA)** solutions and aims to improve the cost-efficiency, accuracy and the speed of condition assessment processes. The **UNICA** solution, will consist of five scientific/technical (S/T) platforms:

- **Platform 1- Inspection:** autonomous inspection methods, using unmanned aerial vehicles (UAVs) – to minimize intrusion on the transport flow, cover large inspection areas and minimize exposure to safety hazards for the inspectors and users;
- **Platform 2 - Interpretation:** automated vision-based data collection and interpretation– to detect and quantify geometrical and visual anomalies in 3D on infrastructure;
- **Platform 3 - Damage quantification**– to identify the damage, underlying mechanism (e.g. corrosion, frost, ASR, etc.) and to quantify the structural consequence of the damage;
- **Platform 4 - Prediction:** advanced structural simulation combined with deterioration models– to leverage the damage patterns for a reliable performance prediction; and
- **Platform 5 - BIG DATA, Cloud computing and Internet of things:** fusing assessment data with Building Information Modelling (BIM) – to enable a network connectivity.

Recent advances in structural health monitoring of existing structures enable condition assessment data to be collected more accurately and more frequently than ever before. Such repository of 4D (3D + time) condition assessment data may leverage updating leaps in service-life prediction models only if they are coupled with advanced structural simulations. Advanced 3D Nonlinear Finite Element (NLFE) analyses are difficult to couple with visual inspection data and are numerically expensive and thus incomprehensible for full-scale practical applications. Thus, the present study aims to initiate an attempt in coupling advanced 3D NLFE analysis with condition assessment data, which is particularly related to the fourth platform mentioned above.

In this study, the influence of corrosion has been introduced in 3D NLFE analysis using three approaches. While 1D-ARC and bond-corrosion methods have been previously introduced in the literature [1-3], the third method, Re-FEM, is recently developed and will be introduced in this paper for the first time. These approaches were utilized to model earlier tested pull-out specimens that had been subjected to accelerated corrosion process, and the force-displacement response, ultimate crack pattern and failure mode observed were compared with those in the experiments.

2. METHODOLOGY

To investigate the effects of replication of crack pattern into a FE model, three different approaches were used:

- 1D-ARC: the effect of corrosion has been included by adjusting the bond-slip relation using the 1D-ARC method developed by Lundgren et al. [1]. Thus, the bond will be deteriorated due to corrosion, but the corrosion induced cracks will not be directly replicated in the analysis.
- Bond-Corrosion: bond-corrosion model for interface elements will be used along with a separate corrosion phase in the simulation procedure. The bond model and the corrosion model were developed by Lundgren [2] and later extended by Zandi et al. [3]. Using bond-corrosion model, a pressure will be introduced around the rebar; thus, some cracks may develop in the first phase.
- Re-FEM: the third approach, which will be called Re-FEM in the rest of this paper, allows for replication of the inspected corrosion-induced cracks in the structural simulation. Therefore, a prior knowledge of crack pattern and crack width is required in this approach. The material properties of these elements will be changed in order to apply the corrosion induced cracks on the model. The generated model is coupled with deteriorated or reference bond-slip properties using different bond-slip models. Thus, three cases of Re-FEM will be investigated: (1) Re-FEM + reference 1D-ARC, (2) Re-FEM + shifted/corroded 1D-ARC, (3) Re-FEM + bond model

3. EXPERIMENTS

Replication of crack pattern into the FE model needs a prior knowledge of crack pattern and crack width. Berrocal et al. [4] performed a corrosion test on cylinders reinforced with a $\phi 16$ mm ribbed bar (Figure 1(a)). The compressive cube strength, f_{cm} , was 56 MPa, tested on 100 mm cubes and the splitting tensile strength, f_{ctm} , was 4.2 MPa, tested on 150 mm cube. Three reference (without corrosion) and three corroded specimens underwent the mechanical pull-out test. Accelerated corrosion tests were carried out and crack path of all visually detectable cracks were investigated and documented. Measurement of crack width was possible for the dominant crack in each specimen (Figure 1(b)). The other cracks were too narrow for a sophisticated measurement. The corrosion level was calculated for each bar using gravimetric steel loss measurements, assuming that the measured loss was uniformly concentrated on the 70 mm bar length embedded in the concrete, and showed an average of 8.43% steel loss. Then, pull-out tests were performed on both reference and corroded specimens. Final results are shown in Figure 1 (c) and (d). The curves mentioned by “RefSp#” show the results of pull-out test on reference specimens and the curves mentioned by “CorSp#” show the same results for corroded ones [5].

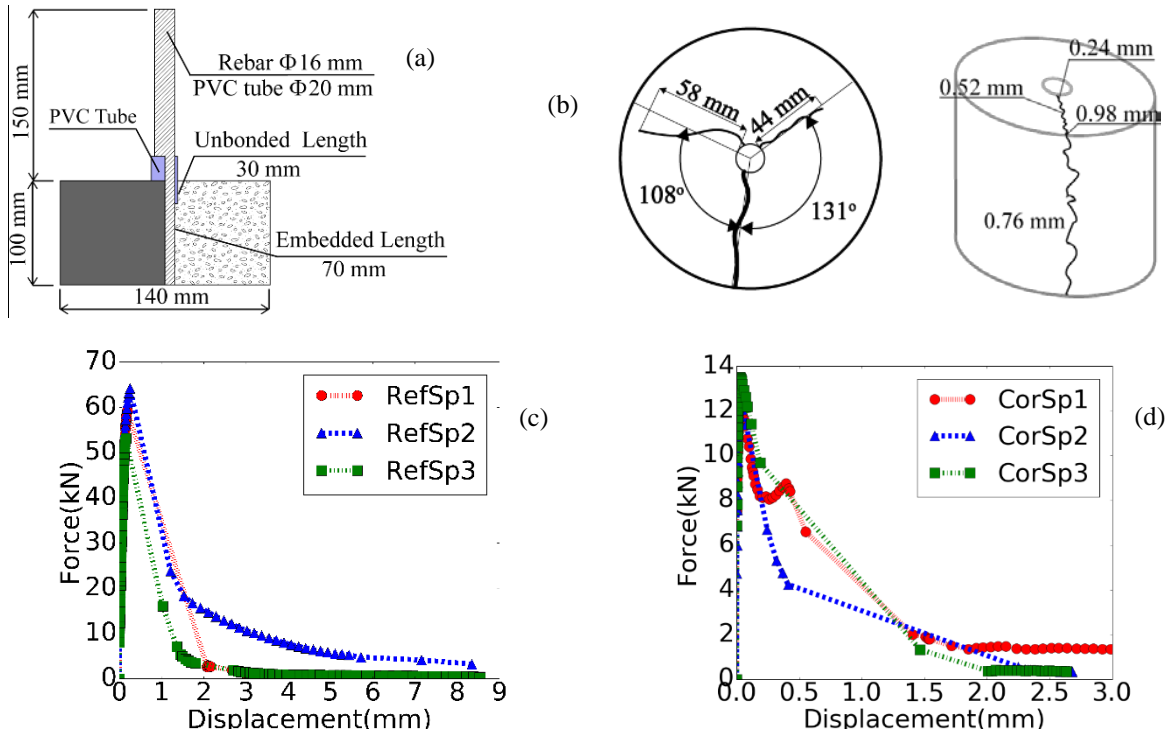


Figure 1 – (a) Dimensions of the specimens and (b) crack path and crack width due to corrosion, Pull out force versus passive slip for (c) reference and (d) corroded specimens [5]

4. FINITE ELEMENT MODEL

Finite element models were made in DIANA finite element package [6]. The fracture energy was derived from MC1990 guidelines [7]. The material properties of steel and concrete are shown in Table 1. Young modulus as well as compressive and tensile strengths of concrete are measured during the experiments. The nodes on the bottom surface of the concrete cylinder and the reinforcement in Figure 2 were fixed in vertical direction and displacement was applied on the free end of the reinforcement. The meshing process was done using 4 mm tetrahedral elements. Interface elements were introduced to describe the interaction between concrete and steel, and the associated impact of corrosion on the concrete-steel integration. For the third approach, cracked elements were also extracted based on the crack path shown in Figure 2 (right). The final FE models are shown in Figure 2.

In 1D-ARC approach, a local bond-slip relation was extracted from experimental results and used instead of the analytical bond-slip relation from CEB FIP 1990 [7] in order to get a correct reference model. Figure 3 (a, b) shows force-displacement curve and principal strain contours for 1D-ARC approach. The failure mode and crack pattern are not correct, but the force-displacement curve is reasonably accurate. The principal strain is used to monitor crack development. If strain of an element exceeds 10^{-3} , it will be considered a cracked element here.

Table 1 – Material properties of steel and concrete in FE model

Steel Properties		Concrete Properties	
Young's Modulus	200 GPa	Young's modulus	35.8 GPa
Plasticity Model	Von Mises	Total strain based rotating crack model	
		Tensile curve, strength	Hordjik [8], 3.76 MPa
		Mode I tensile fracture energy	77 N/m
		Compressive curve, strength	Thorenfeldt [9], 38.7 MPa



Figure 2 – FE model of the specimens (left) and cracked elements (right)

In bond-corrosion approach, the bond and corrosion models with calibrated parameters reported in [10] were used for interface elements, while keeping all other properties the same as the previous case. Figure 3 (a, c) shows a splitting failure mode with accurate crack path and the force-displacement curve is close to the experimental results.

5. RESULTS

The verified FE model was utilized in order to simulate the pull-out phase for corroded specimens. The corrosion was applied in different manners as described in the 2nd section.

1D-ARC: Adjusting the 1D-ARC input based on the level of corrosion will deteriorate the bond-slip characteristic of the interface elements. The corrosion penetration for the specimens was about 340 μm . As shown in Figure 3 (d, e), the model was failed in a pure pull-out manner, which is in contrast with what is observed in the experiments and the crack pattern is not accurate. On the other hand, the force-displacement curve is quite close to the experimental observation.

Bond-corrosion: as stated earlier, in this approach, a corrosion phase will be executed before the mechanical pull-out phase. Because the flow of corrosion, which is the movement of corrosion products to the surface using the crack openings, has not been implemented in the subroutine, the measured corrosion level could not be applied in the analysis. Thus, the maximum corrosion penetration, without computational divergence, is about 140 μm . In Figure 3 (d, f), the splitting failure of the model in mechanical phase is shown and the force-

displacement curve slightly overestimates the measured pull-out force. All results are reported up to the last converged step in the analysis.

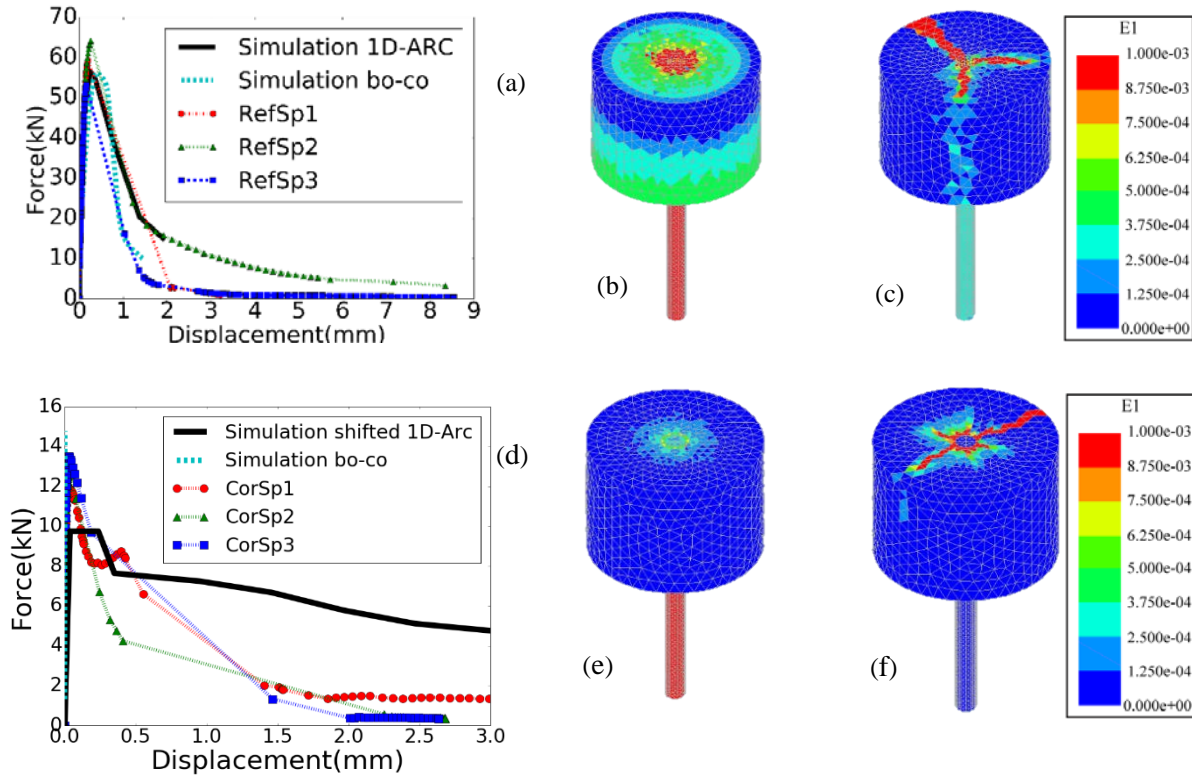


Figure 3 – (a) Force-displacement curve of pull-out test on reference model and principal strain in the same analysis using (b) 1D-ARC, and (c) bond-corrosion, (d) force-displacement curve of pull-out test on corroded model and principal strain in the same analysis using (e) 1D-ARC, and (f) bond-corrosion

Re-FEM: The material properties of extracted elements, shown in Figure 2, were changed. In order to study the effects of changing material properties, four different cases were considered. The Young's modulus, tensile strength and fracture energy of these cases were 85%, 50%, 25% and 1% of the reference values, respectively. Modifying Young's modulus and tensile strength simultaneously will keep the crack strain fixed. Adding cracked elements does not influence the deterioration of bond-slip capacity. Therefore, this method is used along with different bond-slip model.

- **Re-FEM + reference 1D-ARC:** here, Re-FEM was coupled with reference 1D-ARC input. As shown in Figure 4 (left), the force-displacement is not satisfying. Also, while the contour shows the first stages of crack development, the failure mode is pull-out.
- **Re-FEM + adjusted 1D-ARC:** in this case, the force-displacement was not changed by introducing cracked elements into a model with adjusted 1D-ARC input. Therefore, it can be concluded that effects of bond deterioration are significantly more than cracking for this case and changing material properties in any amount will not have any significant effects. The failure mode is still incorrect here.

- **Re-FEM + bond-corrosion:** it is obvious from Figure 4 (right) that the crack is developed on the path which is specified earlier. The failure mode is correct here, but the force displacement result is not near the experimental observations. Although, the trend shown in force-displacement curve is promising.

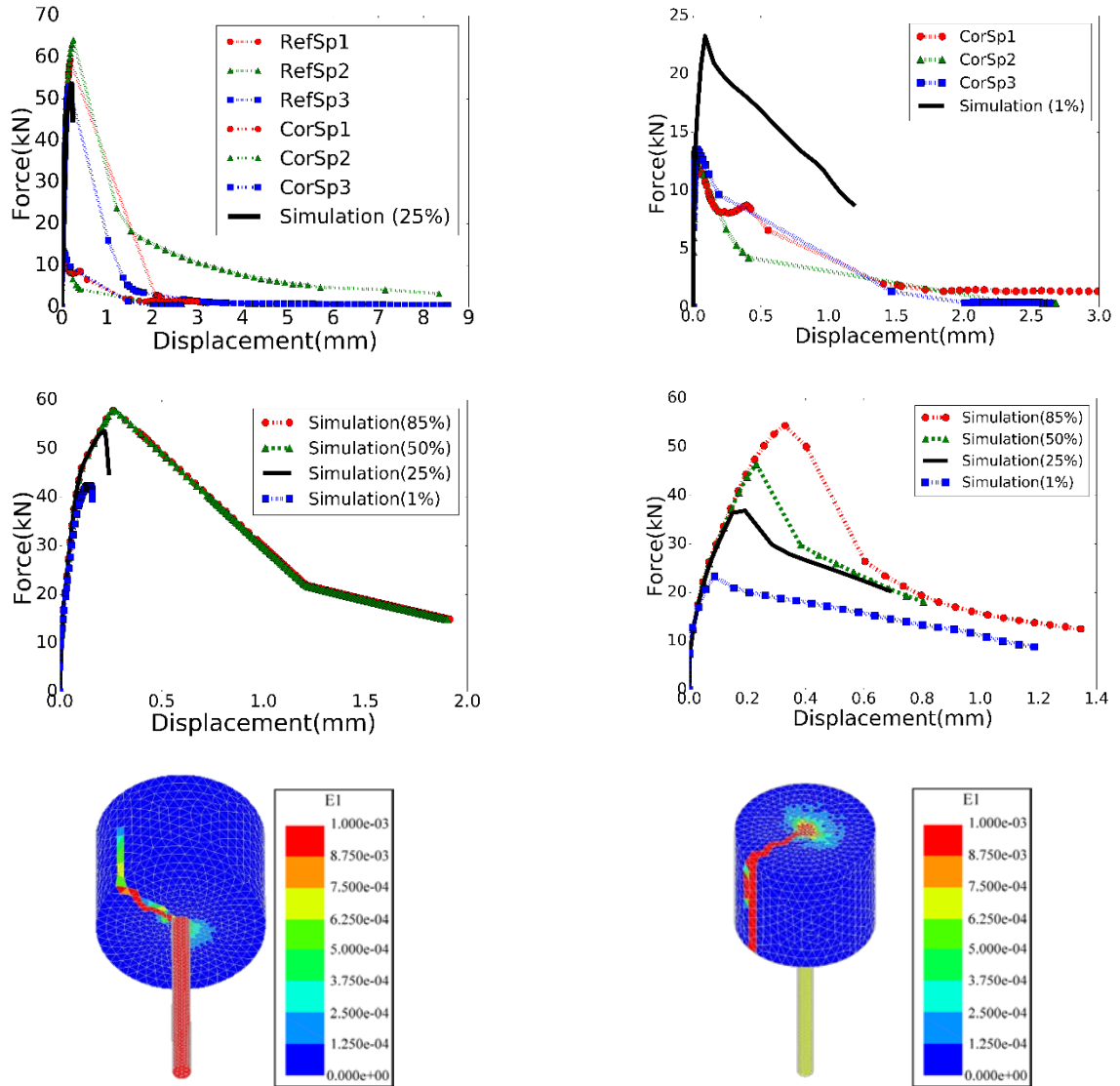


Figure 4 – Force-displacement curve and principal strain of pull-out test on corroded model using (left) Re-FEM + reference 1D-ARC, and (right) Re-FEM + bond

6. CONCLUSION

In this paper, a FE model was used in order to study the effectiveness of different corrosion models for reinforced concrete. The results showed that 1D-ARC model produces a promising force-displacement output, but the failure mode was incorrect. It is an expected feature, because 1D-ARC had been introduced to produce a rough approximation of the bond capacity of the structure. Using bond corrosion model, the force-displacement response was accurate upon the maximum force, but the analysis diverged after that point. Also, failure mode were correct for

this model, because it always considers confinement changes after corrosion. This paper introduced a new method for adding cracked elements to the FE model named Re-FEM. Using this method, the force-displacement response for the corroded specimens was overestimated about 70%, but showed a correct trend. The failure mode and crack pattern were correct, because the model considers the confinement changes as well as dominant cracks. Moreover, the analysis continued after the peak and the behavior of specimen can be monitored in the softening regime. The results are summarized in Table 2. Notwithstanding these features, further developments are required in order to justify the correct amount of material deterioration due to cracking and modify the overestimation.

Table 2 – Summary of the results

<i>Model</i>	<i>Failure mode</i>	<i>Crack path</i>	<i>Force-displacement</i>
<i>ID-ARC</i>	Incorrect	Incorrect	Promising
<i>Bond-Corrosion</i>	Correct	Correct	Accurate up to maximum force
<i>Re-FEM + reference ID-ARC</i>	Incorrect	Promising	Not satisfying
<i>Re-FEM + adjusted ID-ARC</i>	Incorrect	Incorrect	Promising
<i>Re-FEM + bond-corrosion</i>	Correct	Correct	Promising with a proper trend

REFERENCES

1. Lundgren, K., et al., "Analytical model for the bond-slip behaviour of corroded ribbed reinforcement." *Structure and Infrastructure Engineering* 8.2, 2012, pp. 157-169.
2. Lundgren, K., "Bond between ribbed bars and concrete. Part 2: The effect of corrosion." *Magazine of Concrete Research* 57.7, 2005, pp. 383-396.
3. Zandi Hanjari, K., et al. "Three-dimensional modelling of structural effects of corroding steel reinforcement in concrete." *Structure and Infrastructure Engineering* 9.7, 2013, pp. 702-718.
4. Berrocal, C. G., et al., Influence of fibre reinforcement on the initiation of corrosion-induced cracks. International RILEM Conference on Materials, Systems and Structures in Civil Engineering, 22-24 August 2016, Technical University of Denmark, Lyngby, Denmark
5. Berrocal, Carlos G., et al. "Corrosion-induced cracking and bond behaviour of corroded reinforcement bars in SFRC." *Composites Part B: Engineering* 113 (2017): 123-137.
6. Diana finite element analysis, 2015. User's Manual – release 10.0. Delft, The Netherlands: *TNO Building and Construction Research*.
7. CEB-FIP. "CEB-FIP Model Code 1990." *Comité Euro-International du Béton*, 1993.
8. Cornelissen, H.A.W., et al., "Experimental determination of crack softening characteristics of normalweight and lightweight concrete". *Heron* 31, 2, 1986
9. Thorenfeldt, E., et al., "Mechanical properties of high-strength Concrete and applications in design." In *Proc. Symp. Utilization of High-Strength Concrete (Stavanger, Norway)* (Trondheim, 1987), Tapir.

10. Jansson, A., et al. "Experimental investigation of surface crack initiation, propagation and tension stiffening in self-compacting steel–fibre-reinforced concrete." *Materials and structures* 45.8, 2012, pp. 1127-1143.

The Role of the Active Corrosion Phase in the Service Life of Concrete Facades Exposed to Nordic Climate



Arto Köliö
 Researcher, D.Sc.
 Dept. of Civil Engineering, Tampere University of Technology
 Korkeakoulunkatu 5,
 FI-33720 Tampere
 E-mail: arto.kolio@tut.fi



Jukka Lahdensivu
 Adjunct professor, D.Sc.
 Dept. of Civil Engineering, Tampere University of Technology
 Korkeakoulunkatu 5,
 FI-33720 Tampere
 E-mail: jukka.lahdensivu@tut.fi



Matti Pentti
 Professor, D.Sc.
 Dept. of Civil Engineering, Tampere University of Technology
 Korkeakoulunkatu 5,
 FI-33720 Tampere
 E-mail: matti.pentti@tut.fi

ABSTRACT

There is a rising national concern in Finland on increasing maintenance needs of the existing building stock. Active corrosion was studied as an extension to the service life of concrete facade panels in Nordic climate. The project combined statistical analysis of a large database of condition investigation data to the more in-depth analysis of twelve case-study buildings and field measurement data on reinforcement corrosion to produce a model for the corrosion propagation phase in concrete facade panels. Although carbonation resistance remains as the primary factor in ensuring proper service life, it was found that the modelling of active corrosion may provide a considerable extension to it.

Key words: Concrete, Carbonation, Corrosion, Facades, Service life, Modelling.

1. INTRODUCTION

1.1 General

The effects of reinforcement corrosion have resulted in high maintenance costs for concrete infra-structure in varying climates around the world, and the Finnish climate is no exception. The corrosion of the reinforcement in concrete structures has two basic effects. Firstly, it can cause cracking of the concrete cover, and secondly, the effective steel cross-section is reduced (Broomfield 2007). Cracking occurs in structures where the reinforcement is placed relatively close to the surface of the concrete. The cracking accelerates the penetration of agents which are harmful to concrete and causes unsightly visual defects to the concrete structures, which is especially visible on the facades. Cracking can be considered as a limit based on the appearance or serviceability of the structure (DuraCrete 2000) where the needed intervention would be patch repairs and coatings. A further-developed form of visual damage would be spalling, where a whole segment of the concrete cover will fall from the concrete surface. However, there is still an undefined period of residual life after cracking and/or spalling, during which the structure will still continue to function adequately until a final limit is reached (DuraCrete 2000), when the structural failure is so severe as to require either rehabilitation or demolition. The occurrence of visible damage is a natural way of judging the service life of concrete facade panels, since all of the renovation and maintenance decisions are made after inspections which are usually commissioned after these visible warning signs have appeared. However, different strategies taken on the maintenance finally dictate the selection of a suitable limit.

Basically, two different durability design strategies can be followed (DuraCrete 2000): A) avoid the degradation caused by the environment or B) select optimal material composition and structural detailing to resist degradation for a specified time period (service life). On the other hand, the following division of strategies (renovation options) based on the level of intervention needed is given in SFS-EN 1504-9 standard: a) do nothing for a certain time but monitor, b) re-analyse the structural capacity, possibly leading to downgrading in function, c) prevent or reduce further deterioration, d) strengthen or repair and protect all or part of the concrete structure, e) reconstruct or replace all or part of the concrete structure or f) demolish all or part of the concrete structure. It is obvious from this set of options that some are suitable only for early intervention and some are such that are needed, when the intervention is based on realized repair need.

Private and public buildings built of concrete make up 34 % of the whole building stock in Finland, of which almost 40 % is now 30-50 years old. The majority of the existing concrete facades in Finland have been built in time when service life design practice was not yet established (compared to a common service life requirement today of 50 years). The reinforcement service life is in Finnish guidelines (by50 2012) defined as only corrosion initiation. This means that the target service life should be achieved by carbonation resistance alone. This strategy withholds additional safety since no damage at all has happened yet at the chosen end of service life. In addition in new construction carbonation can be fairly easily accounted for by engineering concrete composition and reinforcement cover depths accordingly. Concerning existing buildings a problem is formed since these properties are already fixed. Also, the initiation phase is in many cases already passed. This makes the assessment of the residual service life of these structures problematic in two ways: (i) the residual service life is, by the definition, zero even though no damage at all has happened, (ii) there is no methods available to evaluate the residual service life.

1.2 Research objective

A recent doctoral research (Köliö 2016) focused on the service life design and maintenance strategies for existing concrete facades and balconies constructed in Finland between twenty-five and fifty years ago, (1965–1990). The motivation was to find a way to manage the constantly growing need for renovation of the Finnish housing stock. The aim was to be able to combine a Carbonation model and an Active Corrosion Phase model to give a more comprehensive picture of the service life of these structures. By producing a reliable model for the corrosion propagation phase, new criteria can be applied to define the end of the service life of buildings, which can considerably extend their predicted service life. The residual service life of these facades cannot be estimated by carbonation resistance alone, since this phase has already passed. The most relevant results are summarised and discussed in this article.

2. BACKGROUND

2.1 Carbonation initiated reinforcement corrosion

The corrosion of steel reinforcement in concrete is commonly regarded as an electrochemical phenomenon in that the corroding reinforcement works as a mixed electrode where cathodic and anodic areas are formed on the steel surface. Corrosion due to carbonation occurs generally over the surface of the reinforcement, as the cathode and anode areas are evenly spaced and may alter with the changes in the corrosion environment. (Page 1988). Due to its alkalinity, concrete protects the steel reinforcement from corrosion. Its high pH (approximately 13) is due to the pore solution in the microscopic pores of the concrete, which contain high concentrations of calcium, sodium and potassium hydroxides. This high alkalinity protects the steel from corrosion by creating a thin passive oxide film on the steel's surface. Because the concrete acts as a protective layer for the reinforcement, corrosion is not initiated immediately. This fact is taken into account by depicting reinforcement corrosion as a process consisting of two or more consecutive phases i.e. the initiation and propagation phases (Tuutti 1982).

Concrete carbonation is a reaction between carbon dioxide gas in the atmosphere and the alkaline hydroxides in the concrete (Broomfield 2007). Most commonly, these are calcium silicate hydrate, calcium hydroxide and various calcium aluminate or ferro-aluminate hydrates (Parrott 1987). The carbon dioxide dissolves in the pore water in the concrete and forms carbonic acid, which neutralizes the alkalis in the pore water. The reaction forms calcium carbonate on the pore surfaces of the concrete. The reservoir of calcium hydroxide bound in the concrete is larger than can be dissolved in the pore water, which helps maintain the concrete's high pH during the carbonation reaction (Broomfield 2007). The reaction can only occur when sufficient pore water is available. This means that concrete in low humidity does not react to any significant extent. On the other hand, the reaction also requires the diffusion of carbon dioxide gas to the carbonation front, which is slowed down when there is a lot of moisture (Parrott 1987). Eventually, the reservoir is used up and the carbonation reaction penetrates further into the concrete as a carbonation front. The propagation of the carbonation front inside concrete roughly follows the laws of diffusion, which state that the carbonation rate is proportional to the carbonation distance. The carbonation depth of concrete is therefore commonly described by a square root relationship with the exposure time (Tuutti 1982).

Many of the models which have so far have been proposed to illustrate carbonation make use of the square root of time relationship (Parrott 1987). However, empirical measurements have

indicated using this relationship in the model results in an overestimation of the degree of carbonation, especially in cases where the concrete is exposed to rain (Tuutti 1982, Huopainen 1997). Therefore, the square root equation should be regarded as an upper limit for carbonation in such cases. The carbonation coefficient, k , is used to adjust the models so that they can describe the carbonation of different concretes in different environments. (Monteiro et al. 2012, Tuutti 1982).

Another approach has been to incorporate the effect of different environments by modifying the exponent of time (Parrott, 1987). A number of studies, such as (Thiery et al. 2007, Hyvert et al. 2010) have utilised physical models to show the reaction kinetics of carbonation. These studies were aimed at discovering the points at which the carbonation reaction is controlled by reaction kinetics, and those at which it is controlled by the diffusion resistance of concrete to carbon dioxide. Neves et al. (2012) improved the square root equation so that it distinguishes between the influences of individual internal and external factors which affect carbonation. The influences of specific factors have been isolated (fib 2006) which gives more flexible parameters than the original one-parameter model.

Once the steel is de-passivated it will start to corrode. The principal chemical reaction in corrosion is independent of the way the corrosion is initiated (Broomfield 2007) and can be described in simplified form by anodic and cathodic reactions (Ahmad 2003). Ferrous hydroxide is formed from the ferrous ions and hydroxyl ions as a combined result of the anodic and cathodic reactions. This ferrous hydroxide then reacts further with available oxygen and water to form various final reaction products, i.e. rust. (Bažant 1979). This ferrous hydroxide may react further to produce ferric hydroxide and more hydrated ferric oxide. (Broomfield 2007). The final corrosion product varies depending on the constituents available. It has been observed that the corrosion products form layers of different composition around the reinforcement (Huet et al. 2007). The different corrosion products also have distinctive densities and therefore the corrosion of a certain mass of Fe may result in the formation of a greater volume of corrosion products. This means that different corrosion circumstances generate different expansion of corrosion products.

According to (Huet et al. 2007), the conductive oxide layer consists mainly of magnetite (Fe_3O_4) while the non-conductive oxide layer is mainly lepidocrocite ($\gamma\text{-FeOOH}$) and/or goethite ($\alpha\text{-FeOOH}$). Marcotte and Hansson (2007) have found magnetite (Fe_3O_4), goethite ($\alpha\text{-FeOOH}$) and haematite ($\alpha\text{-Fe}_2\text{O}_3$) in laboratory experiments on reinforcement corrosion with immersion in a NaCl solution. In their experiments, haematite in particular formed above the solution line environment, i.e. not a constantly-wet environment. These results imply that the hydroxide types of rust are formed in high moisture conditions, while the oxide type rust occurs in not-constantly-wet conditions. Suda et al. (1993) detected magnetite, goethite and lepidocrocite from a concrete specimen exposed to a marine environment for five years. Corrosion products observed on rebars by Jaffer and Hansson (2009) under chloride-induced corrosion in mechanically generated cracks included haematite, maghemite ($\gamma\text{-Fe}_2\text{O}_3$), goethite and Ferric hydroxide ($\text{Fe}(\text{OH})_3$).

2.2 Service life modelling

The most common concept (Tuutti 1982) in assessing the service life of reinforced concrete is the division of the service life into two phases, an initiation phase and a propagation phase (Fig. 1). This dual phase model illustrates that the main pre-condition for the corrosion of steel in

concrete is the de-passivation of the reinforcing steel, which occurs during the initiation phase. The de-passivation happens via carbonation of the surrounding concrete. It should be noted here that no actual corrosion (or damage) has yet occurred during this initiation phase.

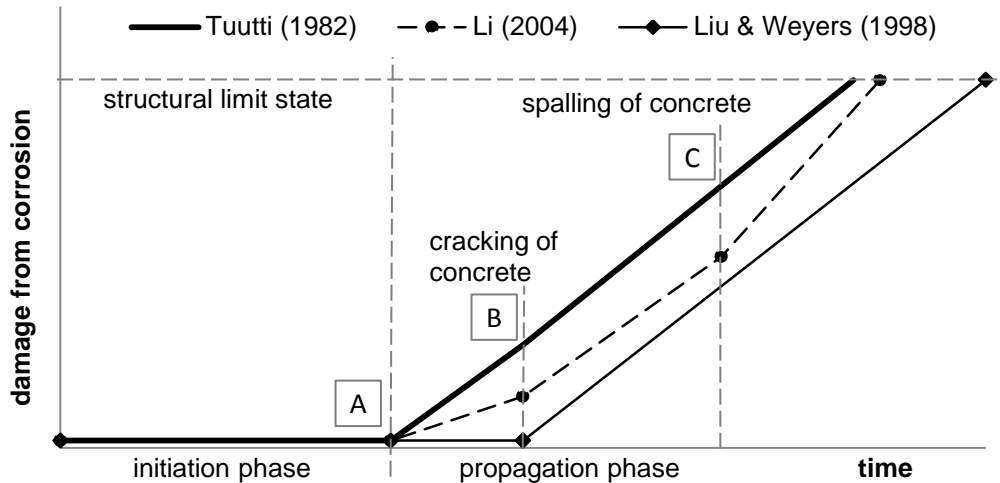


Figure 1 – The model of reinforcement corrosion usually utilizes the principle of initiation and propagation phases.

After initiation comes the propagation phase, in which the reinforcement corrodes, generating ferrous oxides, i.e. rust. As with most chemical reactions, the type and rate of corrosion is influenced by the corrosion environment, affected in this case by fluctuations in the temperature and the moisture and pH levels of the concrete (Ahmad 2003).

The dual phase model can be used in service life design, either as a whole unit (comprising both phases) or only in terms of the initiation phase. In the latter case, the initiation of corrosion, (i.e. the point when carbonation has reached the reinforcement) is regarded as the end of the structure's service life (point A in Fig. 1). The problem with this strategy is that it sets the end of structure's service life at a point where no damage has yet occurred, i.e. there is still a wide safety margin. Yet, the approach of early intervention is good. If both phases are taken into account, this safety margin can be effectively utilised, and a number of other factors can be used to determine the end of the structure's service life, such as concrete cracking and/or spalling (points B and C in Fig. 1), critical deflection or collapse (Li 2004).

Since the introduction of the dual phase model, the theories about what actually happens in the porous zone around the concrete reinforcement have advanced considerably. Liu and Weyers (1998), for example, have identified factors which can delay the accumulation of corrosion damage in concrete (Fig 1). According to their theory, the delay is caused by the fact that rust first accumulates in the vacant pores in the porous zone, which does not raise the tensile stress. Another widely discussed theory is the acceleration of the rate of damage once certain limits, such as cracking or spalling, have been reached (e.g. Li 2004). This theory has given rise to a multitude of studies on reinforcement corrosion (both initiation and propagation) in cracked concrete.

Corrosion propagation can be modelled by (i) empirical, (ii) numerical or (iii) analytical approaches (Otieno et al. 2011). The empirical models can be further divided into three types:

expert Delphic oracle models, fuzzy logic models and models based on the electrical resistivity and/or oxygen diffusion resistance of concrete. The empirical models are based on the experimentally achieved relationship between the degree of corrosion and the controlling parameters (see DuraCrete 2000).

There are three different approaches to developing the numerical models: the finite element method (FEM), the boundary element method (BEM) and a method based on resistor networks and transmission lines. The numerical models rely on complex computation which divides the larger entities into small elements connected to each other by boundary conditions (FEM, BEM) (e.g. Gulikers and Raupach 2006).

In general, the analytical models usually apply a ‘thick-walled cylinder’ approach. Division into a cracked inner cylinder and an un-cracked outer one has also been developed. The analytical models are based on the closed-form solving of mathematical equations derived from the geometry of the problem (e.g. Goltermann 1994).

A traditional way of modelling corrosion propagation is to modify the corrosion rate with the diameter of the reinforcement and the thickness of the concrete cover. (Siemes et al. 1985) The corrosion rate itself is related to the wetness and temperature of the structure, and this can be modelled by, for example, measuring the potential electrolytical resistivity of the concrete (DuraCrete 2000).

3. RESEARCH METHODS AND MATERIAL

The propagation of corrosion on concrete facades in Finnish environmental conditions was studied by a series of field and laboratory studies conducted on twelve residential concrete buildings located in different parts of southern Finland. The studies were conducted in tandem with the normal condition assessment inspections for these buildings. In addition, the extent to which the corrosion rates in concrete facades are affected by the outdoor environment was analysed using long-term (25 months) field measurements from concrete facades under natural weather conditions. These experimental results were compared with statistical information on 947 buildings.

The additional research material for this particular study was gathered from 12 buildings, chosen because of their consistency with larger statistical data. The buildings were all located in southern Finland, and ranged from 1971 to 1984 in their years of construction. A total of 27 sample cores with a diameter of 50 mm were drilled from the outer layer of the facade panels directly on visually observable corrosion cracks or spalls. The length of the active corrosion phase could be calculated by determining the time of initiation from carbonation depth measurements, and then subtracting that figure from the total age of the samples. The reinforcing bars trapped inside the carbonated layer of concrete were extracted from the core samples and studied under an electron microscope. The types and critical quantities of the corrosion products in the concrete and reinforcement samples, which formed visible damage, were studied by electron microscopy and X-ray diffractometry.

Mattila (Mattila and Pentti 2008) took long-term corrosion current density measurements based on linear polarisation resistance between 2000 and 2002. He fitted instruments on the concrete facades and balconies of two residential buildings in Finland, one inland (Fysiikanpolku 5, Tampere), built in 1978, and the other on the coast near Helsinki, at Joupirinne 4, Espoo, also

built in 1978 (Mattila and Pentti 2008). The measurement facades were both in south-facing directions, the one in Tampere faces southeast (154 degrees from north, clockwise) while the one on the coast faces south-west (223 degrees from north, clockwise). This data was in this research combined with long term weather observation data from the same period.

The weather observation data for this study was collected by the Finnish Meteorological Institute (FMI). The data was then further refined to form four weather parameters: Temperature (T, [°C]), relative humidity (RH, [%]), amount of wind-driven rain on the measured wall surface (IWA, [mm]), amount of direct and diffuse solar radiation on the measured wall surface (RAD, [kJ/m²]). The data, taken at three-hour time intervals, was taken from the records of the weather observation stations nearest to the case buildings. Finally, multi-linear regression analysis was used to determine the partial influence of single or a sequence of weather parameters on the observed corrosion current density. From a relatively large number of analyses (525 analyses with different combinations of weather parameters, seasons, etc.) the best performing combinations were judged by the coefficient of determination (R^2) of the model. Initially, separate models were produced for the facades and balconies in both the inland and the coastal areas. However, in cross-checking the models' functionality (by using the coastal area model inland and vice versa) the models were found to have a fairly good fit (R^2 of 0.49–0.53) (Fig. 2).

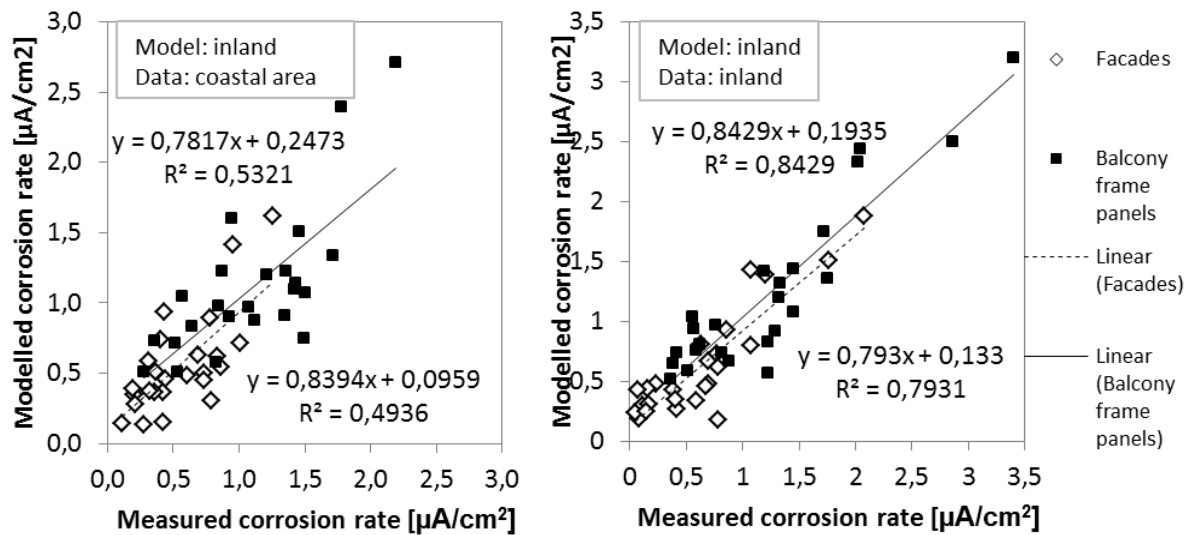


Figure 2 – The correlation between the model generated from the inland data and the measured corrosion rate in both the inland and the coastal area.

The research material collected from the commercial condition investigations produced a total of 18 cases where the same facade and/or balconies had been subject to two condition assessments within a certain time interval. The majority were built in the 1970s, but they ranged from 1969–1992, and were perfect for this study. This data was used to study the reliability of modelling of the carbonation of concrete facades and balconies using the square root relationship and the carbonation coefficient. During the first condition assessment, the buildings ranged from 9–36 years old (average age 27 years), and during the second assessment, they were 19–42 years old (average age 35 years). The interval between the assessments was 4–14 years (average 8 years). The properties studied were the average carbonation across the entire facade of the subject building and the carbonation depth of parallel samples.

The concrete facades of buildings in Finland have been subject to condition investigations since the late 1980s and much data has been collected using standardised procedures (desk studies, visual observations and ratings, field measurements and laboratory analyses) (Lahdensivu et al. 2013). A database has been amassed from a variety of building condition assessments conducted by various professional engineers between 1992 and 2006. This database includes the condition assessment information of 947 buildings built between 1965 and 1995. (Lahdensivu 2012). This data was subjected to statistical analysis and modelling (e.g. regression analysis, statistical distribution fitting, Monte Carlo simulation) in order to determine major trends in the degradation behaviour of concrete facades and balconies. The condition assessment database was used to perform a statistical analysis of the service life of concrete facades in terms of visible damage caused by reinforcement corrosion. The visible damage ratings given in the condition assessments were studied in order to determine the age at which visible corrosion damage is generally observed in concrete facades. This damage rating was used together with the age of buildings to study the time it takes for corrosion damage to propagate.

From 1965 until 1989, the specified concrete grade used in the facade panels was C20/25. The cement type used in these precast panels is mostly CEM I, ordinary Portland cement. The concrete composition was not analysed as part of the condition assessments, and has to be estimated from what is known.

4. RESULTS AND DISCUSSION

4.1 Statistical analysis of the service life

According to the statistical analysis, the first visible damage had already occurred after 8 years in exposed aggregate facades, and within 15 years for brushed and painted concrete facades (Fig. 3). In the balcony slabs, the first damage was observed after 9 years. The median figure is that visible corrosion damage had formed on the concrete facades within 21 and 25 years of construction for exposed aggregate and brushed painted concrete respectively. The spread of corrosion-related damage has therefore been quite fast in these structures. Corrosion damage is clearly a problem, especially in cases where the concrete cover is shallow, as then both the initiation and the active corrosion occur rapidly.

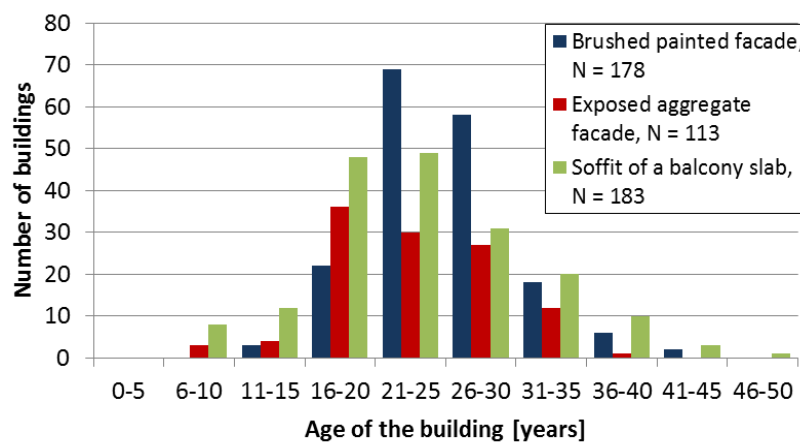


Figure 3 – The age distribution of facades where visible damage had been observed

The propagation phase was estimated by extracting from the total age (Fig. 3) a known initiation phase based on carbonation depth measurement data (Fig. 4). According to the calculation, the length of the propagation phase is 0.6–1.4 years when adopting a commonly used 5 % safety level (Fig. 5). It relates to corrosion of reinforcement with extremely small cover depth or in very capillary concrete. However, this safety level may be too strict compared to empirical knowledge. On average, the length of the propagation phase has been 6–10 years depending on the type of structure.

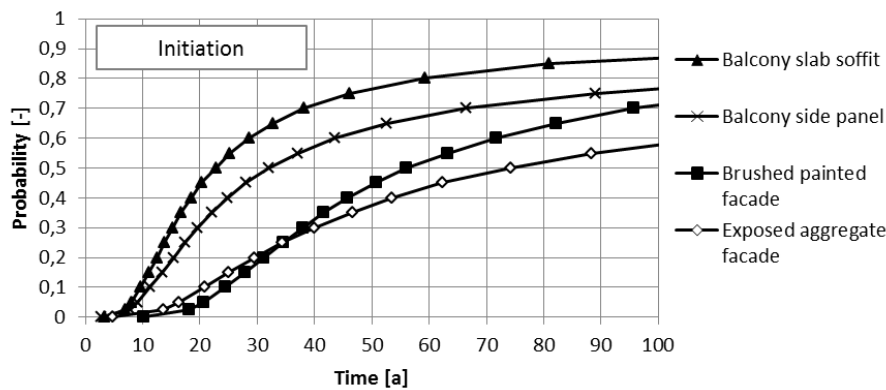


Figure 4 – The length of the initiation phase in concrete facades and balconies based on a Monte Carlo simulation on statistical condition assessment data from buildings constructed in 1965–1990

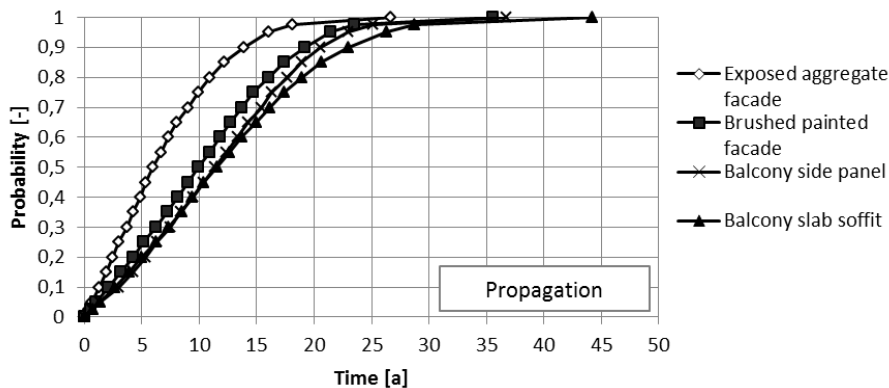


Figure 5 – The length of the propagation phase in concrete facades and balconies based on a Monte Carlo simulation on statistical condition investigation data

As the statistical analysis shows, approximately 80 % of the service life of concrete is accounted for in the initiation phase, although there are slight differences between different structure surfaces. (Table 1). Therefore, when assessing the total service life of a building, it is critical to ensure the structures have the required resilience to carbonation in terms of concrete composition, concrete quality and cover depths. If the properties of the initiation phase are already fixed (as is the case in existing structures) it seems clear that accurate information about the propagation phase will have to be utilized to extend a structure's service life.

Table 1 – The relationship of initiation and propagation phases in concrete facade and balcony panels (av. in brackets)

Structure surface	Share of the initiation phase in the total service life, average in parenthesis (%)	Share of the propagation phase in the total service life (%)
brushed painted concrete facade	85–98 (88)	2–15 (12)
exposed aggregate concrete surface	91–99 (94)	1–9 (6)
balcony slab soffit	66–94 (72)	6–33 (28)
balcony side panel	72–99 (80)	1–28 (20)

4.2 The influence of weather on corrosion rates

The corrosion rate was determined to be the combined effect of the weather parameters on already carbonated concrete structures exposed to the outdoor environment. A set of long-term corrosion rate data from 2 locations was combined with weather data from the same locations for the same time period. Besides being somewhat scattered, the corrosion current densities are in general rather high (Fig. 6). However, the initial assumption that the corrosion rates would be higher on the site located in the coastal region was not confirmed by the measurements, certainly not over the period in question, anyway. In fact, the inland structures faced 47 % more wind-driven rain than those on the coast, and their corrosion rates were 11–18 % higher. This highlights the importance of taking both the geographical position and the micro climate around the building into consideration when assessing the degradation rate. On the bottom surfaces of the balcony slabs, the corrosion rates are clearly much lower than in the other, environmentally-exposed parts. This clearly indicates that structures which are sheltered from wetting do not corrode as fast as those which are exposed to the weather.

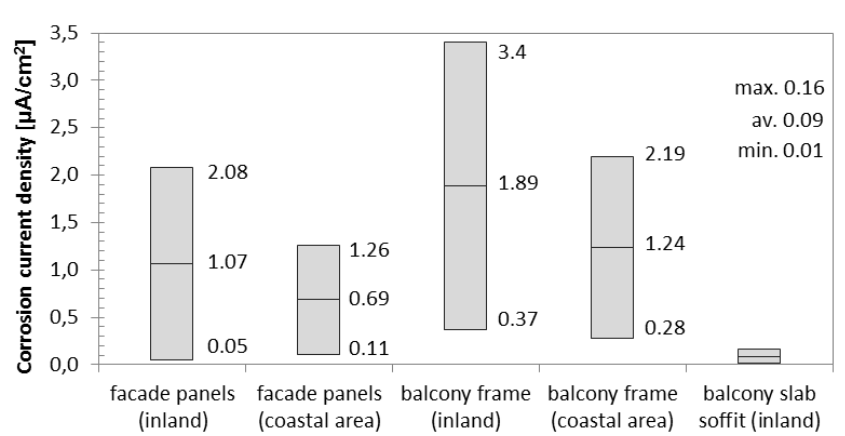


Figure 6 – Monthly average corrosion current densities recorded in field measurements in an inland area and a coastal area in Finland

The measured corrosion current densities were compared with the four weather parameters recorded from the same time period for each area. These were temperature (T , °C), relative humidity (RH , %), wind-driven rain (I_{WA} , mm) and solar radiation (RAD , kJ/m^2). A regression model was formed on the basis of linear regressions between the weather parameters and the

corrosion rate. Corrosion rates estimated with the regression model using a 30-year weather observation data in current climate (1979–2009) are presented in Table 2.

Table 2 – Modelled corrosion rates ($\mu\text{A}/\text{cm}^2$) in facades and balconies with varying geographical locations in Finland averaged over weather data from 1979–2009 with the corresponding corrosion penetration ($\mu\text{m}/\text{year}$) in parenthesis.

	XC4				XC3
	North facing facade	South facing facade	North facing balcony side panel	South facing balcony side panel	Balcony slab soffit
Helsinki-Vantaa (South coastal Finland)	1.00 (11.6)	1.83 (21.2)	1.51 (17.5)	2.98 (34.6)	0.07 (0.85)
Jokioinen (Southern Finland)	0.97 (11.2)	1.43 (16.5)	1.46 (16.9)	2.31 (26.8)	0.06 (0.68)
Jyväskylä (Mid-Finland)	0.86 (9.9)	1.07 (12.4)	1.33 (15.4)	1.74 (20.2)	0.04 (0.51)
Sodankylä (Northern Finland)	0.72 (8.4)	0.81 (9.4)	1.08 (12.5)	1.26 (14.7)	0.03 (0.34)

In the most exposed facades (facing south) the overall average level was $1.8 \mu\text{A}/\text{cm}^2$ in the coastal area and $1.1\text{--}1.4 \mu\text{A}/\text{cm}^2$ in inland. These corrosion rates correspond to a steel loss of $21 \mu\text{m}/\text{year}$ and $12\text{--}17 \mu\text{m}/\text{year}$, respectively, derived from the Faraday's law. These corrosion levels can be considered high (Andrade & Alonso 2001) in carbonation initiated outdoor concrete structures. In south facing balcony structures the corrosion level is even higher than on facades, being $3 \mu\text{A}/\text{cm}^2$ in the coastal area and $1.7\text{--}2.3 \mu\text{A}/\text{cm}^2$ in inland.

4.3 The critical extent of corrosion

Concrete structures studied by characterization methods (SEM, EDS, XRD) were on average 38.8 years old. The average time under active corrosion was for the cracked locations 26.0 years. It should also be noted that for all of the samples corrosion has been initiated quite fast (by average 12.6 years) which indicates that both concrete resistance against carbonation has been poor and the environmental conditions favourable to carbonation (somewhere between exposure classes XC3 and XC4). Corrosion products associated with carbonation initiated corrosion on the studied concrete facade panels were mostly hydroxide type of rusts with a unit volume of roughly 3 times the volume of iron. Taking the determined relative volume of the rust layer into account the required corrosion penetration to initiate visually observable cracks in the studied facade panels was by average $67.5 \mu\text{m}$ (total range of $22.2\text{--}119.1 \mu\text{m}$) with a corresponding rust thickness of $202.5 \mu\text{m}$.

Based on the modelled corrosion rate and the measured critical corrosion penetration, the length of the propagation phase is estimated to be approximately 1.5–8 years in inland and 1–6 years in the coastal area in south facing facades.

5. CONCLUSIONS

The research project confirmed that the active corrosion phase can provide a considerable extension to the service life of concrete facade panels in a Nordic climate especially in mild exposure to weather. Our statistical analyses show that the length of this period can be from just a few to up to tens of years. A more in-depth analysis of the case-study buildings, however, showed that the service-life extension for XC4 exposure conditions is, in practice, likely to be limited to below ten years. It has to be noted that the limit is based on the occurrence of visible corrosion damage on the structure surfaces. Even this is therefore not the ultimate end of service life for these structures. It appears, that the potential for extending a structure's service life with the propagation phase is in some cases considerable (by average 6–12 %). The majority of the service life of concrete is accounted for already in the initiation phase. Therefore, when assessing the total service life of a building, it is critical to ensure that the structures have the required resilience to carbonation in terms of concrete composition, concrete quality and cover depths. If the properties of the initiation phase are already fixed (as is the case in existing structures) it seems clear that accurate information about the propagation phase will have to be utilized to extend a structure's service life.

The ability to model or forecast corrosion rates on concrete facades will enhance the capability of realtors to react on upcoming repair needs. This kind of model would be able to predict the residual service life of a certain structure, but it could also be used in creating renovation strategies for a larger building stock by revealing the order of importance or the urgency of single renovation projects. The knowledge on active corrosion phase will enhance the capability of the owner to utilize the delaying options with more confidence. Especially this knowledge will help in pointing out the cases where these options are applicable and where they are not. It also illustrates clearly the influence of the delaying of renovation, which will in eventually render lighter repair options not applicable due to increasing degradation.

The occurrence of visual damage is a natural way of judging the service life of these structures since all of the renovation and maintenance decisions are made based on investigations usually commissioned based on these visual signs. This, however, means that lighter remedial actions are not anymore available and repair & protect options have to be considered to some extent. In order to be able to utilize only protective options, the service life should not include propagation phase. The intervention should in this case be taken directly in the end of the initiation phase.

Corrosion induced damage occurred on the studied structures commonly on the lap splicing locations of rebars, in the edges and window openings of the panels and in locations with pronounced moisture load due to poorly functioning flashings and rain water runoff control. If the ratio of concrete cover to reinforcement diameter was small (below 1.5) corrosion related damage had emerged as spalling. If the ratio was well over 1.5 the damage more probably emerged as cracking. Careful design of the above mentioned details will allow longer propagation phases to be taken into account in service life.

The definition of the end of service life by corrosion initiation serves the durability design strategy A) of avoiding damage. It also enables early intervening when the available remedial options are many and they are in general fairly light. On the other hand, strategy B) of optimizing service life leads to need-based renovation already requiring some level of intrusive repair. A strategy aiming at maximizing the available service life of the existing structure will lead to heavy renovation, replace or demolition eventually. A conventional limit for the early intervention strategy is the initiation of corrosion. However, it is shown that this strategy is not

compromised even when the service life is extended to the propagation phase via a propagation phase model. Same set of renovation options will be available until the occurrence of damage as cracking or spalling. This information can be utilized in planning of the renovation of structures, where the initiation phase has already passed. Modelling the length of the propagation phase will allow a time-span of up to 8–10 years for planning and budgeting of the renovation work without compromising the choice of strategy.

REFERENCES

1. Ahmad, S. 2003. Reinforcement corrosion in concrete structures, its monitoring and service life prediction – a review. *Cement & Concrete Composites* 25:459-471.
2. Andrade C, Alonso C (2001) On-site measurements of corrosion rate of reinforcements. *Construction and Building Materials* 15:141–145.
3. Bažant, Z.P. 1979. Physical model for steel corrosion in concrete sea structures—theory. *J. of the Engrg. Mech. Div., Proc. ASCE*, 105, Pp. 1137–1153.
4. Broomfield, J. 2007. *Corrosion of steel in concrete*. 2nd ed. Oxon: Taylor & Francis.
5. DuraCrete project. 2000. Probabilistic performance based durability design of concrete structures. The European union – Brite EuRam III, DuraCrete. Final technical report of DuraCrete project, document BE95-1347/R17. CUR, Gouda, Nederland.
6. fib Bulletin No.34. 2006. Model Code for Service Life Design. International Federation for Structural Concrete, Lausanne.
7. Goltermann, P. 1994. Mechanical predictions on concrete deterioration. Part 1: Eigenstresses in concrete. *ACI Materials Journal* 91(6):543–50.
8. Gulikers, J., Raupach, M. 2006. Numerical models for the propagation period of reinforcement corrosion: comparison of a case study calculated by different researchers. *Materials and Corrosion* 57(8):618–27.
9. Huet, B., L'hostis, V., Santarini, G., Feron, D., Idrissi, H. 2007. Steel corrosion in concrete: Determinist modeling of cathodic reaction as a function of water saturation degree. *Corrosion Science*, 49(4):1918–1932.
10. Huopainen, J. 1997. Carbonation of Concrete Facades - a Field Study (MSc thesis), Tampere University of Technology. (in Finnish).
11. Hyvert, N., Sellier, A., Duprat, F., Rougeau, P., Francisco, P. 2010. Dependency of C-S-H carbonation rate on CO₂ pressure to explain transition from accelerated test to natural carbonation. *Cement and Concrete Research* 40:1582-1589.
12. Jaffer, S.J., Hansson, C.M. 2009. Chloride-induced corrosion products of steel in cracked concrete subjected to different loading conditions. *Cement and Concrete Research* 39:116–125.
13. Köliö, A. 2016. Propagation of Carbonation Induced Reinforcement Corrosion in Existing Concrete Facades Exposed to the Finnish Climate. TUT Publ. 1399. 61p+app.
14. Lahdensivu, J. 2012. Durability properties and actual deterioration of Finnish concrete facades and balconies. Tampere University of Technology, TUT Publ. 1028. 117p.
15. Lahdensivu J, Varjonen S, Pakkala T, Köliö A (2013) Systematic condition assessment of concrete facades and balconies exposed to outdoor climate. *Int. J. of Sustainable Building Technology and Urban Development* 4:199–209.
16. Li, C.Q. 2004. Reliability service life prediction of corrosion affected concrete structures. *ASCE J Struct. Eng.* 130(10):1570–7.
17. Liu, Y., Weyers, R.E. 1998. Modelling the time-to-corrosion cracking in chloride contaminated reinforced concrete structures. *ACI Materials Journal* 95(6):675–81.

18. Mattila J, Pentti M (2008) Residual service-life of concrete façade structures with reinforcement in carbonated concrete in Nordic climate. *Tailor Made Concrete Structures*, Taylor & Francis Group, London. Pp. 75-79.
19. Marcotte, T. D., Hansson, C. M. 2007. Corrosion products that form on steel within cement paste. *Materials and Structures* 40:325–340.
20. Monteiro, I., Branco, F.A., de Brito, J., Neves R. 2012. Statistical analysis of the carbonation coefficient in open air concrete structures, *Construction and Building Materials* 29 263-269.
21. Neves, R., Branco, F. A., de Brito, J. 2012. A method for the use of accelerated carbonation tests in durability design. *Construction and Building Materials* 36:585-591
22. Otieno, M., Beushausen, H., Alexander, M. 2011. Modelling corrosion propagation in reinforced concrete structures – a critical review. *Cement & Concrete Composites* 33:240–5.
23. Page, C.L. 1988. Basic principles of corrosion. In: Schiessl P, editor. *Corrosion of steel in concrete*. London: Chapman and Hall. Pp. 3–21.
24. Parrott, L.J. 1987. *A Review of Carbonation in Reinforced Concrete*, Cement and Concrete Association, Slough, UK.
25. Suda, K., Misra, S., Motohashi, K. 1993. Corrosion products of reinforcing bars embedded in concrete. *Corrosion Science* 35(5-8):1543–1549.
26. Thiery, M., Villain, G., Dangla, P., Platret, G. 2007. Investigation of the carbonation front shape on cementitious materials: Effects of the chemical kinetics. *Cement and Concrete Research* 37:1047-1058.
27. Siemes, A.J.M., Vrouwenvelder, A.C.W.M., van den Beukel, A. 1985. Durability of buildings: a reliability analysis. *Heron* 30(3):3–48.
28. Tuutti, K. 1982. *Corrosion of steel in concrete*. Stockholm. Swedish Cement and Concrete Research Institute. CBI Res 1982;4(82):304.

Feasibility Study of Moisture Measurement of a Concrete Pavement Tile Employing a 1.7 GHz Coaxial Surface Probe



Dr. Martta-Kaisa Olkkonen
Department of Electrical Engineering and Automation
previously with Department of Radio Science and Engineering
Aalto University
Maarintie 8
02150 Espoo, Finland
martta-kaisa.olkkonen@alumni.aalto.fi

ABSTRACT

Non-destructive moisture measurement of a homogeneous concrete test sample was conducted employing a coaxial surface probe at approximately 1.7 GHz. The change in the measured resonant frequency shift of the sensor was related to the moisture content variations so that larger resonant frequency shifts were recorded at higher moisture content levels. The absolute moisture content during the experiment varied from 0.1 to 4.9 percent of mass of the sample. In conducting the data post-processing, the relative resonant frequency shift was related to the results by using linear and parabola fit, giving $R^2 = 0.94$ and $R^2 = 0.96$, respectively.

Key words: Microwaves, moisture measurement, resonator, statistical fitting

1. INTRODUCTION

A special demand in evaluation of built environment is to observe moisture leakages causing health problems by measuring the moisture content of walls or floors in old buildings, where microbe growth has possibly already begun. Literature presents many commercial moisture sensors available for destructive moisture measurement of concrete. One of them is a commercial Vaisala relative humidity (RH) sensor [1], based on the borehole method, which requires drilling a hole for placing the sensor. Typically moisture sensors are embedded in building walls at the time of construction in order to monitor the drying process of concrete. Also, risky areas (prone to moisture damages) such as bathrooms can be monitored later [2]. However, it is preferable to investigate further the possibility of employing non-destructive, microwave moisture sensing methods. Several non-destructive techniques (NDT) were combined for the assessment of concrete in [3]–[5].

One traditional and destructive moisture evaluation method is oven-drying, where a sample is dried in the oven. Traditionally, moisture content is defined by a gravimetric method, which means that a sample is weighed before and after drying. The quantity of evaporated water is calculated as the difference of the weights. However, the accuracy in definition of the dry mass is compromised if some amount of water is confined in the pores of the material. Further, the gravimetric moisture content can be defined by either dry- or wet-basis. The percentage moisture content is calculated on a wet basis as a ratio of mass of water to the total mass of moist material

$$M = \frac{m_w}{m_w + m_d} \times 100\%, \quad (1)$$

where m_w is the mass of water and m_d is the mass of dry material. The definition using dry-basis gives the ratio of water in the material to the mass of dry material. The definition using volumetric moisture content would give the ratio of the volume of water in the material to the total volume of the sample.

This paper, extending the methodology of previous work [6], focuses on development of non-destructive microwave methods so that the moisture content of structures could be evaluated even after the construction. We aim to find a statistical correlation directly between the moisture content and the resonant frequency shift of the sensor, while it is assumed that only one parameter, moisture, affects the measurement of a homogeneous sample.

2. MATERIALS AND METHODS

2.1 Theoretical background of analysing moisture readings employing microwave sensors

Electromagnetic wave interaction in a medium is described by the complex permittivity [7, pp. 9–12] and it is denoted using the electrical engineering convention $j^2 = -1$ as

$$\varepsilon = \varepsilon_0 \varepsilon_r = \varepsilon_0 (\varepsilon_r' - j \varepsilon_r''), \quad (2)$$

where ε_r' is the real and ε_r'' is the imaginary part of the dimensionless complex relative permittivity (ε_r) while the permittivity of vacuum is $\varepsilon_0 \approx 8.854 \times 10^{-12}$ F/m (farads per meter). The real part of the complex permittivity ε_r' relates to the speed of propagation of an electromagnetic wave in the material, while the imaginary part ε_r'' accounts for losses i.e., energy dissipation. Interaction with the magnetic field is omitted in this paper because concrete is a non-magnetic material.

Dielectric values given in the literature vary depending on the composition of the concrete, moisture content level and thereby also the frequency. For dry concrete ε_r' was found to be approximately 4 and for wet concrete ε_r' was 11–15 across the measured frequency band 0–20 GHz in [8]. The loss tangent was measured for dry and wet concrete giving values below 0.16 for wet concrete and below 0.04 for oven-dried concrete. Measurement of the complex permittivity of dielectric materials using a similar coaxial sensor as in this research is presented in numerous references. An open-ended coaxial probe was designed for measurement of concrete in [9] and the measurements were made from 100 MHz to 900 MHz because these frequencies are typical in civil engineering applications. Concrete with different porosity levels

was measured giving permittivity values for the most porous concrete 4–4.5 at 900 MHz and the most compact concrete 6.5–7.5 at 900 MHz. The aggregate sizes varied between 5 and 20 mm but at least in this frequency range, the standard deviations were of the same order as that of the more heterogeneous limestone.

The coaxial probe used in the experiments of this paper operates as a resonator, and generally the resonance of a resonator is changed when it is loaded with a dielectric sample. When such a material is present in the resonator volume, the resonance condition will be met at a lower frequency compared to an unfilled resonator, as illustrated in Fig. 1. The measurement of an empty resonator can be used as a basic calibration.

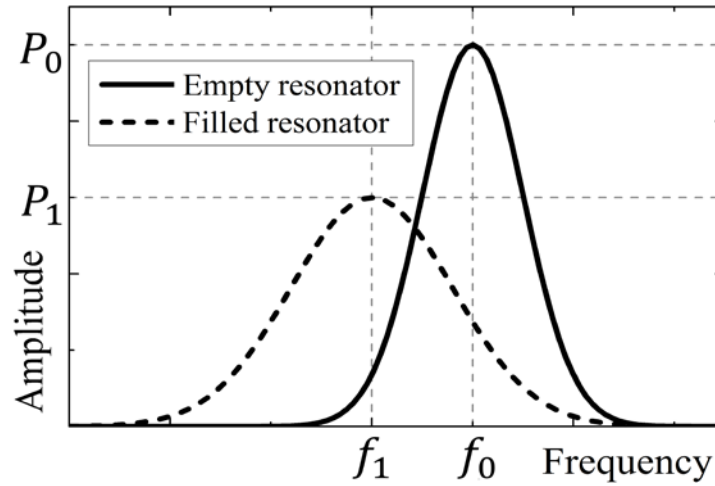


Figure 1 – Shift in the resonant frequency and attenuation of the signal of an empty and a filled resonator, examples of the phenomena are given in [10].

An approximation for the relation between the resonant frequency shift and ε_r' of the material yields in case of low losses [11, pp. 26–27]

$$\varepsilon_r' \approx \left(\frac{f_{r0}}{f_r} \right)^2, \quad (3)$$

where f_{r0} is the resonant frequency of an empty resonator and f_r that of a filled resonator. The relative resonant frequency shift (4) is a convenient quantity as it describes the resonant frequency in relation to the empty resonator:

$$\frac{\Delta f_r}{f_{r0}} = \frac{f_r - f_{r0}}{f_{r0}}. \quad (4)$$

2.2 Experimental setup

The surface sensor chosen for the moisture measurement is a coaxial probe. The diameter of the opening of the coaxial sensor is 40 mm, the centre conductor is 9 mm in diameter and the resonator cavity is 40 mm high. The footprint of the measurement i.e. the measurement resolution is determined approximately as the size of the resonator opening. The resonant frequency of an empty resonator was determined $f_{r0} = 1.715$ GHz. Fig. 2 a) shows the cross

section of the sensor and in Fig. 2 b) the resonator sensor is placed on a concrete test sample, which is a pavement tile purchased from a hardware store. Unfortunately, the exact composition or age of the sample could not be traced. Even though the origin of production is not known, reference values for pavement tiles are available in the literature, and the effect of water-to-cement ratio on the strength of pavement tiles was studied in [12]. A reasonable variation for w/c was considered to be between 0.45 and 0.65 for 15 % cement content and 0.50 to 0.70 for 12 % cement content, the upper limit seeming an overestimation. However, the microwave method assumes that only the amount of free water molecules affects the result, and samples with different w/c ratios would not differ in terms of the theoretical behaviour (Eq. (3)). As the maximum grain size of the concrete test sample is $d_{max} = 2$ mm, it can be considered homogeneous in relation to the measurement resolution. Eventually, the sensor is intended to be used in locations where no prior information about the host material is available. Comparison of the composition of the material with the permittivity is in fact omitted in employing the direct analysis of the moisture content, which relates the resonant frequency to the moisture without deriving the permittivity of material. From the point of view of a microwave measurement, the significant quantity is the amount of free water in the pores, which is removed by oven-drying in the reference measurement. Chemically bound water that is confined in the pores of concrete is harder to detect using microwave methods because it may not be removed prior to the reference measurement of the dry sample. Hence, it is likely that deviation is caused from the statistical fitting compared to free water (linear, parabola fit). In other words, the measurement accuracy can be compromised at low water content levels if there are traces of bound water that are not detected using the sensor.

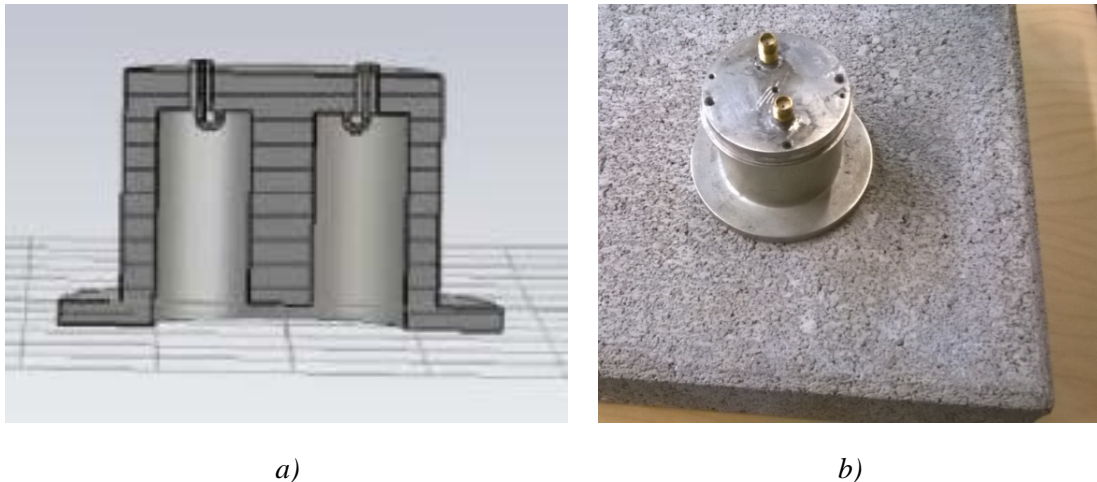


Figure 2 – a) Cross section of the coaxial resonator sensor and b) the sensor placed on a concrete sample.

Commercial coaxial probes and related software are available for example by Agilent Technologies [13]. It was noted that the coaxial probe assumes a half-space or “semi-infinite” configuration, a flat surface and no air gaps between the material and the sensor [13]. Tests indicated that the penetration depth is smaller than the thickness of the sample (55 mm), and the measurement at each moisture level was always made so that the concrete tile was placed on a wooden table. The host material remained the same so this experiment assumed that the accuracy of such a resonator measurement was sufficient. The pavement tile has a smooth surface with roughness less than 1 mm and its thickness is also a constant 55 mm. Due to the flat surface it was possible to press the sensor tightly on the concrete pavement tile. The benefit of the coaxial sensor chosen in this work is that it is a surface sensor opposed to radar which was

used for concrete evaluation studies in [14]. This may become a benefit in some applications where the footprint of the probe is small compared to the spacing of possible metal bars, and the probe can be conveniently placed between them.

2.3 Experiments with a concrete sample at different moisture content levels

The experiment started by soaking the sample in a water bucket until a saturated state was reached. Then, the sample was weighed and placed back to the bucket until the weight did not change anymore. Prior to the resonator measurement, the sample was weighed at the saturated level so that the gravimetric water content could be calculated after the sample was weighed again at a dry state. The resonator sensor was connected to a vector network analyser (VNA) HP8753D, and the sensor was excited from port 1 while the signal was received from port 2.

After the first measurement at the saturated state, the sample was oven-dried and the mass of the dry material was measured on a scale. The sample was dried after each measurement either in room temperature or in the oven until the next moisture content level was reached. In total, a measurement was made at 21 different water content levels. The sample was kept in a plastic bag at least for one night between the measurements so that the moisture would distribute evenly in the sample. Otherwise the moisture content could be lower on the surface of the sample. There was no specific method to confirm the even distribution of moisture besides keeping the sample in the plastic bag, but the sensor has a penetration depth that is only slightly smaller than the thickness of the sample, meaning that the moisture measurement averages over the thickness of the sample. It can be assumed that the moisture was evenly distributed in the measurement area of the sensor if the moisture did not lie exactly on either front or back surface of the sample but rather evenly distributed across the thickness of the sample. This was deemed a sufficient pre-requisite for this measurement.

Finally, for the measurement of the dry sample, it was oven-dried at 80°C until no more water evaporated from it. This is because a normal household oven was used, where it is not possible to adjust the temperature accurately. It was deemed safer to use a lower temperature than having a risk of exceeding 105 C, where one could not be sure if something else than water molecules has evaporated, causing the decline in weight. Anyway, drying of the sample was confirmed by keeping it in the oven as long as the weight loss was stabilized. The measurement series lasted in total for 37 days and there were either one or two days between the 21 different moisture levels. The percentage of water at each moisture level was calculated by comparing to the dry mass. Consequently, the maximum water content level was 4.9 % (wet basis).

3. RESULTS

3.1 Measurement data

Microwave methods enable non-destructive testing but the operation principle differs from traditional relative humidity sensors. The moisture measurement result is superimposed with inclusions of the host material, such as large granularities in relation to measurement resolution. As opposed to relative humidity sensor, employing MW methods for a granular material requires some sort of *noise reduction*, for example averaging. For the pavement tile, the resonant frequency shift was measured for each moisture level at three different locations and an average was taken.

The resonance of the “empty” resonator, without a sample, was measured for each moisture content level measurement due to possible changes in temperature conditions and different position of the cables. This acts as a basic calibration of environmental effects, when measurement of material and of the empty sensor is conducted in the same (room) temperature. The tests were made in a standard laboratory setup with VNA and cables that are sensitive to movement, but the measurements were recorded with the cables at a fixed position. For field use, portable electronics would be designed that allow flexible usage of the device, and moving from one spot to another. This challenge is not related to accuracy of the microwave method itself. An example of three resonances for the lowest moisture level (0.1 %) of the sample and the resonance of the empty resonator are shown in Fig. 3 a). In this case the resonant frequency, which is found at the highest point of the curve, was determined to be 1.522 GHz for the sample. It corresponds to a relative resonant frequency shift of 0.113, calculated using (4). In another example set of resonance curves in Fig. 3 b), the moisture content level of the sample is at maximum, 4.9 % of the weight.

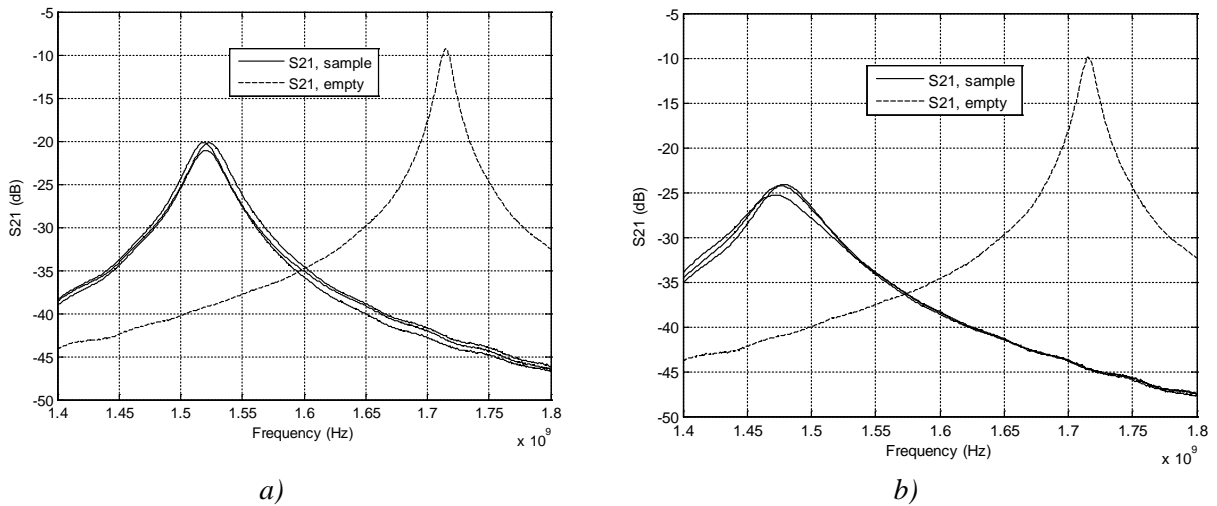


Figure 3 – a) Three resonance curves measured at the minimum moisture content (0.1 %) and resonance of an empty resonator. b) Three resonance curves measured at the maximum (4.9 %) moisture content and resonance of an empty resonator.

3.2 Correlation of the Resonant Frequency Shift to Moisture

The average resonant frequency shift, which was measured with the sample at each moisture level, was related to the gravimetric moisture content of the sample. For the moisture level 3.46% the average resonant frequency shift was calculated of two measurement points, because one point was too high 1.716 GHz, same as the resonant frequency of the “empty” resonator. This indicates that the measurement was made without pressing the sensor tightly onto the sample. Ref. [15] studied different aspects affecting the measurement using a coaxial probe, such as a so-called lift-off of the sensor from the material. Their results showed that an air gap is the most significant factor affecting the measurement accuracy. Such an inaccuracy can be caused by the rough surface of the concrete, even though the roughness of the pavement tile remained below 1 mm due to the smooth surface. For the moisture level 3.15% one point was also higher than the others (1.56 GHz, 1.5 GHz, 1.496 GHz), but the deviant point can be caused by inhomogeneity of the sample or some unevenly distributed moisture and it was left in the analysis. It was concluded in [8] that in practice the porosity of concrete causes the most

standard deviations because the location of the pores might not be even and in the case of wet concrete, water is then unevenly distributed.

Fig. 4 shows the relative resonant frequency shift against the water content in the sample. When the relative resonant frequency shift varied between 0.113 and 0.14, the amount of water (% of weight) varied between 0.15 and 4.89 %. Both a parabola fit and a linear fit were tried for matching the samples and they had $R^2 = 0.96$ and $R^2 = 0.94$, respectively. The parabola fit gives a better matching, and also according to (3), if the losses are low, the real part of the permittivity of the material is inversely proportional to the square of the resonant frequency shift.

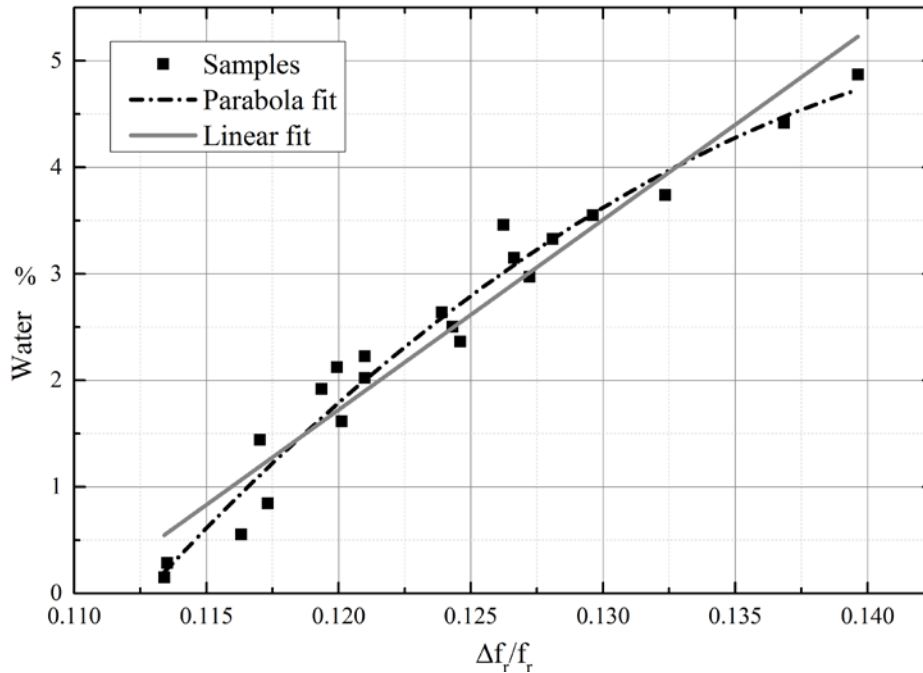


Figure 4 – Relative resonant frequency shift against the amount of water in the sample (% of weight). Parabola fit and linear fit.

4. DISCUSSION AND CONCLUSION

Moisture of concrete was measured using a coaxial surface sensor and a reference oven-drying method. The relative resonant frequency shift varied between 11.3 % and 14 % while the water content varied between 0.1 % and 4.9 % of the weight.

The methodology was based on direct characterization, where the initial assumption was that only one parameter, moisture, affects the measurement. Then, the moisture content of a material can be determined directly with a microwave resonator from the measurement results (f_r), without derivation of the dielectric parameters first. A statistical correlation was determined directly between the moisture content of the concrete and the resonant frequency. A parabola fit and a linear fit were compared and they gave $R^2 = 0.96$ and $R^2 = 0.94$, respectively. The maximum deviation from the parabola is 0.05 percentage points. It is possible to gain such a high accuracy when only one sample is used and an average of three points is taken. However, the repeatability is satisfactory only if the same measurement locations would be measured again, as the permittivity of the dry material varies locally.

In practice there are steel bars in most concrete structures, like floors and walls. Ref. [16] studied the shielding effectiveness of reinforced concrete structures and according to them, the diameter of the reinforcing bars (rebars) typically lies within 10–60 mm and their spacing 90–500 mm. Steel bars or fibres would cause the field pattern at the coaxial probe to distort and hence the resonant frequency shift would become other than expected for a certain moisture content level for homogeneous concrete. The measurement of steel fibre reinforced concrete using a coaxial probe was reported in [17], where a Maxwell-Garnett type analytical relation [18] was derived between the permittivity and the fibre volume fraction. In some cases the effect of the steel bars or fibres and moisture could be superimposed. In this case, it is likely that the uncertainty in the moisture readings becomes too high for using the coaxial probe. It could be an option to make the measurement exactly between the rebars, if their location is known. However, if the spacing of the metal mesh is less than a wavelength, the signal does not penetrate well. Wavelength is inversely proportional to the frequency and it depends on the permittivity of the medium as $c/f\sqrt{\epsilon_r}$. For a comparison, at 3 GHz the wavelength is 5 cm, when $\epsilon_r = 4$ and at a slightly lower frequency $f = 1$ GHz it is already 15 cm.

Microwave methods are very promising for non-destructive testing but some challenges originate from relation of the physical properties of materials with electrical ones, such as temperature. Microwave methods measure the changes in dielectric constant, and in stable temperature conditions and for homogenous host material only the changes in moisture would ideally affect the result. Temperature variations affect the oriental polarization of molecules with permanent dipole moment such as water, thus affecting the observed dielectric constant. Simply, a test with temperature variations would indicate that higher temperature is observed falsely as lower dielectric constant. Studies of compaction of asphalt have dealt with the same problem, where newly-laid asphalt is very hot and the solution could be for example placing temperature sensor and recording the temperature for calibration of results. For the pavement tile, only three recordings were averaged for noise reduction, but for more inhomogeneous cases like mapping a whole highway lane, it is possible to average hundreds of points. This would also require future work in terms of the measurement device and creating algorithms for the calibration, which was out of scope for the feasibility study of the method.

The accuracy of this sensor will be inevitably worse in a real application. As the permittivity of concrete at different moisture states varies from 4 to 15 according to [8], calibration of the sensor is important. It is possible to use the sensor directly for moisture measurements if the concrete in question is known to be homogeneous. One can for example measure on one separate concrete element at a time, if the elements can be distinguished. Then one can monitor the relative differences between wet and dry areas. In this experiment, an average of three measurements on different locations on the sample was taken. This is not advisable, if the moisture on the measurement area is not completely evenly distributed.

Deploying MW sensors for moisture measurement in real applications like building walls would require accurate, real-time information about the reference moisture at each location. Alternatively, the sensor could be used for detecting places with deviating signals and possibly study these locations with a destructive reference method to see if only the thickness has changed without increase in moisture. This research could be continued by testing more samples with different water-to-cement ratios, different mixing ratios of the ingredient materials and different grain sizes. It could be studied, what is the maximum grain size of concrete so that the sensor can detect the moisture variations with a reasonable accuracy and the rock aggregates would not dominate the measurement volume. Different measurement scenarios could be

developed, where the concrete test sample is placed on top of some metal or plastic pipes which simulate the real environment of a wall or a floor with utility pipes or rebars.

ACKNOWLEDGEMENT

The author wishes to thank Finnish Concrete Association for funding this research.

REFERENCES

1. Vaisala SHM40 Structural Humidity Measurement Kit, Available: <http://www.vaisala.com/en/industrialmeasurements/products/humidity/portable/Pages/SHM40.aspx>, [Accessed February 11, 2017].
2. Voutilainen J: "Methods and instrumentation for measuring moisture in building structures," Helsinki University of Technology, Applied Electronics Laboratory. B, Research reports, 17, 2005.
3. Breyse D, Klysz G, Dérobert X, Sirieix C, Lataste J F: "How to combine several non-destructive techniques for a better assessment of concrete structures," *Cement and Concrete Research*, Vol. 38, No. 6, June 2008, pp. 783–793.
4. Villain G, Dérobert X, Sbartaï Z M, Balayssac J: "Evaluation of concrete water content and other durability indicators by electromagnetic measurements," *Proceedings*, 13th International Conference on Ground Penetrating Radar (GPR), 2010, pp. 1–6.
5. Bungey J H: "Sub-surface radar testing of concrete: a review," *Construction and Building Materials*, Vol. 18, No. 1, February 2004, pp. 1–8.
6. Olkkonen M K, Mikhnev V, Huuskonen E: "RF moisture measurement of concrete with a resonator sensor," *Proceedings*, Microwave and Telecommunication Technology (CriMiCo), 2012 22nd International Crimean Conference, 10–14 September 2012, pp. 853–854
7. Pozar D M: "Microwave Engineering," 3rd edition, Hoboken, NJ, John Wiley & Sons, 2012.
8. Rhim H C & Büyüköztürk O: "Electromagnetic Properties of Concrete at Microwave Frequency Range," *Materials Journal*, Vol. 95, No. 3, May 1998, pp. 262–271.
9. Filali B, Boone F, Rhazi J, and Ballivy G: "Design and Calibration of a Large Open-Ended Coaxial Probe for the Measurement of the Dielectric Properties of Concrete," *IEEE Transactions on Microwave Theory and Techniques*, Vol. 56, No.10, October 2008, pp. 2322–2328.
10. Homepage of Material Sensing & Instrumentation: Part 4, "Microwave Cavity Examples," Available: http://www.msi-sensing.com/microwave_cavity.htm
11. Nyfors E: "Cylindrical Microwave Resonator Sensors for Measuring Materials Under Flow," Doctoral dissertation, Radio Laboratory, Helsinki University of Technology, Espoo, Finland, 2000.
12. Tung-Chai L, Md Nor H, Mudiyono R: "The Effect of Cement and Water Cement Ratio on Concrete Paving Block", *Proceedings*, Regional Postgraduate Conference on Engineering and Science (RPCES 2006), Johore, 26-27 July, pp. 89–92.
13. Agilent Technologies, "Basics of Measuring the Dielectric Properties of Materials," Application Note, Available: <http://cp.literature.agilent.com/litweb/pdf/5989-2589EN.pdf>, [Accessed February 11, 2017].
14. Gehrig M D, Morris D V, Bryant J T, (Mar. 2004): "Ground penetrating radar for concrete evaluation studies," *Proceedings*, Foundation Performance Association, pp. 1–17,

Available: http://www.foundationperformance.org/technical_papers.cfm [Accessed February 11, 2017].

15. Koselj J & Bregar V B: "Influence of parameters of the flanged open-ended coaxial probe measurement setup on permittivity measurement," *Journal of Microelectronics, Electronic Components and Materials*, Vol. 42, No. 1, 2012, pp. 36–42.
16. Hyun S Y, Du J K, Lee H J, Lee K W, Lee J H, Jung C, Kim E J, Kim W, Yook J G: "Analysis of Shielding Effectiveness of Reinforced Concrete Against High-Altitude Electromagnetic Pulse," *IEEE Transactions on Electromagnetic Compatibility*, Vol. 56, No. 6, December 2014, pp. 1488–1496.
17. Van Damme S, Franchois A, De Zutter D, Taerwe L: "Nondestructive determination of the steel fiber content in concrete slabs with an open-ended coaxial probe," *IEEE Transactions on Geoscience and Remote Sensing*, Vol. 42, No. 11, November 2004, pp. 2511–2521.
18. Sihvola A: "Electromagnetic Mixing Formulas and Applications," *Electromagnetic Waves Series*, London, U.K., Inst. Elect. Eng., 1999, pp. 40–41.

The Critical Flow Distance at Freezing of Concrete – Theory and Experiment



Göran Fagerlund
 Professor em.
 Div. Building Materials
 Lund Institute of Technology
 Box 118
 SE-221 00 Lund
 E-mail: goran.fagerlund@byggtek.lth.se

ABSTRACT

The distance between a point in cement paste where water freezes and the closest air-pore is traditionally expressed by the Powers spacing factor [1] or the Philleo spacing factor [2]. Both equations are based on two simplifications: (1) no air-pores are supposed to absorb water, (2) no consideration is taken to the true air-pore size distribution. These obstacles might be overcome by using the concept *flow distance* which is developed in the paper. The method to determine the critical flow distance is shown by an example based on experiments. The size of the critical flow distance can be used for determining the required air content. An example is given.

Key words: Frost resistance, spacing factor, flow distance, air-pore size distribution, critical water content.

1. POWERS SPACING FACTOR

1.1 Theory

The major frost destruction mechanisms, the hydraulic pressure mechanism [1] and the microscopic ice lens formation mechanism [3], both predict the existence of a critical distance from a place where ice is formed to the nearest air-filled void that is big enough to accommodate water that is expelled. The traditional way of calculating a maximum distance is by using the *Powers spacing factor* which is based on the material model in Figure 1. It is assumed that cement paste is the only frost sensitive phase in concrete. The total cement paste volume is divided into a number of equal-sized unit cubic cells containing a spherical air void of constant size in its center. Powers spacing factor is the distance from the corner in the cube to the periphery of the pore. This is the longest distance water has to be transported from the site where it freezes to the nearest air-filled pore. The following geometrical relation is valid [1]:

$$\bar{a} = \frac{3}{\alpha} \left[1.4 \left(\frac{1}{A} \right)^{1/3} - 1 \right] \quad (1)$$

\bar{a} Powers spacing factor, mm

α the specific surface of the air pore, $\alpha=6/D$, mm⁻¹

D the diameter of the air pore, mm

A the air content in the cement paste as fraction of the cement paste volume (volume of air

is included in the volume of cement paste)

The value α is supposed to be equal to the specific surface of the *entire air pore system*, i.e. the total surface area of all air-pores divided by their entire pore volume. The value α can be determined by image analysis of polished concrete surface, or by the linear traverse technique.

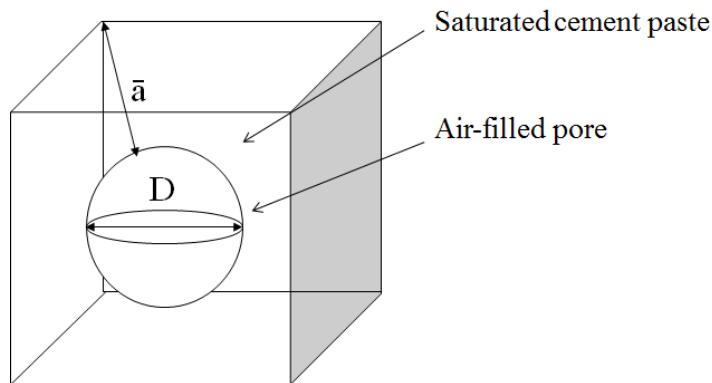


Figure 1 - Model for calculating Powers spacing factor.

1.2 The “effective” Powers spacing factor

The material model behind Powers spacing factor is rather unrealistic since it is based on two dubious assumptions:

1. All air-pores are organized in a regular array that does not represent the real distribution in space.
2. All air-pores are assumed to be of equal size. In reality there is a wide range of pore sizes.

Another big defect is the assumption that the entire air-pore system stays air filled during freeze/thaw. In reality, however, a considerable portion of the air-pore system becomes water-filled [4]. Therefore the calculated Powers spacing factor becomes too small. However, Equation (1) can be used for calculation of the *effective spacing factor* of the active part of the air-pore system, provided one knows the fraction of the air-pore system which is inactivated and the specific surface of the remaining air-filled pore system. The effective spacing factor will always be larger than Powers spacing factor which is shown by the following example:

Total air-pore system: Air content 20%. Specific surface 25 mm^{-1} .

$$\text{Powers spacing factor: } \bar{a} = \frac{3}{25} \left[1.4 \left(\frac{1}{0.20} \right)^{1/3} - 1 \right] = \mathbf{0.17 \text{ mm}}$$

The active air-pore system: Remaining air-content 12%. Remaining specific surface 18 mm^{-1}

$$\text{Effective spacing factor: } \bar{a} = \frac{3}{18} \left[1.4 \left(\frac{1}{0.12} \right)^{1/3} - 1 \right] = \mathbf{0.31 \text{ mm}}$$

2. PHILLEO SPACING FACTOR – PROTECTED VOLUME

2.2 Theory

A more advanced structural model of air-entrained cement paste was developed by Philleo [2]. As a first approximation the air-pore system is represented by arbitrarily distributed points in the saturated cement paste. Thus, every air-pore is supposed to lack volume. Philleo uses the following expression for the probability P that any point in the saturated cement paste shall be located within a given maximum distance D from the closest point.

$$P = 1 - \exp\left\{-N \cdot \frac{4 \cdot \pi}{3} \cdot D^3\right\} = 1 - \exp\{-V_{PR}\} = 1 - \exp\{-k \cdot V_p\} \quad (2)$$

N is the number of points (pores) in the cement paste volume considered

V_{PR} is the protected volume, i.e. the total volume of all spheres with diameter D , mm^3

V_p is the cement paste volume, mm^3

k is a coefficient $k \geq 1$. $k = V_{PR}/V_p$

This equation was first derived by Hertz [5]. The parameter $(4\pi/3)D^3$ describes the volume of a material sphere surrounding each point. According to the equation a bigger volume than the cement paste volume itself has to be protected if the probability shall be high that a big fraction of the cement paste shall be protected. The reason is that individual spheres must overlap in order to cover the entire cement paste volume, see Figure 5.

Equation (2) is plotted in Figure 2. The probability that the entire cement paste volume is protected, is only 63% when $V_{pr}=V_p$. A probability of 90% or 98% requires that $V_{pr}=2.3 \cdot V_p$ and $V_{pr}=3.9 \cdot V_p$.

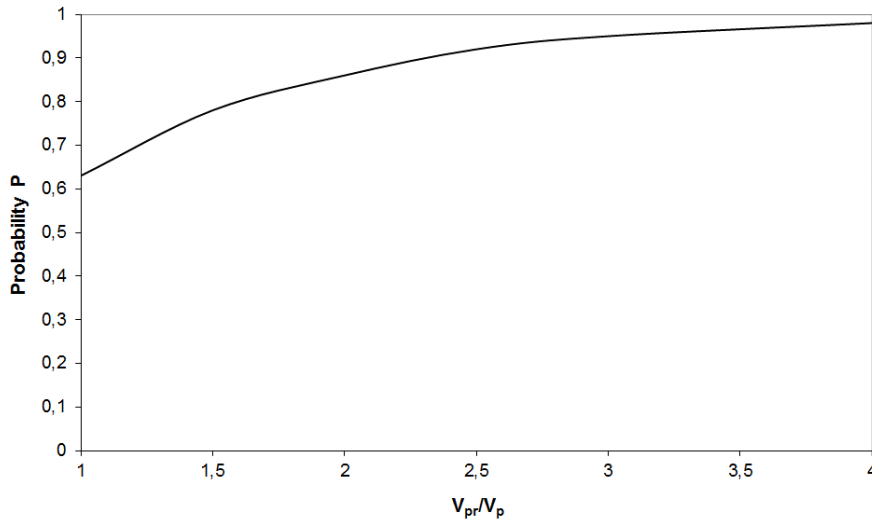


Figure 2 - Plot of equation (2).

Philleo develops Equation (2) further in order to consider the effect of air by letting all points be spheres of finite volumes representing air-bubbles. The result is the following approximate equation that gives the probability P that the entire cement paste is protected:

$$P \approx 1 - \exp\left\{-\left[4.19 \left(S \cdot N^{\frac{1}{3}}\right)^3 + 7.80 \left(S \cdot N^{\frac{1}{3}}\right)^2 \cdot [-\log(1 - A)]^{\frac{1}{3}} + 4.84 \left(S \cdot N^{\frac{1}{3}}\right) \cdot [-\log(1 - A)]^{\frac{2}{3}}\right]\right\} \quad (3)$$

Where A is the air content as volume fraction of the cement paste volume including the air pores. S is the *Philleo spacing factor*, i.e. the maximum distance between any point in the cement paste and the edge of the nearest air-pore, see Figure 3. Frost damage occurs when S is bigger than the critical distance S_{CR} .

Thus, the air volume A together with the parameter $S \cdot N^{1/3}$ determine the volume fraction of protected cement paste. The number of air-pores at a given air content depends on the pore size, the larger the number of pores the smaller the air-pore. Therefore, N is a measure of the specific surface of the air-pore system.

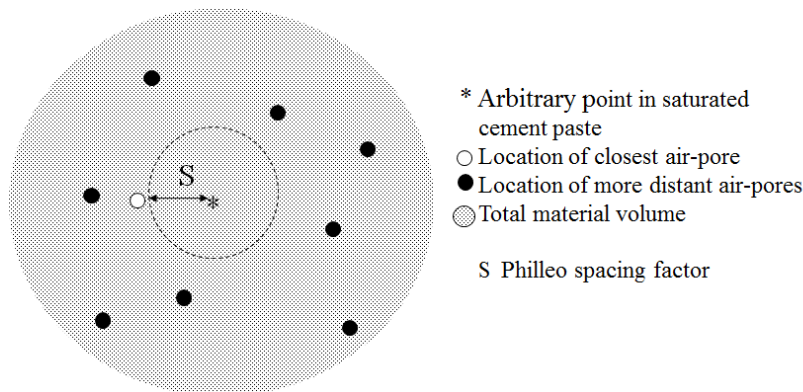


Figure 3 - Illustration of Philleo spacing factor.

Example:

$A=10\%$ i.e. $0.1 \text{ cm}^3/\text{cm}^3$ paste.

Number of air-pores $N=13\,800$ per cm^3

Critical Philleo spacing factor $S_{CR}=0.02 \text{ cm}$ (assumed value)

$S_{CR} \cdot N^{1/3}=0.02(13\,800)^{1/3}=0.478$

Inserting these values in Equation (3) gives:

$P=1-\exp\{-1.39\}=0.75$ Thus, only 75% of the cement paste is protected.

90% of the cement paste would be protected ($P=0.9$) provided the critical Philleo spacing factor was increased to 0.25 mm, or the number of air-pores was increased to 28 000 per cm^3 , or the air content was increased to 17%.

The value of the critical Philleo spacing factor is unknown. It might be possible to calculate its value by Equation (3) using results from experimental determination of the number of air-pores and the air content for a great number of concretes that have turned out to be frost resistant and not resistant.

2.2 Philleo spacing factor-comments

Philleo spacing factor is more practicable than Powers spacing factor since it makes it possible to estimate the probability that a certain volume fraction is protected. However, like Powers spacing factor the Philleo spacing factor as defined by Equation (3) can be criticized for the following reasons:

1. No consideration is taken to the real size distribution of air-pores, only to the number of pores.
2. No consideration is taken to the fact that a portion of the air-pore system is water-filled.

The second obstacle can be overcome by replacing the total air volume A by the air volume A_{eff} , which stays air-filled. The total number of air-pores N is replaced by the number of air-pores N_{eff} that actually are air-filled. Then, one must also consider that the critical Philleo spacing factor becomes higher when air-pores are supposed to be inactivated by water.

2.3 Comparison between Philleo spacing factor and Powers spacing factor

According to Equation (2) 98% of the cement paste is protected when the following condition is satisfied:

$$P = 1 - \exp(-3.9) = 0.98 \quad (4)$$

The parameter $S \cdot N^{1/3}$ is then given by Equation (3), which is:

$$4.19 \left(S \cdot N^{1/3} \right)^3 + 7.80 \left(S \cdot N^{1/3} \right)^2 \cdot [-\log(1 - A)]^{1/3} + 4.84 \left(S \cdot N^{1/3} \right) \cdot [-\log(1 - A)]^{2/3} = 3.9 \quad (5)$$

The number of air-pores N is approximately calculated from the specific surface α of the pores:

$$N = \frac{A}{\frac{4}{3} \cdot \pi \cdot r^3} = \frac{3 \cdot A}{4 \cdot \pi} \cdot \left(\frac{\alpha}{3} \right)^3 \quad (6)$$

r is the air-pore radius. The parameter $S \cdot N^{1/3}$ becomes:

$$S \cdot N^{1/3} = S \cdot \left(\frac{3 \cdot A}{4 \cdot \pi} \right)^{1/3} \cdot \frac{\alpha}{3} \quad (7)$$

The application of this model in comparison with the Powers spacing factor is shown by two examples:

Example 1: The air content A is supposed to be 10%, i.e. $A=0.10$.

Equation (5) is satisfied when the parameter $S \cdot N^{1/3}=0.76$. Thus:

$$S \cdot \left(\frac{3 \cdot 0.1}{4 \cdot \pi} \right)^{1/3} \cdot \frac{\alpha}{3} = 0.76$$

The pore radius is supposed to be 0.1 mm. Then $\alpha=3/0.1=30 \text{ mm}^{-1}$. This gives:

$S=0.264 \text{ mm}$

The Powers spacing factor for the same air content and specific surface is:

$$\bar{a} = \frac{3}{30} \left[1.4 \left(\frac{1}{0.1} \right)^{1/3} - 1 \right] = \mathbf{0.201 \text{ mm}}$$

Example 2: Air content 20%, i.e. $A=0.20$. The same specific surface as in Example 1

Equation (5) is satisfied when the parameter $S \cdot N^{1/3}=0.70$.

$$S \cdot \left(\frac{3 \cdot 0.2}{4 \cdot \pi} \right)^{1/3} \cdot \frac{30}{3} = 0.70 \quad \mathbf{S = 0.193 \text{ mm}}$$

$$\bar{a} = \frac{3}{30} \left[1.4 \left(\frac{1}{0.2} \right)^{1/3} - 1 \right] = \mathbf{0.139 \text{ mm}}$$

According to these examples the Philleo spacing factor for 98% protection is about 30 à 40% higher than the Powers spacing factor according to which 100% of the cement paste is protected, see Figure 1.

The reason for this difference could not be the small difference in protection. A main reason is that according to the Philleo spacing factor the air-pores are supposed to be arbitrarily distributed in space and not arranged in the ordered manner illustrated by Figure 1. Another reason is that in the calculation above all air-pores were assumed to have the same size.

3. THE FLOW DISTANCE

3.1 Theory

A more realistic flow distance is obtained by using the real size distribution of air-pores in the calculation. The total volume of the empty pore system is:

$$A = K \cdot \int_{r_{min}}^{r_{max}} f(r) \cdot \frac{4\pi}{3} r^3 \cdot dr = K \cdot \frac{4\pi}{3} \cdot \mu_3 \quad (8)$$

- A the total air-pore volume in the cement paste volume considered
- $f(r)$ the frequency function (probability density function) of the air-pore distribution
- r air-pore radius, mm. r_{max} and r_{min} are the biggest and smallest air pores
- K is a coefficient transferring the “unit air volume” μ_3 to the total air volume A
- μ_3 the third statistical moment of the frequency function

The i :th statistical moment is defined:

$$\mu_i = \int_{r_{min}}^{r_{max}} r^i \cdot f(r) \cdot dr \quad (9)$$

The value of K depends on the total air-pore volume A :

$$K = \frac{A}{\frac{4\pi}{3} \cdot \mu_3} \quad (10)$$

Each air-pore is supposed to be surrounded by a shell of thickness t . This is supposed to have the same thickness for all pores, see Figure 4 left. The shell thickness is:

$$t = R_i - r_i \quad (11)$$

The shell is allowed to grow from $t = 0$ to $t = t_i$. The value of t_i is gradually increased. At a certain value of t_i the expanding spheres from adjacent pores will touch each other, see Figure 4 right.

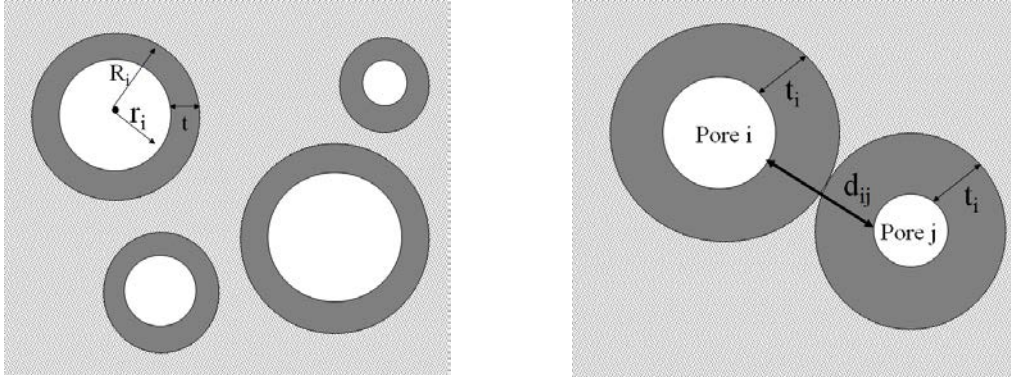


Figure 4 - Left: Four spherical air-pores with different radius r_i surrounded by a spherical shell with the same thickness t for all pores. Right: Two adjacent growing shells touch. The sum shell thickness is $d_{ij}=2t_i$.

The more the shells expand, the bigger is the fraction of cement paste that is occupied by spheres. At a certain expansion the total sphere volume corresponds to the entire cement paste volume V_p . But, when this happens there still is a portion of the cement paste that is not occupied by spheres. This is illustrated by Figure 5.

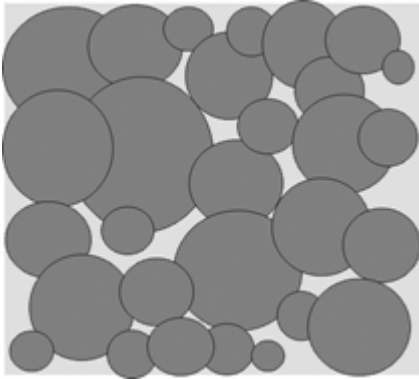


Figure 5 - Expanded spheres having the same total volume as the cement paste volume. There is paste areas that are not occupied by spheres.

The total volume of all expanded spheres is:

$$V = K \cdot \int_{r_{min}}^{r_{max}} f(r) \cdot \frac{4\pi}{3} \cdot R^3 \cdot dr \quad (12)$$

Inserting Equation (8):

$$V = K \cdot \int_{r_{min}}^{r_{max}} f(r) \cdot \frac{4\pi}{3} \cdot (t + r)^3 \cdot dr \quad (13)$$

Developing the equation:

$$V = K \cdot \int_{r_{min}}^{r_{max}} f(r) \cdot \frac{4\pi}{3} \cdot (t^3 + 3t^2r + 3tr^2 + r^3) \cdot dr \quad (14)$$

i.e.

$$V = K \cdot \frac{4\pi}{3} \left[\int_{r_{min}}^{r_{max}} t^3 \cdot f(r) dr + \int_{r_{min}}^{r_{max}} 3t^2 r \cdot f(r) dr + \int_{r_{min}}^{r_{max}} 3t r^2 \cdot f(r) dr + \int_{r_{min}}^{r_{max}} r^3 \cdot f(r) dr \right] \quad (15)$$

Expressed as statistical moments:

$$V = K \cdot \frac{4\pi}{3} (t^3 \mu_0 + 3t^2 \mu_1 + 3t \mu_2 + \mu_3) \quad (16)$$

μ_0 is the area below the frequency curve and is by definition equal to 1. μ_1 is the mean pore radius. μ_2 is a measure of the total surface area of all air-pores. μ_3 is a measure of the total volume of all air pores. Inserting Equation (8) in Equation (16) gives:

$$V = \frac{A}{\mu_3} (t^3 \mu_0 + 3t^2 \mu_1 + 3t \mu_2 + \mu_3) \quad (17)$$

$$V = A \left\{ t^3 \frac{\mu_0}{\mu_3} + 3t^2 \frac{\mu_1}{\mu_3} + 3t \frac{\mu_2}{\mu_3} + 1 \right\} \quad (18)$$

The specific surface of the empty air-pore system is:

$$\alpha = \frac{\int_{r_{min}}^{r_{max}} 4\pi r^2 \cdot f(r) dr}{\int_{r_{min}}^{r_{max}} \frac{4\pi}{3} r^3 \cdot f(r) dr} = 3 \frac{\mu_2}{\mu_3} \quad (19)$$

$$\mu_3 = 3 \frac{\mu_2}{\alpha} \quad (20)$$

Inserting this expression in Equation (18):

$$\frac{V}{A} = \left\{ \frac{t^3}{3} \alpha \frac{\mu_0}{\mu_2} + t^2 \cdot \alpha \frac{\mu_1}{\mu_2} + t \cdot \alpha + 1 \right\} \quad (21)$$

Equations (18) and (21) satisfy the condition $V = A$ when $t = 0$, i.e. when no expansion of air-pores has yet started.

The maximum flow distance, i.e. the maximum distance water has to be transported in order to reach the nearest air-filled pore, corresponds to the value t which is given by Equation (21). The value will depend on the cement paste volume V covered by the expanded spheres. A lowest value is obtained when the total volume V corresponds to the total cement paste volume V_p , i.e.

$$V = V_p \quad (22)$$

But, then there are areas that are not covered by expanded spheres, see Figure 5. A more relevant value may be:

$$V = k \cdot V_p \quad (23)$$

Where k is a coefficient >1 .

3.2 Example - triangular air-pore distribution

A triangular frequency function is shown in Figure 6. All pores with radii < 0.02 mm are neglected since they can hardly function as recipients for water during freezing.

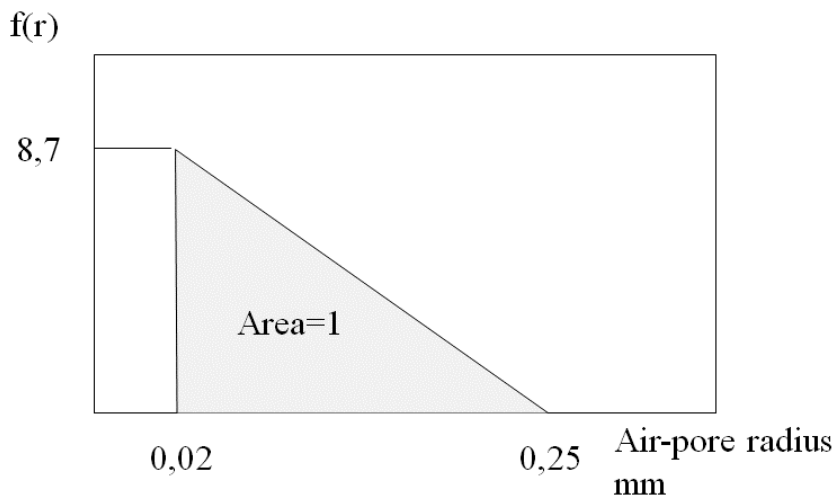


Figure 6 - Triangular frequency function of air-pores. $f(r) = 9.5 - 38 \cdot r$

The statistical moments are:

$$\begin{aligned} \mu_0 &= \int_{0.02}^{0.25} (9.5 - 38r) r^0 \cdot dr = 1 & \mu_1 &= \int_{0.02}^{0.25} (9.5 - 38r) r \cdot dr = 0,097 \\ \mu_2 &= \int_{0.02}^{0.25} (9.5 - 38r) r^2 \cdot dr = 0.0123 & \mu_3 &= \int_{0.02}^{0.25} (9.5 - 38r) r^3 \cdot dr = 0.00186 \end{aligned}$$

The specific surface is:

$$\alpha = 3 \frac{\mu_2}{\mu_3} = 3 \frac{0.0123}{0.00186} = 20 \text{ mm}^{-1}$$

The air content is supposed to be 10%, i.e. $V/A=10$.

Equation (22) is supposed to be valid, i.e. the expanded volume V is equal to the entire cement paste volume V_p . Then Equation (21) is:

$$10 = \frac{t^3}{3} 20 \frac{1}{0.0123} + t^2 20 \frac{0.097}{0.0123} + 20 \cdot t + 1 = 542t^3 + 158t^2 + 20t + 1$$

This gives the following maximum flow distance:

$$t=0.155 \text{ mm}$$

Equation (23) with $k=1.5$ is supposed to be valid. Then Equation (21) is:

$$1.5 \cdot 10 = 542t^3 + 158t^2 + 20t + 1$$

$$t=0.195 \text{ mm}$$

Powers spacing factor for the triangular air-pore system above is:

$$\bar{a} = \frac{3}{20} \left[1.4 \left(\frac{1}{0.1} \right)^{1/3} - 1 \right] = \mathbf{0.302 \text{ mm}}$$

The maximum flow distance, which considers the real size distribution of air-pores, calculated above is considerably lower than the Powers spacing factor. However the maximum flow distance equals the Powers spacing factor when k in Equation (23) is $k=3.7$.

3.3 Effect of water absorption in the air-pore system

In normal situations in the field or in a freeze/thaw test a fraction of the air-pore system is inactivated by water absorption. This means that also the maximum flow distance will be changed. This is exemplified by analyzing the effect of water absorption in a pore system of the type shown in Figure 7. The total air content with no water in the pores is 10%.

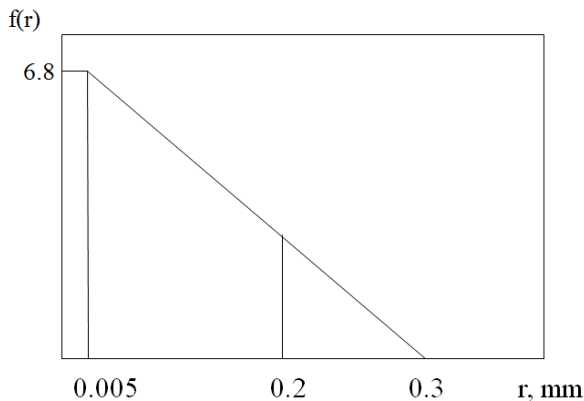


Figure 7 - Triangular frequency function of air-pores. $f(r)=6.9-23 \cdot r$

Two different possibilities are investigated:

- 1: No air-pores are water-filled.
- 2: All pores smaller than 0.2 mm are water-filled.

Possibility 1: No water absorption in the air-pore system

The calculation below is valid for the total air-pore system.

$$\mu_0 = \int_{0.005}^{0.3} (6.9 - 23r) dr = 1 \quad \mu_1 = \int_{0.005}^{0.3} (6.9 - 23r)r \cdot dr = 0,104$$

$$\mu_2 = \int_{0.005}^{0.3} (6.9 - 23r)r^2 \cdot dr = 0.0155 \quad \mu_3 = \int_{0.005}^{0.3} (6.9 - 23r)r^3 \cdot dr = 0.0028$$

The specific surface is:

$$\alpha = 3 \cdot \frac{0.0155}{0.0028} = 16.6 \text{ mm}^{-1}$$

The total air content is supposed to be 10% of the cement paste volume. Equations (21) and (22) give:

$$\frac{V}{A} = 10 = \frac{t^3}{3} 16.6 \frac{1}{0.0155} + t^2 16.6 \frac{0.104}{0.0155} + 16.6 \cdot t + 1$$

$t=0.19 \text{ mm}$

Possibility 2: All pores with radius <0.2 mm are water-filled

$$\mu_0 = \int_{0.2}^{0.3} (6.9 - 23r) dr = 0.115 \quad \mu_1 = \int_{0.2}^{0.3} (6.9 - 23r)r \cdot dr = 0.027$$

$$\mu_2 = \int_{0.2}^{0.3} (6.9 - 23r)r^2 \cdot dr = 0.0063 \quad \mu_3 = \int_{0.2}^{0.3} (6.9 - 23r)r^3 \cdot dr = 0.0015$$

$$\alpha = 3 \frac{0.0063}{0.0015} = 12.6 \text{ mm}^{-1}$$

The effective air content $A_{effective}$ is proportional to the statistical moments μ_3 before and after absorption:

$$A_{effective} = 10 \cdot \frac{0.0015}{0.0028} = 5,3\%$$

Equations (21) and (22) give:

$$\frac{V}{A_{effective}} = \frac{1}{0.053} = 19 = \frac{t^3}{3} 12.6 \frac{0.115}{0.0063} + t^2 12.6 \frac{0.027}{0.0063} + 12.6 \cdot t + 1$$

$t=0.40 \text{ mm}$

The maximum flow distance has been increased from 0.19 mm to 0.40 mm when a volume of about 50% of the air-pore system has been inactivated by water absorption.

4. EXPERIMENTAL DETERMINATION OF THE CRITICAL FLOW DISTANCE

Frost damage occurs when the actual flow distance t exceeds a critical value t_{CR} which is individual for each cement paste composition but independent of the air-pore structure, viz. t_{CR} is primarily determined by properties of the cement paste matrix such as water-cement ratio, tensile strength and permeability. The critical flow distance can be calculated from an experimental determination of the critical degree of saturation and a determination of the air-pore size distribution [4] The method and an example is given below.

4.1 Determination of the critical air pore absorption

An experimental method for determination of the critical degree of saturation is presented in [6]. An example for an air-entrained concrete with w/c-ratio 0.57 is shown in Figure 8 [7]. S_{CR} was found to be 0.80 for the actual concrete.

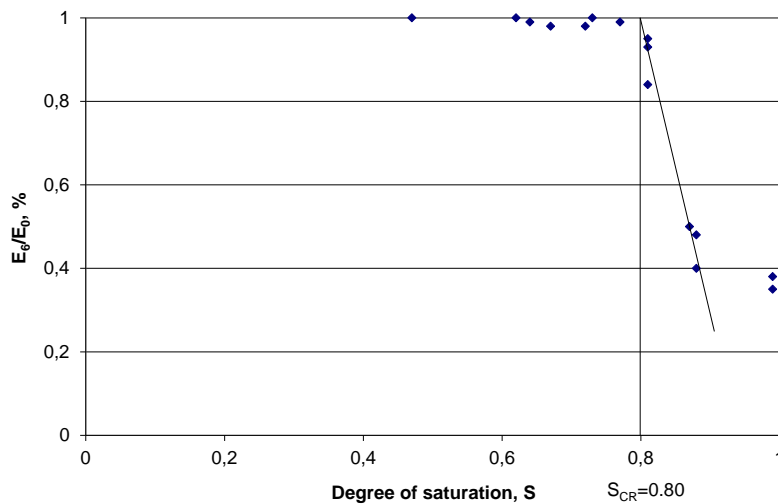


Figure 8 - Determination of the critical degree of saturation S_{CR} for an air-entrained concrete. E_0 and E_6 are the dynamic E-modulus before freeze/thaw and after 6 cycles.

A block diagram for the concrete is shown in Figure 9.

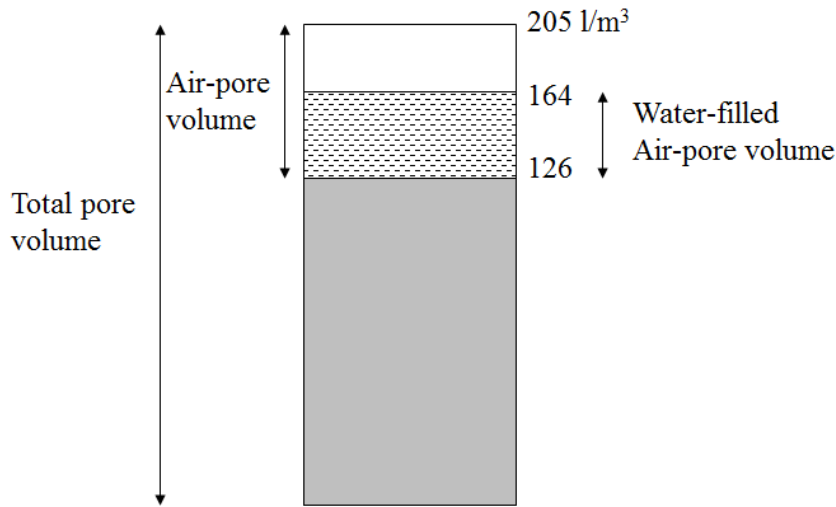


Figure 9 - Block diagram for the concrete in Figure 8.

Total pore volume: 205 litres/m³. Critical water content: $0.8 \cdot 205 = 164$ litres/m³. Air-pore volume: 79 litres/m³. Pore volume except air-pores: $205 - 79 = 126$ litres/m³. Amount of water in air-pores: $164 - 126 = 38$ litres/m³. Volume fraction of water-filled air-pore volume: $38/79 = 0.48$.

4.2 Determination of the air-pore distribution

The air-pore size distribution of the concrete has been determined by the linear traverse method. A large number of air-pore chords are crossed and their length registered. The chord distribution for the concrete in Figure 8 is shown in Figure 10.

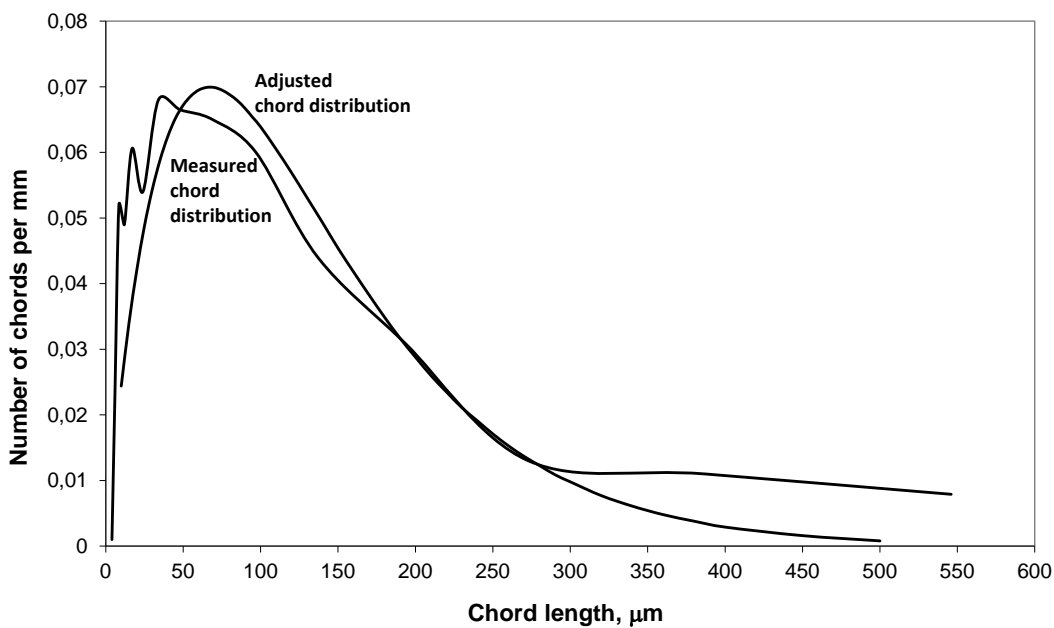


Figure 10 - Chord size distribution for the concrete in Figure 8.

In the actual example, the chord distribution is adjusted to a suitable continuous frequency function. The following function gives fairly good agreement with the measured distribution within the important range 50-300 μm . This type of function was suggested by Larson et al. [8].

$$\phi(L) = \frac{a \cdot L}{b^L} \quad (24)$$

L is the chord length (μm)

a and b are coefficients. $a=2.8 \cdot 10^{-3}$, $b=1.0146$

The chord distribution is transformed into a pore-radius distribution using the following equation [9]:

$$\phi(r) = -\frac{a}{2\pi} \cdot \frac{d}{dL} \left[\frac{1}{\frac{\phi(L)}{L}} \right] \quad (25)$$

Exchanging L for the radius r and inserting Equation (24) gives:

$$\phi(r) = -\frac{a}{2\pi} \cdot \frac{d}{dr} \left[\frac{1}{b^r} \right] = \frac{a}{2\pi} \cdot \frac{\ln b}{b^r} \quad (26)$$

The frequency function (density function) $f(r)$ is given by the condition that the area under the curve shall be 1, thus $\mu_0=1$.

$$\mu_0 = \frac{a \cdot \ln b}{2\pi} \cdot \int_0^{r_{max}} \frac{1}{b^r} \cdot dr = 1 \quad (27)$$

r_{max} is the radius of the largest air-pore. The lower integration limit is put to zero since pores smaller than about 10 μm give negligible contribution to the air-pore volume.

Integration gives:

$$\frac{a \cdot \ln b}{2\pi} \cdot \left[-\frac{b^{-r}}{\ln b} \right]_0^{r_{max}} = 1 \quad (28)$$

Inserting the integration limits finally gives the coefficient a :

$$a = \frac{2\pi \cdot b^{r_{max}}}{b^{r_{max}} - 1} \quad (29)$$

Inserting this value in Equation (25) gives the relative frequency function:

$$f(r) = \frac{b^{r_{max}}}{b^{r_{max}} - 1} \cdot \frac{\ln b}{b^r} \quad (30)$$

r_{max} is put to 1000 μm , see Figure 11. Thus $b^{1000}/(b^{1000}-1) \approx 1$.

Inserting this and the coefficient $b=1.0146$ in Equation (30) gives:

$$f(r) = \frac{\ln 1.0146}{1.0146^r} \quad (31)$$

4.3 Calculation of the biggest water-filled air pore

The relevant statistical moments of the actual distribution between the limits 0 to ∞ are calculated by Equations (32) and (33) below with the lower integration limit r_{min} changed to 0. The result is:

$$\begin{aligned} \mu_0 &= 1 & \mu_1 &= \frac{1}{\ln 1.0146} = 69 \\ \mu_2 &= \frac{2}{(\ln 1.0146)^2} = 9.52 \cdot 10^3 & \mu_3 &= \frac{6}{(\ln 1.0146)^3} = 1.97 \cdot 10^6 \end{aligned}$$

The specific surface of the total air-pore system is:

$$\alpha = 3 \frac{\mu_2}{\mu_3} = \ln 1.0146 = 0.0145 \mu m^{-1} = 14.5 mm^{-1} \text{ (Mean radius: } 3/\alpha = 0.21 \text{ mm).}$$

Note: The specific surface is equal to $\ln b$ where b is defined by Equation (24).

Total pore volume is 79 litres/ m^3 , i.e. $79 \cdot 10^{15} \mu m^3/m^3$. But, total pore volume is also calculated by, see Equation (8):

$$K' \cdot \mu_3 = K' \cdot 1.97 \cdot 10^6 = 79 \cdot 10^{15} \quad \text{thus} \quad K' = 4.0 \cdot 10^{10}$$

Experimentally determined critical water-filled air-pore volume is 38 litres/ m^3 , i.e. $38 \cdot 10^{15} \mu m^3/m^3$.

It is assumed that a smaller air-pore is water-filled before a larger pore is filled. The radius of the largest water-filled pore can then be calculated by:

$$4.0 \cdot 10^{10} \cdot \mu_3 = 38 \cdot 10^{15} \quad \mu_3 \text{ is the volume of the water-filled air-pore system.}$$

or

$$4.0 \cdot 10^{10} \cdot \ln 1.0146 \int_0^{r_{max}} r^3 \cdot 1.0146^{-r} dr = 38 \cdot 10^{15}$$

Integration gives (integration is more easily performed by substituting $-r$ for x):

$$4.0 \cdot 10^{10} \left[1.0146^{-r} \left((-r)^3 - \frac{3(-r)^2}{\ln 1.0146} + \frac{6(-r)}{(\ln 1.0146)^2} - \frac{6}{(\ln 1.0146)^3} \right) \right]_0^{r_{max}} = 38 \cdot 10^{15}$$

i.e.

$$4.0 \cdot 10^{10} \left\{ 1.0146^{-r_{max}} \left(-r_{max}^3 - \frac{3r_{max}^2}{\ln 1.0146} - \frac{6r_{max}}{(\ln 1.0146)^2} - \frac{6}{(\ln 1.0146)^3} \right) + \frac{6}{(\ln 1.0146)^3} \right\} = 38 \cdot 10^{15}$$

The relation between the largest water-filled pore r_{max} and the water content in air-pores is shown in Figure 11. The measured critical water absorption 38 litres/m³ corresponds to the pore radius 250 μm .

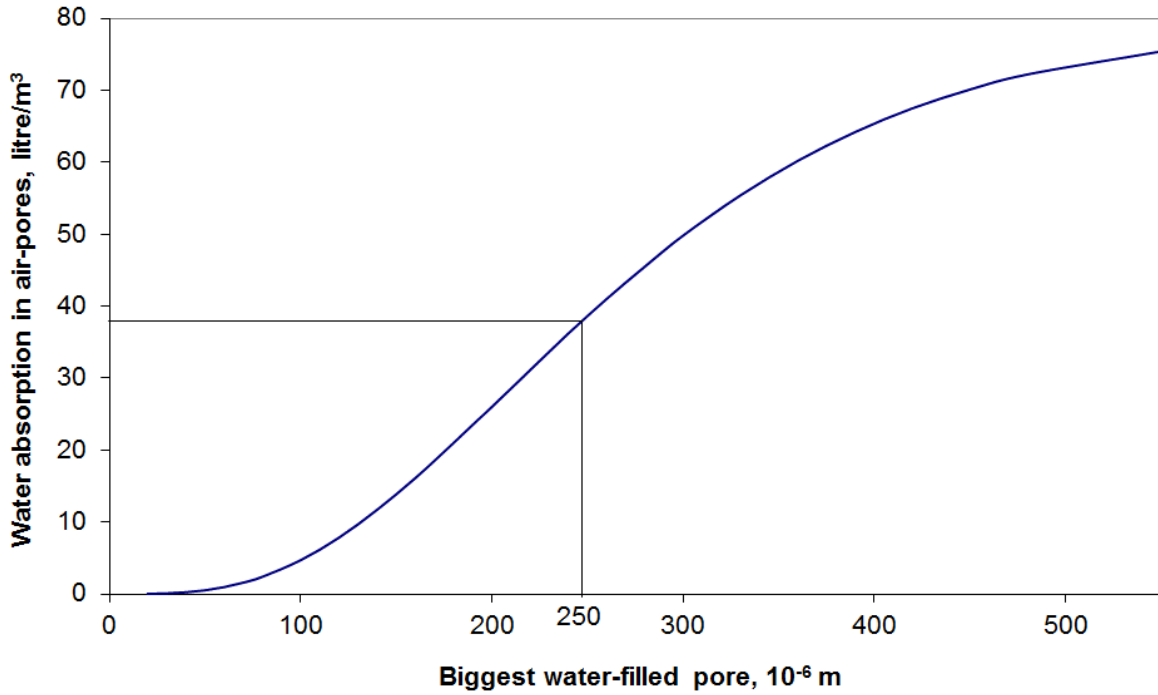


Figure 11 - Relation between biggest water-filled air-pore and absorbed amount of water.

4.4 Determination of the critical flow distance

The experimentally determined value of S_{CR} together with the experimentally determined air-pore distribution can be used for calculating the critical flow distance. Equations (32) and (33) are used for calculating the statistical moments of the air-filled part of the pore system. The lower integration limit is 250 μm .

$$\mu_0 = 1.0146^{-250} \quad (32)$$

$$\mu_{i>0} = 1.0146^{-250} \left(250^i + \frac{i \cdot 250^{i-1}}{\ln 1.0146} + \frac{i \cdot (i-1) 250^{i-2}}{(\ln 1.0146)^2} + \frac{i!}{(\ln 1.0146)^i} \right) \quad (33)$$

The statistical moments become:

$$\mu_0 = 0.027 \quad \mu_1 = 10.4 \quad \mu_2 = 3096 \quad \mu_3 = 10^6$$

The specific surface of the residual air-filled pore system is:

$$\alpha = 3 \frac{3096}{10^6} = 0.0093 \mu\text{m}^{-1} = 9.3 \text{ mm}^{-1}$$

Thus, the surface is reduced by about 35% due to water absorption.

The critical flow distance is obtained from Equation (18):

$$\frac{V_p}{A_{c,effective}} = t_{CR}^3 \frac{0.027}{10^6} + 3t_{CR}^2 \frac{10.4}{10^6} + 3t_{CR} \frac{3096}{10^6} + 1$$

The cement paste volume V_p for the actual concrete is 34%.

The effective air-pore volume in the actual concrete $A_{c,effective}$ is: 7.9%-3.8%=4.1%.

Equation (22) with $k=1.0$ is supposed to be valid, i.e. the volume of expanded spheres equals the total cement paste volume. It gives $V_p/A_{c,effective}=34/4.1=8.3$. The critical flow distance becomes:

$$t_{CR} = 330 \mu\text{m} = 0.33 \text{ mm}$$

The critical Powers spacing factor defined by Equation (1) is:

$$\bar{a}_{CR} = \frac{3}{14.5} \left[1.4 \left(\frac{34}{7.9} \right)^{1/3} - 1 \right] = 0.26 \text{ mm}$$

The critical *effective* Powers spacing factor considering only the air-filled part of the air-pore system is:

$$\bar{a}_{CR,eff} = \frac{3}{8.5} \left[1.4 \left(\frac{34}{4.1} \right)^{1/3} - 1 \right] = 0.65 \text{ mm}$$

5. APPLICATION OF THE CRITICAL FLOW DISTANCE

There are two applications of the critical flow distance:

1. Estimation of the required air content for a given service life.
2. Analysis of the mechanism behind frost damage.

Only the first application is treated in the present article.

Theoretically the required air content for a given service life can be calculated from the critical flow distance. Information needed is:

1. The air-pore distribution
2. The rate by which the air-pore system becomes water-filled in the actual environment.

The principles are shown by an example. Consider a concrete with the same mix composition and the same general type of air-pore distribution as in the example above, Equation (24). The cement paste content is 32%. The specific surface of the air-pore system is assumed to be 30 mm^{-1} ($0.030 \mu\text{m}^{-1}$). Then, the coefficient b in Equation (24) is:

$$\ln b = 0.030 \quad b = 1.0305$$

The total air-pore volume A_c in concrete is:

$$A_c = K' \cdot \mu_3 = K' \cdot \ln 1.0305 \cdot \int_0^{\infty} r^3 \cdot 1.0305^{-r} dr = \frac{6 \cdot K'}{(\ln 1.0305)^3} = K' \cdot 2.2 \cdot 10^5$$

The outer environment is such that one can assume that all pores smaller than 150 μm are water-filled after the desired service life 50 years. The air-filled air pore volume is calculated by Equation (33) with the lower integration level is changed to 150 μm and the coefficient 1.0146 changed to 1.0305:

$$A_a = K' \cdot \mu_3 = K' \cdot \ln 1.0305 \cdot \int_{150}^{\infty} r^3 \cdot 1.0305^{-r} \cdot dr = K' \cdot 7.55 \cdot 10^4$$

The air-filled part of the air-pore system is $7.55 \cdot 10^4 / 2.2 \cdot 10^5 = 0.34$ (34%).

The statistical moments of the effective, air-filled part of the pore system are calculated by Equations (32) and (33) using the coefficient 1.0305 and the lower integration level 150 μm :

$$\mu_0 = 0.011 \quad \mu_1 = 2.39 \quad \mu_2 = 407 \quad \mu_3 = 7.55 \cdot 10^4$$

The required volume of air-filled pores is obtained by Equation (18) using the value of the critical flow distance. This is supposed to be the same as calculated above in paragraph 4.4 since the concrete composition is supposed to be the same, i.e. $t_{CR} = 0.33 \text{ mm} = 330 \mu\text{m}$. Then Equation (18) is:

$$\frac{V_p}{A_{c, \text{effective}}} = 330^3 \cdot \frac{0.011}{7.55 \cdot 10^4} + 3 \cdot 330^2 \cdot \frac{2.39}{7.55 \cdot 10^4} + 3 \cdot 330 \cdot \frac{407}{7.55 \cdot 10^4} + 1 = 21.9$$

$A_{c, \text{effective}} = 32 / 21.9 = 1.5\%$. The required total air content is: $A_c = 1.5 / 0.34 = 4.4\%$

A theoretical analysis of the rate of water absorption in air-pores during capillary water uptake is performed in [4]. The time needed is proportional to the volume of the pore and is dependent on the diffusion coefficient of dissolved air in the water saturated pore system.

When freezing takes place in the presence of salt the water absorption is probably accelerated meaning that larger air-pores are water-filled at each water absorption time. Besides, the critical flow distance is probably changed. The net effect, however, is reduced service life if the air content is not increased.

6. CONCLUDING REMARKS

The required air content in frost resistant concrete can be determined by a freeze/thaw test that is representative for the actual use of the concrete. A more rapid method is to calculate the required air-content theoretically by using the Powers spacing factor, Equation (1), or as an alternative, by using the more advanced Philleo spacing factor, Equation (3). Both methods are based on the assumption that there exists a maximum allowable, or critical, distance between a place where water freezes and the nearest air-pore that can relieve the pressure caused by freezing. In both cases information is needed on the mean size of the air-pores, or the number of air pores in a unit volume of the cement paste. There are two drawbacks with both methods besides the fact that information on the true value of the critical spacing for different types of concrete is lacking:

1. No consideration is taken to the fact that a certain portion of the air-pore system is water-filled when freezing takes place. This fraction depends on the actual moisture conditions to which the concrete is exposed.
2. No consideration is taken to the real size distribution of air-pores.

Principally, the first drawback can be coped with by considering only the air-filled, *effective*, part of the pore system when calculating the spacing factor. The second draw-back cannot be handled by these two spacing factor concepts.

By using the concept flow distance described in this article consideration is taken to the real pore size distribution. Therefore, theoretically it might be possible to find the critical flow distance considering also the water absorption in air-pores. The critical flow distance is determined experimentally by measuring the critical air-pore absorption using a freeze/thaw test together with a determination of the air-pore distribution. The method is described and exemplified. The critical flow distance for the tested concrete is found to be about 0.33 mm.

The critical flow distance can be used for determination of the required air content for a given moisture environment and service life. The method is described and exemplified. The time-moisture field in the air-pore system of concrete is required for the calculation. A method for estimating this is described in [4].

REFERENCES

1. Powers T.C. The air requirement of frost-resistant concrete. *Highway Research Board*, Proceedings No 29, pp 184-202. 1949.
2. Philleo R.E. A method for analyzing void distribution in air-entrained concrete. Tentative manuscript. *Portland Cement Association*, Chicago. 1955.
3. Powers T.C. & Helmuth R.A. Theory of volume changes in hardened portland cement paste during freezing. *Highway Research Board*, Proceedings No 32, pp 285-316. 1953
4. Fagerlund G. A service life model for internal frost damage in concrete. *Div. of Building Materials, Lund Institute of Technology*. Report TVBM-3119. Lund 2004.
5. Hertz P. Über den gegenseitigen durchschnittlichen Abstand von Punkten die mit bekannter mittlerer Dichte im Raume angeordnet sein. *Math Ann.* pp 387-398. 1909.
6. Fagerlund G. The critical degree of saturation method of assessing the freeze/thaw resistance of concrete. *Materials and Structures*, 1977(10):58. pp 217-229.
7. Fagerlund G. The international cooperative test of the critical degree of saturation method of assessing the freeze/thaw resistance of concrete. *Ibid.* pp 231-253.
8. Larson T.D., Cady P.D. & Malloy J.J. The protected paste volume concept using new air-void measurement and distribution techniques. *Journal of Materials*, Vol 2 No 1, pp202-224. 1967.
9. Reid W. P. Distribution of sizes of spheres in a solid from a study of slices of the solid. *Cambridge, Mass. J. of Mathematics and Physics*, Vol 34, pp 95-102. 19. 1955.

Thermal Crack Risk of Concrete Structures – Evaluation of Theoretical Models for Tunnels and Bridges



Jonny Nilimaa
M.Sc., Ph.D., Ass. Sr. Lecturer
Luleå University of Technology
SE-971 87 Luleå
E-mail: jonny.nilimaa@ltu.se



Anders Hösthagen
M.Sc., Ph.D. student
Luleå University of Technology
SE-972 87 Luleå
E-mail: anders.hosthagen@ltu.se



Mats Emborg
M.Sc., Ph.D., Professor
Luleå University of Technology
SE-972 87 Luleå
E-mail: mats.emborg@ltu.se

ABSTRACT

An approach for thermal crack risk estimations was introduced in the Swedish design guidelines BRO 94. The cracking occurs during the early hardening process because of the exothermic reactions between water and cement and often result in high repair costs and delayed construction. This paper studies and validates the inherent safety levels for one typical case of concrete structure. Three slab-frame structures were analysed and the original crack risk estimations were compared to the actual cracking and post-calculations were carried out, using actual parameters. This paper shows that walls with computed strain ratios over 70% were affected by thermal cracks.

Key words: Thermal cracking, Structural Design, Sustainability, Concrete Tunnels.

1. INTRODUCTION

Thermal cracking may occur during the early hardening process of concrete [1]. The exothermic reactions of the hydration process leads to increasing core temperatures in the structure and thereby inducing thermal expansion of the concrete. However, prohibited deformation due to different types of restraints leads to compressive strains in parts of the structure. As the hydration rate reduces, the core starts cooling, inducing shrinkage and tensile strains within the restrained structure. The tensile strains may also be associated to uneven expansion and contraction of the concrete due to differential temperatures in the inner core and the outer layers.

In some cases the tensile strains exceed the ultimate strain of the concrete and thermal and shrinkage cracks appear. Thermal cracks are usually identified as through cracks, emerged in the cooling phase, and supported by restraints. These types of cracks are generally associated with massive concrete infrastructure such as dams, foundations and tunnels, where the core temperature may become high and vary considerably internally. More slender structures may also be subjected to thermal cracks if e.g. high temperature differences arise between a newly cast wall and a previously cast slab. Thermal cracks may also emerge during the heating phase if the internal temperatures vary considerably and the cracks can be located both in the slab and the wall. Another type of cracks that usually emerge during the heating phase is surface cracks. These cracks are restricted to the concrete surface and thereby remain thin, with widths below 0.1 mm [2]. Surface cracks may also emerge due to rapid surface cooling associated with form removal or rapid shifts in the weather.

Factors influencing the heat of hydration and thereby the thermal crack risk of concrete, may, according to [2] be divided into internal and external factors as stated in Table 1. The internal factors are governed by the concrete recipe and may be decided by adiabatic or semi-adiabatic tests. The external factors are mainly governed by the casting procedure and other environmental factors and may not be adjusted by changing the concrete properties.

Traditional crack preventing actions generally aims at reducing the tensile strains within the structure, typically by reducing the temperature differences within a massive concrete structure or between old and new concrete members. Existing slabs can for example be pre-heated before a new wall is cast to account for the thermal effects of the concrete hydration. Cooling pipes can also be installed in the new wall to avoid high temperatures and strains.

Table 1 – Factors influencing the heat of hydration [2].

Internal factors	External factors
Concrete recipe	Casting procedure and environment
Cement content and -type	Concrete temperature at casting, T_c
Aggregate content and -type	Air temperature, T_{air}
Aggregate size, d_{max}	Temperature of supporting structures, T_{slab}
Water-cement ratio	Heating/cooling
Additives	Formwork, insulation and hardening process
	Wind velocity, solar radiation, etc.

Effects of restraint have been studied in e.g. [3-5]. The degree of restraint may vary between 0 and 100%, where the case of full restraint comprises casting on a completely rigid support, for example crack free bedrock or massive slabs, with full bond to adjoining structures, and no restraint represents casting on a bond-free surface. The main factors influencing the restraint of a concrete wall is the geometry of the wall, the adhesion between new and old members, the geometry and stiffness of the base slab, and the flexibility and stiffness of the ground.

This paper considers two types of casting procedures: (1) casting of a free wall on top of a slab and (2) casting of a wall on top of a slab with one edge adjoining an existing wall while the other edge remains free. Figure 1 illustrates the restraint distribution for these two cases.

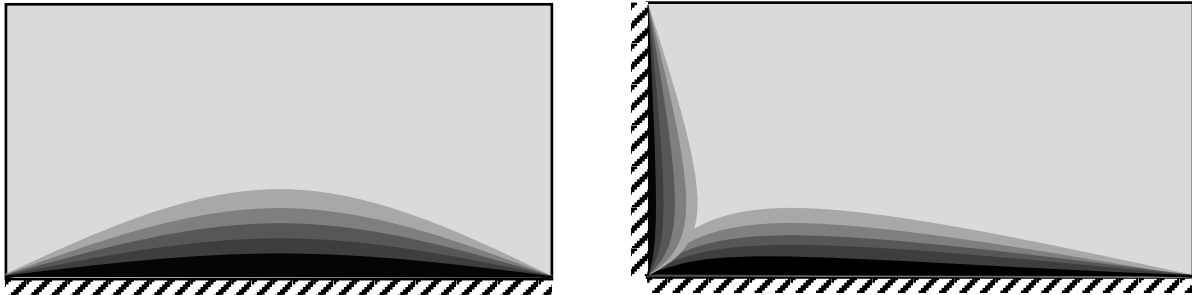


Figure 1 – Restraint distribution for the two types of castings studied in this paper.

The risk of thermal cracking, η , may be calculated as the structural stress ratio, or alternatively the strain ratio:

$$\eta = \left(\frac{\sigma_t(t)}{f_{ct}(t)} \right)^{max} \approx \left(\frac{\varepsilon_t(t)}{\varepsilon_{ct}(t)} \right)^{max} \quad (1)$$

where

- $\sigma_t(t)$ is the tensile stress at the time t
- $f_{ct}(t)$ is the tensile strength at the time t
- $\varepsilon_t(t)$ is the tensile strain at the time t
- $\varepsilon_{ct}(t)$ is the ultimate tensile strain at the time t

The safety level for cracking, Γ , is defined as the inverse of η :

$$\Gamma = \frac{1}{\eta} \quad (2)$$

If the crack risk η is too high according to AMA Anläggning [6], measures are needed to mitigate the risk of cracking. Typical methods for such thermal crack prevention aim at reducing the temperature differences within a concrete casting, between different castings or between a concrete member and its surroundings. This can be accomplished by installing heating cables in the slab or cooling pipes in the wall. The degree of restraint may also be regulated by, for example, expansion joints or optimizing the casting order to avoid adjoining walls for critical members, and the concrete properties may be customized to alter the heat of hydration and reduce the risk of thermal cracking.

The prevailing concept for crack risk estimations was introduced in the Swedish construction standards BRO 94 [7], and can today be found in AMA Anläggning [6]. The concept aims at reducing the risk of thermal cracking of concrete structures by introducing different safety levels for different exposure classes (previously denoted environmental classes). Originally there were three major safety levels and today the design approach has expanded into five levels, as shown in Table 2. Unknown material parameters require higher safety levels, while tested parameters result in lower requirements for the safety level. The untested concrete has been divided into two levels depending on the cement content, where a higher heat of hydration and thereby higher safety factor is expected for the higher cement content, C .

The safety factor for thermal cracking of concrete infrastructure is given in the Swedish guidelines AMA Anläggning [6] and depends mainly on the structures exposure class, the cement content or whether the material parameters have been fully investigated. A summary of relevant safety factors is presented in Table 2.

Table 2 – Safety factors (and corresponding strain ratios) for thermal cracking of concrete structures given in AMA Anläggning [6].

Exposure class	Tested material parameters	Untested material parameters	
		$360 \leq C \leq 430 \text{ kg/m}^3$	$430 < C \leq 460 \text{ kg/m}^3$
XC2	1.05 (0.95)	1.18 (0.85)	1.33 (0.75)
XC4	1.11 (0.90)	1.25 (0.80)	1.42 (0.70)
XD1, XS2	1.18 (0.85)	1.33 (0.75)	1.54 (0.65)
XD3, XS3	1.25 (0.80)	1.42 (0.70)	1.67 (0.60)
Structures exposed to one sided water pressure			
All	1.42 (0.70)	1.67 (0.60)	2.0 (0.50)

The risk of thermal cracking should, according to AMA Anläggning, be reduced by applying one of the following three methods for crack prevention:

Method 1: Temperature requirements may be applied for the concrete and the surrounding air. Certain requirements for the geometry, cement content and structural restraints should also be fulfilled.

Method 2: Some typical design cases were studied in [2] and the most representative case, with associated design parameters and crack preventing actions, may be applied.

Method 3: Using sophisticated computer software to calculate the risk of thermal cracking and customize the crack preventing actions. The applied software should be thoroughly validated and the material parameters should be known.

The objective of this paper is to study the Swedish procedures for crack risk estimation and validate the accuracy of current safety levels for some concrete structures. The study is limited to Method 3 and the use of one commercial and widely applied 2D FE software ConTeSt Pro 5.0 [8]. The study is applied on frame structures where the crack prevention consists of pre-heating the slab before casting the walls.

2. METHOD

The method for this project can roughly be divided into six steps:

1. Identifying relevant structures with adequate documentation.
2. Studying construction documentation.
3. Checking original thermal crack risk estimations and suggested crack preventing measures based on expected parameters.
4. Carrying out post-project thermal crack risk estimations based on actual parameters.
5. Field inventory of emerging thermal cracks.
6. Analysis of the procedure and accuracy of crack risk estimations.

The most critical parameter for this project was identifying relevant structures with adequate documentation of the construction process, with construction drawings, material properties, crack preventing measures, concrete pouring rates and temperature logs. Three concrete structures were chosen for this project: a railway tunnel in Gamla Uppsala (2016) and two existing portal frame bridges in Ulriksdal (1990) and Antuna (1993). The geometry of the 2D FE-models are shown in Figure 2 and structural parameters are found in Table 3. The structures were analyzed with ConTeSt Pro, a commercial FEM software developed for purpose of temperature, strength and crack risk calculations in young concrete [8].

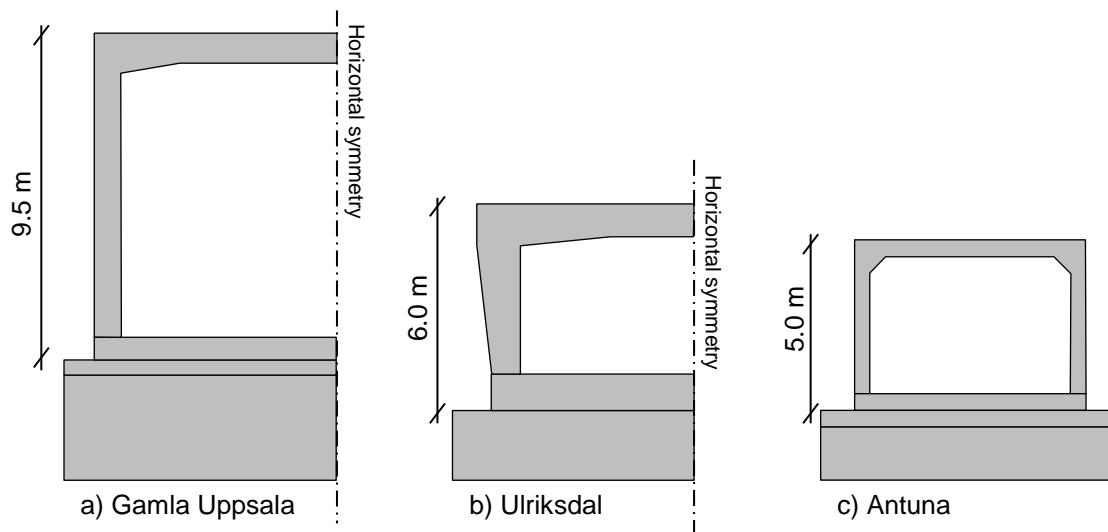


Figure 2 – Geometry of the three slab-frame structures. a) Railway tunnel b-c) road tunnels.

Table 3 – Structures analyzed in this paper.

Name of structure	Year of construction	Length	Casting length (walls)	Height	Wall thickness	References
Gamla Uppsala	2014-2016	610 m	10.0 m	9.5 m	0.7 m	[9-10]
Ulriksdal	1989-1990	41.6 m	10.4 m	6.0 m	0.8-1.2 m	[11]
Antuna	1993	35 m	35 m	5.0 m	0.45 m	[11]

Crack preventing measures were designed according to original crack risk estimations, carried out prior to casting. The crack preventing actions of the structures studied in this paper consisted of heating the slab with either internal heat cables or an external heat mat before and after the frame walls were cast. Construction fans were also used to increase the air temperature inside the tunnel for some castings. The original design was compared to the actual outcome of the project regarding temperatures and construction times. The recorded air and concrete temperatures were thereafter used in ConTeSt Pro for the post-project thermal crack risk estimations.

The material properties are given in Table 4. The heat development within the concrete is highly influenced by the heat transfer coefficient along the boundaries of the structure. All free surfaces (air), formwork and expanded polyethylene (EPE) foam were modeled with heat transfer coefficients of 500; 4.7 and 3.6 W/m²·K, respectively. A frame wall had for example heat transfer coefficient of 4.67 until the formwork was removed, whereon the heat transfer coefficient increased to 500 W/m²·K as the boundary surface was exposed to air.

The structures were visually inspected and the presence of cracks was recorded. The railway tunnel in Gamla Uppsala was thoroughly inspected for all types of cracks and all small cracks (< 0.1 mm) were divided into 8 zones for each casting sequence (wall) as seen in Figure 3. Only cracks in the mid-part of the wall with openings larger than 0.1 mm were considered as thermal cracks. The cracking was finally compared to the previous estimations.

Table 4 – Material properties.

Structure	Parameter	Soil	Gravel	Slab	Frame
Uppsala	Material/strength class	Fine soil	coarse soil	C30/37	C30/37
	Density, kg/m ³	1700	2200	2350	2350
	Thermal capacity, J/Kg K	1950	1400	1000	1000
	Thermal conductivity, W/m K	1.4	2.1	0-120 h: 1.7 120- h: 2.1	0-120 h: 1.7 120- h: 2.1
	Cement type	-	-	Anläggning*	Anläggning*
	Cement content, kg/m ³	-	-	365	365
	Water/cement	-	-	0.48	0.48
Ulriksdal	Material/strength class	Not used	coarse soil	C32/40	C32/40
	Density, kg/m ³	-	2200	2350	2350
	Thermal capacity, J/Kg K	-	1400	1000	1000
	Thermal conductivity, W/m K	-	2.1	1.7	0-24 h: 1.7 24- h: 2.1
	Cement type	-	-	Anläggning*	Anläggning*
	Cement content, kg/m ³	-	-	390	390
	Water/cement	-	-	0.45	0.45
Antuna	Material/strength class	Fine soil	coarse soil	C32/40	C32/40
	Density, kg/m ³	1700	2200	2350	2350
	Thermal capacity, J/Kg K	1950	1400	1000	1000
	Thermal conductivity, W/m K	1.4	2.1	1,7	0-24 h: 1.7 24- h: 2.1
	Cement type	-	-	Anläggning*	Anläggning*
	Cement content, kg/m ³	-	-	390	390
	Water/cement	-	-	0.45	0.45

*CEM I 42.5N – Anläggning Degerhamn, Cements AB, Sweden

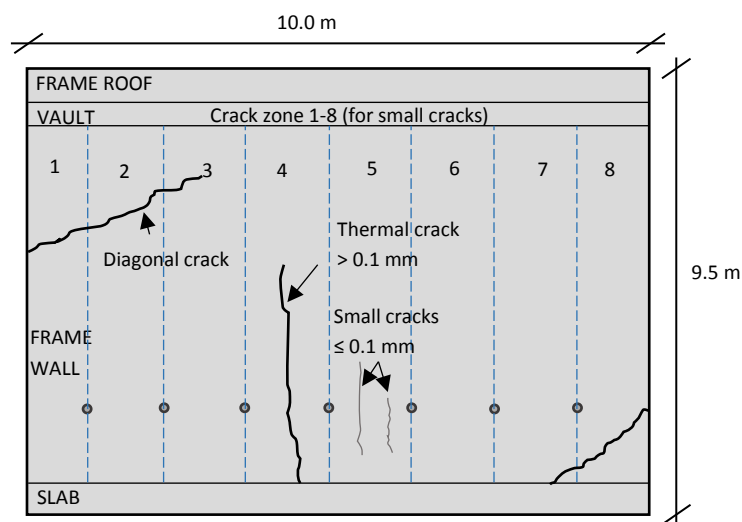


Figure 3 – Example crack types and crack zones (1-8) for the visual inspection of Gamla Uppsala.

3. RESULTS

3.1 Original design of thermal crack prevention

The original crack risk design was aimed at avoiding thermal cracks in the concrete members of Gamla Uppsala, Ulriksdal and Antuna. For Gamla Uppsala. Some typical cases were identified and the construction of each casting sequence was adjusted according to the prevailing conditions, depending on the type of casting, the concrete temperature at delivery, T_c , and the air temperature, T_{air} . The type of casting was either: a) casting of a free wall, without previously cast adjacent walls, or b) casting of a wall in direct contact to one adjacent wall. The crack preventing actions based on the original design were pre- and post-heating of the previously cast slab to avoid large strain differences between the slab and the wall. The original design cases of the Gamla Uppsala tunnel are presented in Table 5.

Table 5 – Original design of the Gamla Uppsala tunnel.

Type of casting	T_c °C	T_{air} °C	Pre-/Post-heating h/h	Form removal h	T_{max} °C	η Limit Design limit	η Original Calculated ratio	strain
Free seq.	15	-5	48/48	120	42.9	0,80	0.57	
Free seq.	15	5	0/0	72	43.1	0,80	0.77	
Adj. wall	15	-5	144/48	120	43.1	0,80	0.77	
Adj. wall	15	5	96/24	120	43.1	0,80	0.77	
Adj. wall	15	10	72/24	72	42.2	0,80	0.79	
Adj. wall	25	20	72/24	72	58.0	0,80	0.80	

*Free sequence corresponds to a wall without adjacent walls at casting

Figure 4 illustrates the typical crack preventive measures for wall casting in the Gamla Uppsala tunnel in cold weather, between -5°C and $+5^{\circ}\text{C}$. The slab was pre-heated with heat cables of type 1 and 2 according to Figure 4. Both types of cables had an output of 40 W/m , but as the wall was cast, the type 1 cables under the wall were switched off and only the type 2 cables were used for post-heating. The slab was insulated with a 10 mm layer of EPE foam which was removed as the post-heating was terminated. For temperatures over 5°C , the type 2 cables furthest from the wall were removed and no heat cables on the bottom reinforcement were used for temperatures over 10°C .

Figure 5 illustrates an example of temperature evolution for the case of casting a wall in direct contact to an existing adjacent wall, with $T_{\text{air}} = -5^{\circ}\text{C}$ and $T_c = 15^{\circ}\text{C}$. The horizontal axis represents the time after casting the slab, while the vertical axis represents the temperature to the left and the strain ratio to the right. Casting of the wall started at the relative time $t = 0\text{ h}$ with a concrete temperature of 15°C . The concrete temperature increased to a maximum of 36°C due to the exothermic reactions, and after the peak, the concrete started to cool off. The concrete exhibited a negative strain ratio (compression) of about $\eta = 0.40$ relatively fast where after it was subjected to a strain ratio of maximally $\eta = 0.77$. The crack preventing actions can also be seen by the temperature development within the slab. The temperature of the slab was governed by the air temperature until the heating was started at $t = -158\text{ h}$ (the slab was covered/insulated 16 h later). The heating ended at $t = 0$ and 24 h for the type 1 and 2 cables, respectively. The slab was also uncovered 24 h after the wall was cast. Note that the temperature gauge in the slab was located directly below the wall and the slab temperature was strongly influenced by the temperature development in the wall.

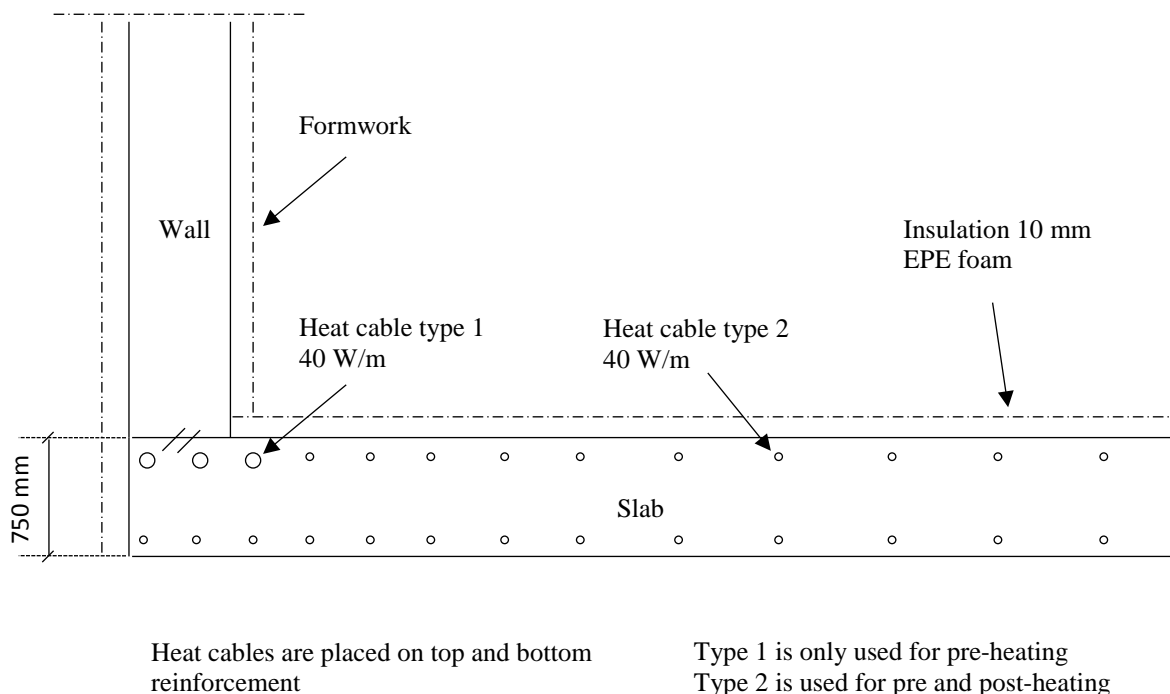


Figure 4 – Typical approach for crack prevention with heating cables for Gamla Uppsala.

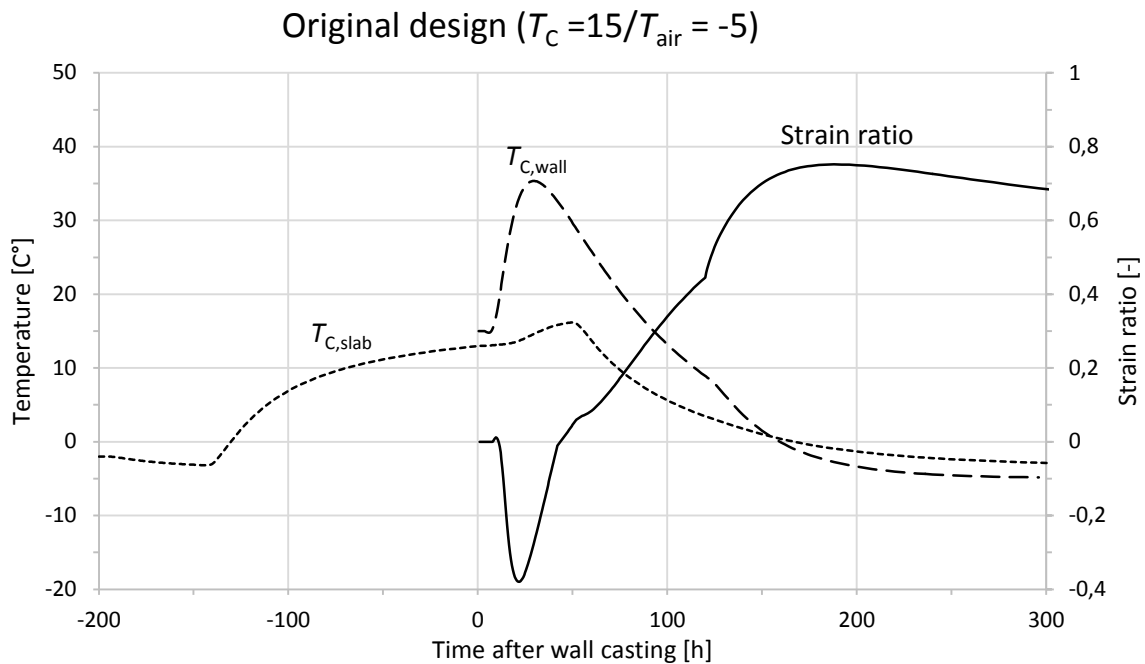


Figure 5 – Example of temperature evolution in the Gamla Uppsala Tunnel for the original design case with $T_{air} = 15^{\circ}\text{C}$ and $T_c = -5^{\circ}\text{C}$.

3.2 Post design of thermal crack prevention

Figure 6 presents the air (T_{air}), wall (T_{wall}) and slab (T_{slab}) temperatures. Each temperature is given for the original and post-design, as well as the actual measured values. The figure shows that the measured air temperature was much higher than assumed in the original design and the post-design was carried out according to a simplified temperature curve with straight lines between temperature peaks. Due to the assumed lower temperatures in the original design, the maximum temperature in the wall, as well as in the slab, was substantially underestimated. However, the post-design shows a relatively good adaption to the measured temperatures in the wall as well as the slab. The figure shows a common problem where the air temperature changes considerably after the crack preventing actions have already started. For this casting sequence, the typical case with an air temperature of $+5^{\circ}\text{C}$ would have been more suitable.

Figure 7 illustrates the strain distribution for casting sequence 5.1.2 of Gamla Uppsala at the time of maximum strain. Thermal cracks are assumed to develop as the average strain in a cross section exceed the ultimate strain of the concrete [12]. The strain ratio was calculated as an average value over a region of $0,7 \cdot 0,2 \text{ m}^2$, centered over the point of maximum strain, see the magnified part in Figure 7. The maximum strain developed in the center of the wall, approximately 0,7 m over the slab. Previous research has shown that thermal cracks in wall-slab structures typically initiate at a height corresponding to the wall thickness above the joint [13-14]. The maximum strain ratio for sequence 5.1.2 was $\eta = 1,02$ and the average strain for the shadowed region of Figure 7 was $\eta = 0,90$. This value can be compared to the strain ratio $\eta = 0,77$ from the original design and the strain limit of $\eta = 0,90$ for exposure class XC4 and tested material parameters.

inspection. The compilation in Table 6 shows a large number of small cracks for all casting sequences of the Gamla Uppsala tunnel. The amount of small cracks ranged from 6 – 38 cracks for each casting.

For Ulriksdal, one out of four casting sequences exceeded the limiting strain ratio $\eta = 0.70$ (based on exposure class XD3/XS3 and a cement content of 390 kg/m^3) in the post-design and temperature cracks were found on two sections during the visual inspection. The single casting of Antuna was not supposed to crack according to neither the original design, nor the post-design, and no temperature cracks were actually detected.

Table 6 – Summary of the original and post-designs for thermal crack risks.

Seq.	Exposure class	η Limit	η Original	η Post	Temp. cracks > 0.1 mm	Average crack width, mm	Small cracks $\leq 0.1 \text{ mm}$
Gamla Uppsala							
3.1.1			0.57	0.58	1	0.20	25
3.1.2			0.77	0.55	0	-	6
3.2.1			0.77	0.97	1	0.20	30
5.1.1			0.77	0.67	0	-	23
5.1.2	XC4/XF4		0.77	0.90	1	0.30	38
5.2.1			0.77	1.01	1	0.20	27
5.2.2	Tested	0.90	0.77	0.75	1	0.30	11
6.1.1	material		0.77	0.65	1	0.20	28
6.1.2	parameters		0.77	1.04	2	0.40	15
6.2.1			0.77	0.69	0	-	31
8.1.1			0.57	0.49	0	-	13
9.1.2			0.77	0.81	4	0.40	8
9.2.2			0.77	0.74	2	0.20	32
10.2.2			0.77	0.84	3	0,37	17
Ulriksdal							
1	XD3/XS3		0.70	0.69	1	0.4	-
2			0.70	0.46	0	-	-
3		0.70	0.70	0.44	0	-	-
4	$360 < C < 430$		0.70	0.81	3	0.27	-
Antuna							
1	XD3/XS3	0.70	0.70	0.55	0	-	-

4. ANALYSIS AND DISCUSSION

Traditional crack preventing actions generally aims at reducing the tensile strains within the structure, typically by reducing the temperature differences within a massive concrete structure or between old and new concrete members. Existing slabs can for example be pre-heated before a new wall is cast to account for the thermal effects of the concrete hydration. Cooling pipes can also be installed in the new wall to avoid high temperatures and strains. All three structures within this study had their slabs pre-heated prior to casting the walls. The crack prevention was not always completely successful due to a number of factors and thermal cracks could be found in 12 of the 19 studied wall castings (63%).

Based on the results of this study it is observed that a correct weather forecast is crucial for an accurate original design, and can ultimately be the factor determining whether the structure remains crack-free or not. Under- or overestimated air temperatures in the original design leads

to improper crack preventing actions, typically due to rapid temperature changes after the actions have started. Table 5 showed that six typical cases were used for the original design of the Gamla Uppsala tunnel. However, Fig. 5 showed that a constant air temperature of -5°C was chosen for the original design of casting sequence 5.1.2, but the measured temperature was in fact up to 15 degrees higher. This resulted in a higher wall temperature than anticipated in the original design. The construction process followed the original design restrictions and even though the formwork was removed later than planned, it was still a bit too early.

The concrete temperature was higher than planned at the point of form removal, resulting in a rapid cooling of the wall and accelerating tensile strains, see Figure 8. Instead of the originally anticipated strain ratio of 0.77, the strain ratio for this wall reached the limit $\eta = 0.90$. Other factors that may affect the accuracy of the crack risk estimation are the quality and function of the cooling/heating equipment, the workmanship, effects of sun exposed (locally heated) surfaces, etc. By using accurate quality controls, most functional errors may be avoided. However, the original design could be updated with a more reliable weather forecast and accordingly adjusted actions just before the wall casting starts. Another approach that may be used to reduce the risk of thermal cracks is more comprehensive monitoring of the concrete temperatures and avoiding unnecessary high tensile strains due to premature form removal.

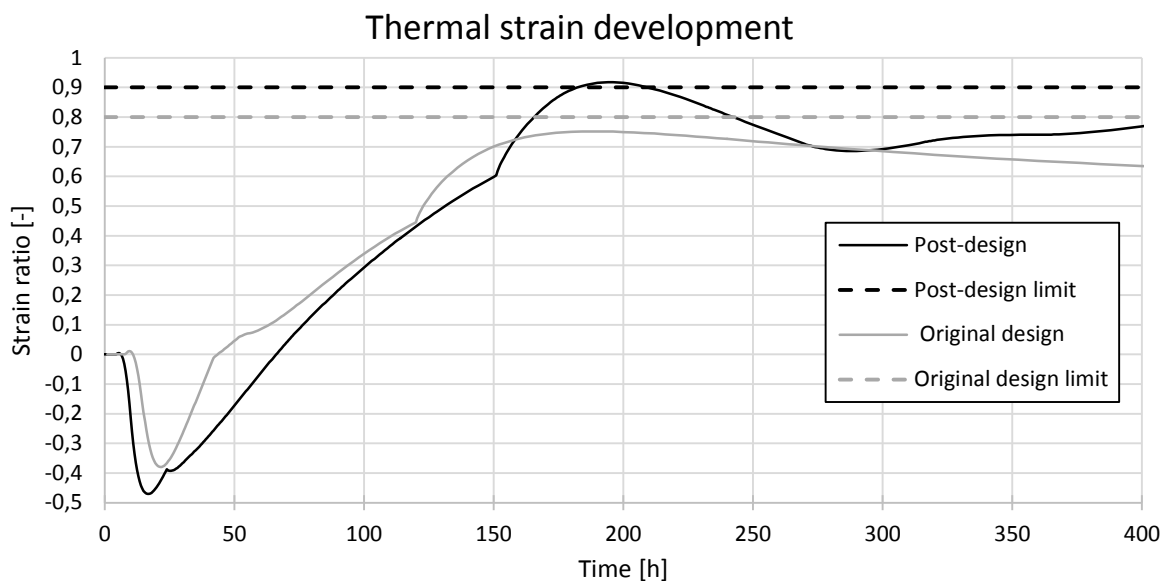


Figure 8 – Comparison of average strain ratios in the original- and post-designs for casting sequence 5.1.2 of the Gamla Uppsala tunnel.

Table 6 showed a presence of thermal cracks for all walls with $\eta > 0.70$ in the post-design and a few thermal cracks could also be seen on walls with even lower strain ratios. A more thorough analysis of the planned and executed crack preventive actions is presented in Table 7. The Table shows that the prescribed pre- and post-heating was relatively well complied, but there was still a high frequency of thermal cracks. Crack risk estimations according to the Swedish standards have probably reduced the amount of thermal cracks in the Swedish infrastructure, but there are still a large number of uncertainties involved in the design. Based on the results of this study, it seems relevant to discuss whether the maximum strain ratio for exposure class XC4 should be 0.90 as it is in the Swedish guidelines today or if it should rather be reduced to 0.70 to avoid certain cracking. However, the results of this study are based on a limited number of slab-frame

structures where the only crack preventing action was pre-heating of the slab. Further studies of relevant structures with different crack prevention are required to validate these results. Finally, the visual crack inspection of the Gamla Uppsala tunnel showed that there was a strong correlation between the wall's degree of restraint and the presence of surface cracks with crack widths < 0.1 mm. Totally 144 frame-walls of the Gamla Uppsala tunnel were inspected and surface cracks were found on each one of them. According to theory [3], the restraint is supposed to be higher in the mid-part of the wall and decrease towards the wall-ends. Figure 9 shows a FE-analysis of the restraint situation for a wall cast in direct contact with an adjacent wall. The frequency of small cracks is plotted in front of the wall to illustrate the correlation between restraint and surface cracks.

Table 7 – Summary of planned and actual parameters for the Gamla Uppsala tunnel.

Seq.	T_{air} Pre-design °C	T_{air} Average °C	Planned heating Pre-/Post- h/h	Actual heating Pre-/Post- h/h	η Original design	η Post- design	η Limit	Cracks > 0.1 mm
3.1.1	-5	+4	48/48	100/50	0.57	0.58		Yes
3.1.2	-5	+6	144/48	150/40	0.77	0.55		-
3.2.1	+5	+10	96/24	150/30	0.77	0.97		Yes
5.1.1	+5	+5	96/24	45/35	0.77	0.67		-
5.1.2	-5	+5	144/48	160/25	0.77	0.90		Yes
5.2.1	-5	0	144/48	160/30	0.77	1.01		Yes
5.2.2	-5	-2	144/48	350/50	0.77	0.75	0.90	Yes
6.1.1	-5	+3	144/48	120/30	0.77	0.65		Yes
6.1.2	+5	+1	0/0	0/0	0.77	1.04		Yes
6.2.1	+5	+5	96/24	140/30	0.77	0.69		-
8.1.1	-5	0	48/48	110/50	0.57	0.49		-
9.1.2	-5	+2	144/48	110/40	0.77	0.81		Yes
9.2.2	-5	+4	144/48	160/25	0.77	0.74		Yes
10.2.2	+10	+12	72/24	25/60	0.79	0.84		Yes

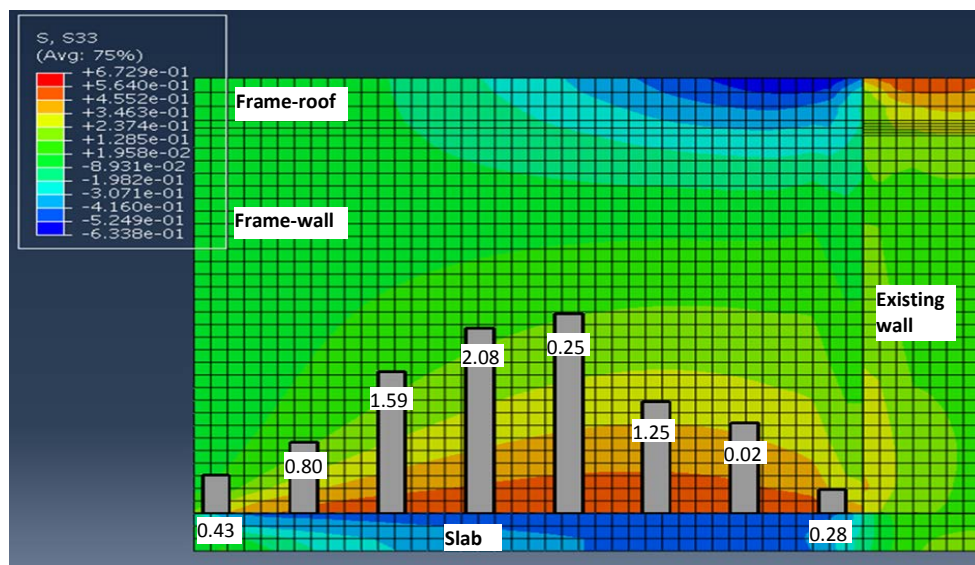


Figure 9 – Illustration of the correlation between wall-restraint and the frequency of small surface cracks (< 0.1 mm). The numbers represent the observed average number of small cracks in each of the eight crack zones (cracks/wall) and the colours represent the calculated degree of restraint.

5. CONCLUSIONS

Thermal crack risk estimations were carried out for three concrete frame structures according to the directions in the Swedish design guidelines AMA Anläggning [6]. The original crack risk estimations are influenced by a large number of uncertainties which may affect the outcome substantially. Typical uncertainties in thermal crack risk estimations include:

- Material properties of concrete, formwork and insulation.
- Environmental conditions, e.g. wind, temperatures, sun exposure.
- Structural properties, e.g. degree of restraint.
- Function and efficiency of heating and cooling equipment.
- Accomplishment of planned activities.

This paper demonstrates how thermal cracks have emerged in structures that were not supposed to crack according to their original crack risk estimations. All structures that reached tensile strains higher than 70% of the concretes ultimate strain within the first weeks after casting were actually cracked. The Swedish guidelines presently allow strain ratios of 0.90 for exposure class XC4 if the material properties have been tested and 0.80 otherwise. However, the results of this paper indicate that the limit should be reduced to 0.70. Further studies are needed to analyse other types of structures and crack preventing measures, and also to validate the results of this paper.

ACKNOWLEDGEMENTS

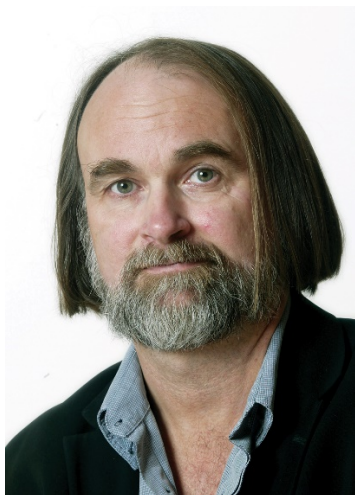
The authors would like to express their appreciation for the financial support from the Swedish Transport Administration, the construction industry's organisation for research and development (SBUF), Heidelberg cement, Cementsa, The Elsa & Sven Thysell Foundation and LTU. Those who have contributed with their knowledge in this project are Petter Eriksson and Jan-Erik Jonasson at LTU, Kjell Wallin at Betong & Stålteknik and Vilmer Andersson-Wass at PEAB.

REFERENCES

1. De Schutter G, Taerwe L: "Degree of hydration-based description of mechanical properties of early age concrete," *Materials and Structures*, Vol. 29, No. 335, July 1996, doi:10.1007/BF02486341
2. Emborg M, Bernander S, Ekerfors K, Groth P, Hedlund H: "Temperature Cracking in Concrete Structures: Calculation Methods for Hydration Stresses and Charts for Some Relevant Typical Cases. Part A, B and C," *Report No. 1997:02*, Dept. of Civil, Environmental and Natural Resources Engineering, Luleå University of Technology, Luleå, Sweden, 1997. (In Swedish)
3. Knoppik-Wróbel A, Klemczak B: "Degree of restraint concept in analysis of early-age stresses in concrete walls," *Engineering Structures*, Vol. 102, Nov. 2015, pp 369–386
4. Nilsson M: "Restraint factors and partial coefficients for crack risk analyses of early age concrete structures," *Doctoral Thesis*, Dept. of Civil, Environmental and Natural Resources Engineering, Luleå University of Technology, Luleå, Sweden, 2003.
5. Weiss J, Yang W, Shah SP: "Shrinkage Cracking of Restrained Concrete Slabs," *Journal of Engineering Mechanics*, Vol. 124, No. 7, July 1998.

6. Svensk Byggtjänst: "AMA Anläggning 13. General Material and Work Descriptions for Construction Work," *Svensk Byggtjänst*, Stockholm, Sweden, 2014, ISBN 9789173336406
7. Vägverket: "BRO 94, Allmän teknisk beskrivning för broar," *VV Publ* 1999:20, Vägverket, Borlänge, March 1999.
8. JEJMS Concrete: "ConTeSt Pro Users manual: Program for temperature and stress calculations in concrete," *Manual*, Jejms Concrete, Luleå, 2008.
9. Vass-Andersson V: "Temperature Cracking in Concrete- Development of Methods for Crack Reduction and Study of Cracks in Tunnel Structures," *Master Thesis*, Dept. of Civil and Architectural Engineering, Royal Institute of Technology (KTH), Stockholm, Sweden, Sept. 2015. (In Swedish).
10. Eriksson P: "Temperature Cracking in Early Age Concrete: Follow up of the Swedish Crack Rules," *Master Thesis*, Dept. of Civil, Environmental and Natural Resources Engineering, Luleå University of Technology, Luleå, Sweden, Jan. 2017. (In Swedish).
11. Wallin K, Emborg M, Jonasson J-E: "Heating, an Alternative to Cooling," *Report No.* 1997:15, Dept. of Civil, Environmental and Natural Resources Engineering, Luleå University of Technology, Luleå, Sweden, 1997. (In Swedish).
12. Knoppik-Wróbel A: "Analysis of Early-age Thermal-shrinkage Stresses in Reinforced Concrete Walls," *Doctoral Thesis*, Dept. of Structural Engineering, Silesian University of Technology, Upper Silesia, Poland, Jan. 2015.
13. Al-Gburi M: "Restraint Effects in Early Age Concrete Structures," *Doctoral Thesis*, Dept. of Civil, Environmental and Natural Resources Engineering, Luleå University of Technology, Luleå, Sweden, Sept. 2015.
14. Zhou J, Chen X, Zhang J: "Early age temperature and strain in basement concrete walls: Field monitoring and numerical modelling," *Journal of Performance of Constructed Facilities*, Vol. 26, No. 6, Dec. 2012.

Durable Aluminium Reinforced Environmentally-friendly Concrete Construction – DARE2C



Harald Justnes, PhD
Chief Scientist
SINTEF Building and Infrastructure
Pb 4760 Sluppen, 7465 Trondheim, Norway
harald.justnes@sintef.no

ABSTRACT

A new concept is described for low pH concrete that can allow reinforcement with aluminium metal rods or fibres. In regular concrete the high pH will after short while lead to substantial amounts of hydrogen gas evolution. However, by replacing cement partially by an active pozzolan (e.g. calcined blue clay) in a sufficient amount to consume all calcium hydroxide produced by the cement hydration, the remaining alkalis will have aluminate or silicate as counter ion and metallic aluminium will be stable. Since aluminium is stable towards the environment, the concrete can then be designed with respect to strength class rather than environment classes.

Key words: Aluminium, durability, environment, reinforcement, supplementary cementitious materials

1. INTRODUCTION

1.1 Evolution of environmentally friendly cement

Cement is a key binder component of, for example, concrete production in the building industry. It has started out as a complex hydraulic binder, made up of four main clinker components; alite (Ca_3SiO_5), belite (Ca_2SiO_4), tricalcium aluminate ($\text{Ca}_3\text{Al}_2\text{O}_6$) and ferrite ($\text{Ca}_2\text{AlFeO}_5$), which are milled together with gypsum to regulate setting time. In recent years, the production of cement has been identified as the third largest emitters of carbon dioxide (CO_2), accounting for approximately 5 to 8% of the total global anthropogenic emissions, with 60% coming from

decomposition of limestone in the raw meal and 40% from fuel to reach clinkerization temperatures of 1450°C for a pure Portland cement. Four main methods are currently in place to mitigate this challenge; i) switching from fossil fuels to alternative fuels [1], ii) increase efficiencies in factories [1], iii) implementation of supplementary cementitious materials (SCMs) replacing cement clinker [1, 2] and iv) carbon capture and storage (CCS) [3, 4]. Among which, clinker partially replaced by SCMs is the most promising on a short term [2], whereby significant reduction in CO₂ emission could be expected depending on how much emission is associated with the SCM (transport, calcination energy etc.). Replacing cement with SCM will also reduce the amount of raw meal needed per unit cement and increase the cement production volume of a cement plant. Most of the cement produced today has clinker replaced with SCMs with an average global clinker factor of 0.85 in 2003 [5], but higher clinker replacement with a greater variety of SCMs is expected in the near future. The potential SCMs of the future include combustion ashes, slag, calcined clay and limestone. Fly ash is commonly employed in current cements with replacement of 20% in Norway. Calcined clay or marl is a new and upcoming SCM due to its abundance as increased clinker replacement demands large volumes of available SCMs. Additionally, previous studies displayed that calcined marl is a potential SCM up to a replacement level of 50% in terms of equal 28 day strength to reference [2], but generally it is limited to < 35% replacement if sufficient alkalinity is to be maintained to protect steel from corroding in the long run.

1.2 Alternative concrete reinforcement

The most common reinforcement for structural concrete is rebars made of steel. At the same time the most common degradation mechanism of reinforced concrete is corrosion of the steel initiated by carbonation (i.e. CO₂ from the air diffuse in and lower the pH by neutralization) or by chlorides exceeding a critical limit in spite of maintained pH. Thus, there is a need for concrete reinforcement that will not corrode, but at the same time being composed of common chemical elements since a gross volume of 10¹⁰ m³ concrete is produced annually world-wide. "Stainless steel" exists that will not corrode, but there is "not enough chromium in the world" to make a significant replacement feasible and it is rather pricy. Some efforts have been made to make rebars out of fibre reinforced plastic (FRP). Karlsson [6] recently made a review and evaluation of alternative concrete reinforcement. Naturally, aluminium was not a part of this evaluation since it will be degraded by the high pH of regular concrete and can only function in a sufficiently low pH concrete. On the other hand, aluminium is a very common element in earth's crust.

There is an on-going project called SEACON in the European INFRAVATION program (www.infravation.net/projects/SEACON) with the objective "demonstration of safe utilization of seawater and salt-contaminated aggregates (natural or recycled) for a sustainable concrete production when combined with noncorrosive reinforcement to construct durable and economical concrete infrastructures". The difference from the present concept is that SEACON uses regular concrete binder and a reinforcement of either fibre reinforced plastic (FRP) or basalt. Of course, a low pH binder with aluminium metal reinforcement would also have the benefit of enabling use of chloride contaminated aggregate or even seawater as mixing water. Aluminate containing SCMs will also produce hydrates that have a high capacity of solidifying chlorides (chemical bound as Friedel's salt).

1.3 DARE2C concept

The main durability design of concrete today is in relation to preventing the steel reinforcement from corroding. The major degradation mechanisms; chloride ingress and carbonation, does not jeopardize the integrity of the concrete binder itself. Steel needs the high pH of conventional concrete to be passive towards corrosion while aluminium metal will be corroded by high pH and develop hydrogen gas.

Environmentally friendly concrete is often designed by either using blended cement where maximum 35% of the clinker is replaced by supplementary cementitious materials (SCMs) to secure the presence of calcium hydroxide over time that will buffer a pH of 12.5 passivating steel, or by replacing cement in concrete mixes with corresponding amounts of SCM.

In order to secure long service life for steel reinforced concrete, low w/c is used for low permeability often leading to much higher strength than required. Low w/c will also create complications in the construction phase as lower workability calling for use of super-plasticizing admixtures and higher temperature and subsequent thermal cracking risk generated by hydration heat. The required compressive strength for the bulk of concrete today is still in the range of 25-30 MPa (B25).

The concept is to make environmental friendly concrete with cement replacement > 50% with a combination of SCMs where some are so pozzolanic active that the pH is kept so low that the concrete can be reinforced with aluminium metal rods without formation of hydrogen gas. The w/c can then be so high that it is only determined by required compressive strength and workability should not be a problem and neither hydration generated heat. Permeability is not important as aluminium metal is resilient to atmospheric CO₂ and chlorides, and high initial permeability is in fact beneficial for the concrete to carbonate as fast as possible to reduce the carbon footprint further and lower the pH for the long run. The concrete cover over the reinforcement can be made much thinner (20 mm) than today (50-70 mm) reducing weight and further improving the carbon footprint.

2. APPROACHED TO LOW pH CONCRETE

2.1 Supplementary cementitious materials (SCMs)

The easiest approach to implement low pH concrete by the industry is to make a blended cement with a pozzolanic SCM (i.e. one consuming calcium hydroxide from hydration of clinker minerals) exceeding 35% clinker replacement to a level of 50-60% depending on target strength level.

The calcium hydroxide produced by the hydration of clinker minerals in ordinary Portland cement would lead to a buffered pH of about 12.5, while the alkalis (0.6-1.2% Na₂O_{equivalent}) of the cement clinker will top this to pH 13.0-13.5.

Aluminium metal forms a dense layer of Al₂O₃ in contact with air that prevents further oxidation (or corrosion). This layer may dissolve by alkali hydroxides and open up for further corrosion evolving hydrogen gas;



aluminium reinforcement as aluminium is more resilient towards chlorides. Furthermore, as the SCM produces CAH over time, chlorides will be taken out of solution and bound as Friedel's salt. The soluble calcium in calcium chloride may further depress the initial pH of the pore water due to the common ion effect with calcium hydroxide.

The question is which pozzolanic SCM to choose. It should be one with a high specific surface consisting of silica, aluminosilicate or alumina. If one considers the passive layer of aluminium as alumina, the initial alkali hydroxides from cement should be busy dissolving the SCM rather than the passive layer of the aluminium.

The most common pozzolanic SCM used by cement industry today is fly ash from coal fired energy plants. These are tiny spheres with glassy aluminosilicate walls to put it simple. However, the glass phase reacts rather slowly (i.e. strength improvement after 14 days) compared to for instance silica fume (within a day) and "ordinary blue clay" as dug from the ground with all its contaminations and calcined at about 800°C [8, 9, 10]. A combination of fly ash and calcined clay is possible and demonstrated [11] to give a good workability together.

2.2 Low pH cements

There is a class of cements referred to as "the third cement series" when it was invented in China, but now usually referred to as belite-calcium sulfoaluminate-x cements where x usually is "ferrite" phase ($\text{Ca}_2\text{AlFeO}_5$), but recently a special one was developed where x is ternesite, $2\text{Ca}_2\text{SiO}_4 \cdot \text{CaSO}_4$ [12]. One important feature about these cements is that they do not produce calcium hydroxide of pH 12.5, but rather aluminium hydroxide (yield pH 8.1 in theory) that cannot attack aluminium metal. Only the belite content can contribute with a minor content of calcium hydroxide. Belite-calcium sulfoaluminate-ternesite (BCT) cement was based on waste raw materials, produced at lower kiln temperature than ordinary Portland cement (OPC), required lower grinding energy and was claimed to lead to a 50% reduction in CO_2 -emission compared to OPC [12].

If one uses a calcium sulfoaluminate (CSA) cement with a low belite content, only a minor pozzolan content may be required (if any) to secure no calcium hydroxide present. Since these cements bind high amount of water corresponding to 0.72 water per hydrated cement, a higher water-to-cement ratio (w/c) can be used and still obtain required strength. Ettringite is the main product of CSA, and this will also carbonate eventually in contact with air. Hence, CSA cement is an interesting candidate for aluminium metal reinforcement.

3. PROOF OF DARE2C CONCEPT

As a proof of concept, two paste mixes with $w/c = 0.60$ were made with 100% ordinary Portland cement and 50% calcined marl [8] replacing cement. These pastes were poured into a plastic cup and an aluminium plate placed in each of them as shown in Fig. 1. The paste of pure cement separated and after a few minutes hydrogen gas started to bubble vigorously along the aluminium plate as seen from the left side of Fig. 1, while for the mix with 50% calcined marl some water was added on top for better visualization, but only a few small bubbles were observed.

After the pastes had hardened, the samples were split and the imprints of the front and back of the aluminium plates on the pastes are shown in Fig. 2. It is clearly much more cavities in the OPC sample next to the plate, while only a few small gas voids are seen on the interface for the paste with 50% calcined marl. One cannot rule out that the minor gas voids are due to entrained air by the high shear mixer, and the only way to find out is to capture and measure the evolved hydrogen gas volume.



Reference paste (w/c = 0.60)

50% cement/50% calcined marl (w/c = 0.60)

Figure 1 – Aluminium plates inserted in pastes of different composition for gas observation.



Reference, split front



50% calcined marl, split front

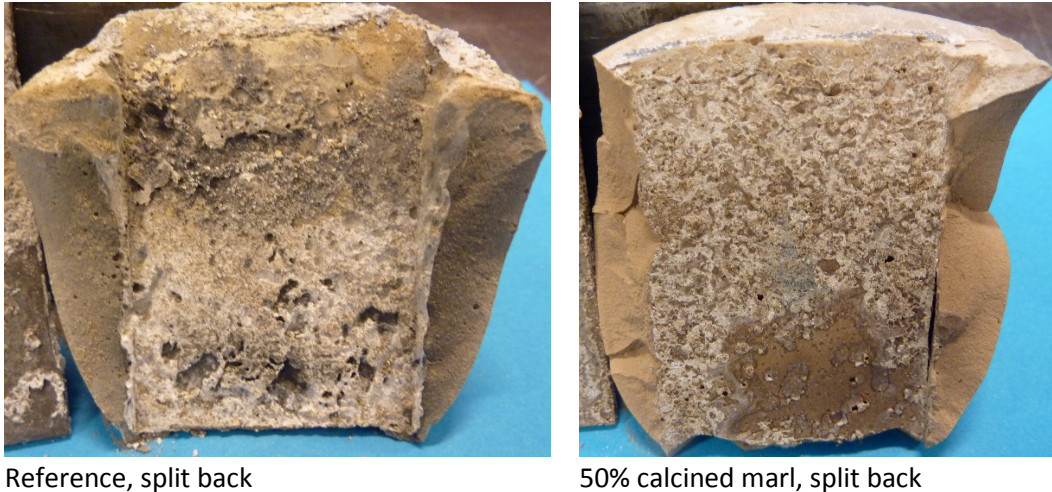


Figure 2 – Interfaces between aluminium plate inserts and pastes after hardening showing the difference in cavities formed by hydrogen gas evolution.

Mortars where 50% cement is replaced by calcined marl on volume basis have been shown to develop sufficient strength for formwork removal (≈ 10 MPa) at 1 day and to achieve equal strength as mortar with 100% cement [10] when cured at 20°C and 90% RH. Furthermore, no sign of calcium hydroxide was found by thermal analysis neither at 28 days nor after 2 years (confirmed by X-ray diffraction) [10]. The above observations and former studies on cement blended with calcined marl or calcined clay give confidence in the DARE2C concept.

4. OTHER BENEFITS OF THE DARE2C CONCEPT

There are several other benefits with the DARE2C concept that can support its applicability:

- Maintenance free reinforced concrete (i.e. no carbonation or chloride induced corrosion).
- Much less cover over rebar needed (save 30 mm concrete cover), probably 20 mm needed for proper anchoring of reinforcement with concrete.
- Higher w/c allowed giving more permeable concrete leading to
 1. Easier to cast as the concrete will need less plasticizers or none
 2. Faster carbonation leading to binding of CO₂ and further reduction of Carbon-footprint
 3. Less thermal expansion/contraction in monolithic concrete.
- Al-reinforced concrete will have significantly lighter unit weight (reduced "dead-weight").

In addition to the preceding bullet points of improvements, the sulphate resistance of the binder will be greatly improved when aluminate containing SCMs are used. This is demonstrated in Fig. 3 and Fig. 4 showing photos of mortar prisms been exposed for 5% sodium sulphate (Na₂SO₄) solution at 5°C for 2 years. The reference mortar mix with 100% cement is clearly deteriorated with material flaking off, while mix M1 (20% cement replaced with calcined marl) is slightly deteriorated in the edges. Mixes M2, M3 and M4 with 35, 50 and 65% cement replacement by calcined marl, respectively, appear to be in pristine condition.

It is clear from Figs. 3 and 4 that mortar with ≥ 35 vol% replacement of cement by calcined marl does not show any visible damage. This is explained by the lack of calcium hydroxide in the samples with 50 vol% (M3) and 65 vol% (M4) cement replacement, while the mortar with 35 vol% (M2) still might have some calcium hydroxide as shown for corresponding paste cured at

20°C and 90% RH for 2 years [10]. The reason for this claim is that the first sulphate attack is the expansive formation of gypsum as pointed out by Justnes [13];



with a solid volume expansion of 124% based on molar volumes. Since this reaction will not happen, or to a limited extent in these mortars, the second step of forming expansive ettringite (AFt) from calcium monosulphoaluminate hydrate (AFm) will not happen. Among the reaction products of calcined clay is more calcium aluminate hydrate, so more AFm will form rather than AFt.

In short, the durability of aluminium reinforced concrete with high content of aluminate containing SCMs will be high since carbonation and chloride intrusion will not attack the binder nor the reinforcement, the binder will be resistant to sulphate attack (Fig. 3 and 4) and there is no alkali hydroxides to induce ASR in the aggregate. The only remaining common concrete degradation mechanism is freeze-thaw action, but that can be avoided with proper air entrainment and distribution when needed.



Figure 3 – Condition of mortar prisms stored in 5% Na_2SO_4 solution for 2 years at 5°C. The light grey, deteriorated (spalled) prisms are the reference with 100% OPC. The brown ones marked M1 and M2 are mortar prisms where 20 and 35 vol% cement is replaced with calcined marl, respectively.

partners. The project is sponsored by the Norwegian Research Council while the remaining finance is cash and in-kind from the industrial partners.

The research focus in the first years is to find stable and functional binders enabling the use of aluminium as reinforcement as well as making aluminium reinforcement with optimum properties for such binders.

In addition to use traditional SCMs and calcined clay as cement clinker replacements, the project will also focus on potential utilization of "red mud" as SCM. "Red mud" is a waste stream from production of alumina serving as the raw material for aluminium production. The concept of transforming "red mud" into a pozzolan was discovered a few years ago and the Brazilian company Votorantim applied for a patent in 2013 [14], albeit so far only tried out on a pilot scale. A secondary option in the project is to utilise "red mud" as raw meal for production of calcium sulfoaluminate cements (CSAs) outlined in section 2.2.

The aluminium rebars will be produced by an extrusion process. The screw extrusion process is patented by Hydro [15], and has been developed through the Norwegian Research Council supported SEAL project [16]. A prototype extruder along with fundamental knowledge of the process have been developed to a level that allows industrial implementation. Compared to the traditional process route based on re-melting and extrusion, direct screw extrusion of scrap material represents a significant reduction in energy consumption [17]. Moreover, this process is well suited for utilization of swarf material from material removal processes such as cutting, milling and turning that is commonly of less value than other scrap types, further contributing to the environmental friendliness of the overall DARE2C concept.

7. CONCLUSION

Low pH concrete reinforced with aluminum metal has been shown to have a potential of being a construction material with extraordinary long service life without maintenance.

Achieving low pH with high content of supplementary cementitious material of pozzolanic nature also makes it more environmentally friendly than ordinary Portland cement.

Since the aluminum reinforcement does not corrode, the concrete can be designed according to required strength only without considering permeability. Higher porosity will make it carbonate faster and contribute further to limiting the overall CO₂ emission.

REFERENCES

1. <http://www.wbcscement.org/pdf/tf2/CEMBUREAU.pdf>
2. Justnes, H. "How to Make Concrete More Sustainable", *Journal of Advanced Concrete Technology*, Vol. 13 (2015) 147-154
3. Bosoga, A., Mazek, O. and Oakey, J.E.: "CO₂ Capture Technologies for Cement Industry", *Energy Procedia*, Vol. 1:1 (2009) 133-140
4. <http://www.zero2.no/projects/norcem-cement-plant-in-brevik-norway>
5. Schneider, M., Romer, M., Tschudin, M. and Bolio, H.: "Sustainable Cement Production – Present and Future", *Cement and Concrete Research*, Vol. 41:7 (2011) 642-650

6. Karlsson, J.: "Alternative reinforcement approaches – Extended service life of exposed concrete structures", MSc thesis 2014:151, Chalmers University of Technology, Department of Civil and Environmental Engineering, Gothenburg, Sweden, 2014, 117 pp.
7. Mercier, D. and Barthés-Labrousse, M.-G.: "The role of chelating agents on the corrosion mechanisms of aluminium in alkaline aqueous solutions", *Corrosion Science*, Vol. 51 (2009) 339-348.
8. Danner, T., Justnes, H., Norden, G. and Østnor, T.: "Feasibility of calcined marl as alternative pozzolan", *Proceedings*, 1st International Conference of Calcined Clays for Sustainable Concrete, Eds. Karen Scrivener and Aurélie Favier, RILEM Book series Vol. 10, Springer, pp. 67-74 (ISBN 978-94-017-9938-6). Lausanne, Switzerland, June 23-25, 2015.
9. Østnor, T., Justnes, H. and Danner, T.: "Reactivity and microstructure of calcined marl as supplementary cementitious material", *Proceedings*, 1st International Conference of Calcined Clays for Sustainable Concrete, Eds. Karen Scrivener and Aurélie Favier, RILEM Book series Vol. 10, Springer, pp. 237-244 (ISBN 978-94-017-9938-6). Lausanne, Switzerland, June 23-25, 2015.
10. Justnes, H., Østnor, T.A. and Ng, S.: "Applicability of Nordic clays as SCM", *Proceedings*, International RILEM Conference on Materials, Systems and Structures in Civil Engineering, Conference segment on Concrete with Supplementary Cementitious materials, 22-24 August 2016, Technical University of Denmark, Lyngby, Denmark, Paper 278, 10 pp.
11. Ng, S., Østnor, T.A.: "A new type of Ternary Cement based on Fly ash and Calcined Marl with improved Rheology", *Proceedings*, 2nd International Conference on the Chemistry of Construction Materials, Munich/Germany (2016) 310–313.
12. Ben Haha, M., Bullerjahn, F., Zajac, M. and Schmitt, D.: "Belite-calcium sulfoaluminate-ternesite (BCT) – A new alternative binder", (Paper 51), *Proceedings*, 1st Concrete Innovation Conference (CIC), 11-13 June 2014, Oslo, Norway.
13. Justnes, H.: "How SCMs Improve Concrete Durability – A Fundamental View", *Proceedings*, 4th Sustainable Construction Materials and Technologies (SCMT4), Las Vegas, Nevada, USA, August 7-11, 2016, 23 pp. (Invited paper).
14. Lannes, J.: "Process for producing a chemical composition for the production of an active additive that can be used as a portland clinker substitute, chemical composition and use of said composition", Pub. No.: WO/2015/039198, Intl. Application No.: PCT/BR2014/000208, Publication Date: 26.03.2015, International Filing Date: 24.06.2014
15. Werenskiold, J.C., Auran, L., Roven, H.J., Ryum, N., Reiso, O.: "Screw extruder for continuous extrusion of materials with high viscosity", European Patent 2 086 697 B1, 01.05.2013, 8 pp.
16. Widerøe F., Welo T.: "Using contrast material techniques to determine metal flow in screw extrusion of aluminium", *Journal of Materials Processing Technology* 213:7 (2013) 1007-1018.
17. Duflou, J.R., Tekkaya, A.E., Haase, M., Welo, T., Vanmeensel, K., Kellens, K., Dewulf, W., Paraskevas, D.: "Environmental assessment of solid state recycling routes for aluminium alloys: Can solid state processes significantly reduce the environmental impact of aluminium recycling?", *CIRP Annals - Manufacturing Technology*, 64 (2015) 37–40.

RE:Concrete - Study on Recycling of Concrete in Sweden



Madumita Sadagopan, M.Sc.
Department of Resource Recovery and Building Technology
University of Borås, S-50190 Borås, Sweden
madumita.sadagopan@hb.se



Katarina Malaga
Adjunct Professor, PhD.
Department of Resource Recovery and Building Technology,
University of Borås, S-50190 Borås, Sweden
C.E.O, CBI Swedish Cement and Concrete Research Institute
katarina.malaga@ri.se

Agnes Nagy
Ph.D., Senior Lecturer,
Department of Resource Recovery and Building Technology,
University of Borås, S-50190 Borås, Sweden
Email: agnes.nagy@hb.se

ABSTRACT

Sweden's concrete waste is recycled for use in low-utility purposes such as in the construction of sub-bases in roads but hardly as aggregates in new concrete. To analyse the potential for high-utility recycling, a literature study was conducted on the regulatory instruments, building standards, production and properties of recycled concrete aggregates and the recycled aggregate concrete for Sweden and European countries.

Results urge statistics to quantify recycled concrete; regulations like source sorting of waste and selective demolition could potentially optimize recycled aggregate production. Also, the compressive strength of recycled concrete aggregate's parent concrete influences the properties of the new concrete.

Key words: Recycled concrete aggregate, Structural applications, Closed-loop recycling, Sustainability.

1. BACKGROUND

Recycled Concrete Aggregates (RCA) are aggregates produced from the crushing and recycling of only concrete or concrete combined with mineral waste sourced from demolition waste, rejects from prefabrication and concrete spill. RCA is useful in road construction and as aggregates in new concrete. The new concrete produced using RCA or a combination of RCA and other aggregates is called Recycled Aggregate Concrete (RAC) [1]. The production of RAC is being implemented in certain European countries for example Spain, where coarse fractions of RCA was used in structural RAC in housing near Madrid [2]. Similarly in Germany, RAC formed about 4% of the total precast concrete products and ready-mixed concrete produced in 2004 [3]. Sweden on the other hand uses RCA in low-grade construction applications. This can be confirmed by national statistics which estimated that Sweden in 2014 used 670,000 ton of crushed concrete and mineral waste for road sub-base construction while disposing 510,000 ton in the landfills [4].

In Sweden, the inclusion of RCA as aggregates in structural concrete is acknowledged by sustainability and environmental certification systems in their methods of assessment [5, 6]. Besides the certification systems, the European standard for concrete EN 206 has proposed regulations for the inclusion of RCA in new concrete. This is to help producers of ready-mixed and prefabricated concrete realize a closed loop recycling by using the waste concrete for the same application as its parent concrete [7].

Generally, the introduction of RCA in the production process of concrete as a replacement for natural aggregates is investment intensive [8], however, environmental benefits can be made from prolonging the life cycle of the parent concrete as aggregates and un-hydrated cement in the new concrete. This also creates opportunity for internal recycling of waste as a raw material in production. Furthermore, if the production of RCA is included in the concrete production (in-house production) it could potentially eliminate transportation costs related with the delivery of natural aggregates to the industry.

This article attempts to list and analyse examples of the regulatory instruments, building standards and production infrastructure for RCA suitable for use in structural and non-structural RAC. Such examples are drawn from European countries that are forerunners in RAC production and are compared with corresponding Swedish examples.

Together with this, reliable examples from the extensive RCA research from Europe and China are presented and critically analysed regarding the influence of RCA in the mechanical, deformational properties and durability of RAC. It is to note that, except for a single research study in Sweden [9] there were no other published attempts relating to RAC produced from RCA.

The comparative analysis with examples are presented as a sequence starting with the production of RCA from concrete waste and finally ending with the properties of RAC produced from such RCA.

2 CONCRETE WASTE TO RCA

The concrete waste received as hardened spill or mixed demolition waste is recycled into RCA by Construction and Demolition Waste (CDW) recycling plants in Germany, Italy, Spain, and

Belgium. Figure 1 is a simplified representation of the treatment processes for RCA production in a CDW plant.

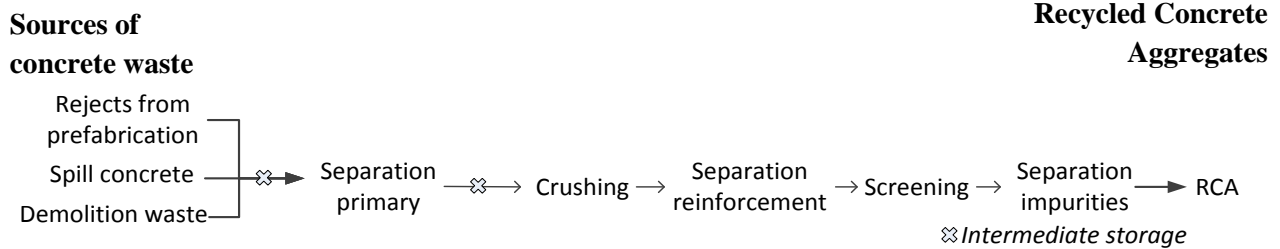


Figure 1 – A simplified representation of the processes involved in the production of RCA.

The processes which are a sequence of crushing, separation of impurities and screening [2, 10] aim to produce RCA free from contaminants and adhered cement mortar that adversely affect the RAC's properties. Examples of such contaminants are unwanted blended CDW fractions such as wood, plastic, paper and gypsum from plaster boards that cause harmful internal expansion in concrete [11]. Fine fractions of gypsum, autoclaved aerated concrete and organic materials can be separated by complex methods such as X-ray transmission [12] and Near Infrared Sorting [13]. The separation processes are, however, not entirely successful in separating the cement mortar adhered to the RCA; which if developed could make possible larger RCA replacements in the RAC [14]. The cement mortar from the parent concrete adhered to the RCA increases the RCA's porosity thereby negatively influencing the mechanical properties and durability of the RAC [15]. Novel thermo-mechanical separation methods include the "closed cycle construction" from Netherlands [12], microwave-assisted technique [16], ADR dry classification technology [17]. These methods have been successful in separating contamination and adhered cement mortar from the finer fractions of RCA that are more susceptible to contamination [18].

The RCA used mainly in un-bound road applications in Sweden is produced in waste treatment facilities following largely the processes shown in Figure 1, however, the separation processes involved are less advanced in comparison with the aforementioned CDW plants. The equipment in the most advanced of Swedish facilities can separate non-ferrous materials and fines in addition to mobile crushers, ferrous metal separation and screening operations [19, 20]. These plants are, however, not tried and tested for producing RCA that could substitute natural aggregates in concrete.

Currently, there exist only few instances of high-utility concrete recycling conducted internally by Swedish concrete producers; as is reported in their product declarations [21, 22]. These instances are however missing from the national statistics along with the information on the amount of RCA produced in treatment facilities to be used in low-grade recycling.

For it to be economically feasible to produce purer RCA fractions suitable for RAC using complex separation methods, a continuous supply of considerably uncontaminated waste is required [23]. According to industrial actors even the intermittent supply of concrete waste to produce RCA is challenged by the long transportation distances resulting from the extensive land area in Sweden. This leads to the accumulation of crushed concrete waste in intermediate storage facilities until a considerable amount is collected to justify the establishment of mobile recycling equipment in the facility. Logistical challenges of this nature reduce the availability of waste for recycling, but can potentially be resolved by alternatives like the establishment of

localized sorting, storage facilities and the creation of material or waste exchange opportunities between industrial clusters [24].

The Swedish waste regulations aim to increase the concrete waste available for recycling but fall short in initiating its use in high-utility applications. Also, certain aspects of the waste regulations seem to indirectly cause landfilling to be a more viable option.

2.1 Regulatory instruments to aid in recycling of concrete waste

Landfill tax in Sweden is charged at SEK 435/ton (approx. EUR 47) as of 2006 with no-fee exceptions for materials useable in landfill construction [25]. Additionally, the quantities of concrete waste and other mineral fraction used in landfill construction is considered recovered by the Swedish Environmental Protection Agency [26]. The use of recovered waste to enhance landfill capacity justifies the claim by the European Environmental Agency that landfill tax is not an efficient driver for recycling. Landfill taxes have, however, increased recycling rates when coupled with mandates such as recycling targets and source-sorting of waste in Germany and Denmark [27].

Mandatory **source-sorting** along with landfill tax in Denmark, Germany and the Netherlands has been effective in reaching high recycling rates for concrete waste. Concrete waste in Denmark is sorted separately as 1 out of 10 waste fractions which has increased the recycling rate in Denmark to 90% [28]. Mandatory source-sorting in Portugal has also helped to create cost savings in the separation processes for the production of RCA free of contaminants [29] and on-site production of RCA in Brazil [30]. However, recycling concrete waste to contaminant-free RCA is challenging in Sweden because source-sorting is not mandatory. But even when such sorting is implemented, the Swedish branch-normative guidelines recommend concrete waste to be sorted as a mineral fraction combined with bricks, stones and asphalt which only increases the chances of contamination [31].

Regulatory measures such as **selective demolition** have been identified in facilitating better recycling and production of lesser contaminated RCA [12, 32] that could potentially be used in RAC. Selective demolition is, however, difficult to implement because of the need of sufficient space on-site for sorting; the cost of which exceeds the costs of processing CDW [33]. For example the Danish Construction Federation's guidelines NMK 96, formulated towards separating hazardous components from CDW has been remarked as ineffective [34]. Additionally, the environmental benefits arising from the increased recycling in selective demolition [35] could in a few cases be lost to increased transportation needs [36]. This could lead to decisions made in favour of conventional demolition.

3. RCA AS AGGREGATES IN RAC

The suitability of RCA for use in RAC depends on likeness of the properties of RCA with the properties of natural aggregates [37]. The RCA properties such as the physical and chemical properties are in turn influenced by the adhered mortar and CDW contaminants that the RCA is composed of [38].

3.1 Constituents of RCA

The constituents and properties of the RCA can vary depending on the waste source, methods of demolition and waste sorting, and the quantities sampled to determine its composition [39, 40]. RCA's constituents also depend on the treatment process; namely the crushing operation that varies the cement-mortar content [41, 42].

Classification of RCA based on its constituents

To ensure quality despite such variation, standards and specifications such as the RILEM, EHE 08 from Spain and the PTV 406 from Belgium include a classification of recycled aggregates especially RCA. This classification delimits the content of certain constituents in coarse RCA [43]. The delimited constituents are those that negatively affect the properties of RAC such as glass, plastic, organic material and light-weight material content [44].

Similarly, the Swedish standard SS 137003:2015 which is the application of EN 206 in Sweden delimits the constituents of coarse RCA and determines the extent of using RCA in RAC. The RCA's constituents are defined by the harmonized European standard SS EN 12620+A1:2008 aggregates for concrete. This definition has resulted in SS 137003:2015 classifying RCA into categories A and B based on their constitution. For coarse RCA to qualify as Type A, 95% of the constituents must originate from concrete and natural aggregates; whereas in Type B the content of similar constituents is reduced to 70%.

Table 1 shows the maximum allowable mass percentage of coarse natural aggregates that could be replaced with Type A and B coarse RCA; as prescribed by SS 137003:2015.

*Table 1 – Maximum permissible mass percentages of RCA
(adapted from Table 6, SS 137003:2015)*

RCA type	Exposure classes			
	X0	XC1,XC2	XC3, XC4,XF1, XA1,XD1, XS1	Other exposure classes
Type A	50%	30%	30%	0%
Type B	50%	20%	0%	0%

From Table 1 it can be inferred that the maximum RCA replacement percentage permitted by the standard is 50% for use in non-reinforced RAC in an indoor environment (X0). The permitted mass percentages are based on the constituents of RCA, the physical properties of the RCA and the resulting properties of the RAC.

Table 2 presents a classification of RCA and compares the allowable content of concrete, natural aggregate, masonry, bitumen, and lightweight materials from standards and specifications from different countries in Europe. Most of the classification stated in this table is derived from the European Standard EN 933-11 of 2009 [38].

The existing information from [38] was updated with the allowable content for constituents from the Swedish standard. The recycled aggregate classifications in the table are considered as RCA by researchers based on the high content of concrete in the aggregate and its suitability in RAC recommended by the respective standard.

Table 2 – Classification of RCA and the allowable content of its constituents
(Adapted from Martín-Morales, Zamorano et al. [38])

Country/ Standard	Standard	Concrete (in %)	Masonry (in %)	Natural aggregate (in %)	Lightweight materials (in %)	Bituminous materials (in %)
Belgium	PTV406	>90	<10	n.a.	n.a.	<5
Denmark	DS 2426	>95	n.a.	n.a.	n.a.	n.a.
Germany	DIN 4226- 100 Type 1	>90	<10	n.a.	n.a.	1
	DIN 4226- 100 Type 2	>70	<30	n.a.	n.a.	1
Netherlands	CUR	>95	<5	n.a.	n.a.	n.a.
	NEN 5905	<80	n.a.	<20	0.1	n.a.
Norway	NB 26	> 94	<5	^b	0.1	1
Portugal	LNEC E 471 Type 1	>90	<10	^b	1	<5
	LNEC E 471 Type 2	>70	<30	^b	1	<5
RILEM [43]	Type II	<100	n.a.	n.a.	0.5	1 ^a
	Type III	<20	<10	>80	0.5	1 ^a
Sweden	SS 137003 Type A	≥90	≤10	^b	≤2	1
	SS 137003 Type B	≥50	≤30	^b	≤2	1

^b included in the crushed concrete content

^a includes metals, glass, soft material and bitumen

n.a. no limit values reported by the standard

Adhered cement mortar content in RCA

RCA basically comprises the original aggregate surrounded by adhered cement mortar that is physically attached to the surface of the aggregate [45]. The adhered mortar is a remnant of the from the RCA's parent concrete that has undergone crushing. This adhered mortar as a result of its porosity has been identified to negatively affect the physical properties of RCA such as lowering its density and abrasion resistance, increasing the water absorption. The sulphate content in the adhered mortar can also increase the sulphate content of the RCA [46].

The porosity of the RCA due to the adhered mortar affects subsequently the mechanical properties of the RAC such as the drying shrinkage [15].

The adhered mortar content in the RCA has been identified to vary with RCA particle size fractions [32, 46, 47]. Padmini, Ramamurthy et al. [48] reasoned that smaller sized aggregates contained a higher adhered mortar content due to the higher surface area available for equal volume of aggregate. Juan and Gutiérrez [46] investigated the adhered mortar content in 15 RCA samples of sizes 4/8 mm and 8/16 mm by thermal treatment. They reported that 4/8 mm size fraction contained between 33-55% and the 8/16 mm between 23-44% adhered mortar.

They also deduced from literature, a tendency for the adhered mortar content to increase with decreasing RCA size fractions. Unable to obtain a significant regression they concluded that there were other factors that influenced the adhered mortar content.

The Building Contractors Society of Japan (BCSJ) determined the adhered cement mortar content in RCA acquired from parent concretes of medium-high compressive strengths [1]. The investigation by dissolution in hydrochloric acid yielded results of the adhered cement mortar content as weight percentages of RCA and is shown in Figure 2. Where the coarser fractions (20-30 mm) contained 20% adhered mortar compared to finer fractions that contained 40-60%; thereby confirming the size-adhered mortar relation. Additionally, the result also shows that RCA of identical size fractions can have different adhered cement mortar contents depending on the strength of the parent concrete, as is seen for RCA of size 0.3 mm.

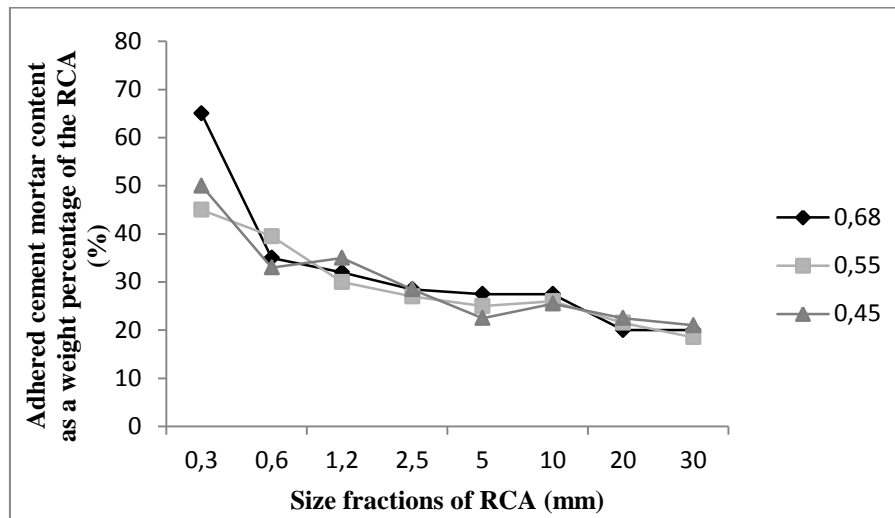


Figure 2 – Adhered cement mortar content varying with RCA size fraction and water/cement ratio of the parent concrete (adapted from Hansen [1]).

3.2 Physical properties of RCA

Density and water absorption

The density of RCA is lesser than that of natural aggregate because of the adhered cement mortar that is relatively less dense. It is the porosity of the adhered cement mortar that reduces the density and increases the water absorption of the RCA [46]. The relationship between the density and water absorption of RCA has been described as a linear relationship [49]. The

factors that could vary the adhered mortar content and thereby influencing the RCA's density include:

- Different stages of crushing [41, 50]
- Compressive strength of the parent concrete [48, 51]

The effects of primary crushing and primary combined with secondary crushing were investigated on the density of coarse RCA prepared from precast and lab concrete rejects. Primary crushing entailed the use of jaw crusher while the combined crushing included the use of the jaw crusher and the impact crusher. It was observed that the primary combined with secondary crushing produced RCA of higher density. The RCA fractions that underwent primary and secondary crushing demanded lesser water for workability of the RAC mix implying that they had reduced water absorption compared to the RCA produced only from primary crushing [41]. The lesser water absorbed by the RCA can be attributed to the reduction in the mortar content with successive crushing.

Padmini, Ramamurthy et al attempted to investigate the influence of the compressive strength of the parent concrete on the physical properties of coarse RCA [48]. They investigated the water absorption and density for fractions of 10, 20 and 40 mm obtained from low, medium and high strength concrete. The results of the particle density and water absorption for the 20 mm RCA for the respective parent concretes are shown in Table 3; also included is a 20 mm crushed granite aggregate used as a benchmark by the authors themselves. The results show higher densities and lower water absorption values for RCA from lower strength parent concrete. The authors observed this to be due to lesser mortar adhered to RCA acquired from a parent concrete of lower strength. Thus they deduced that the adhered mortar content was an outcome of the bond strength between the mortar phases and aggregate which increased with increasing strength of the parent concrete. Therefore RCA from parent concretes of lesser strength, in this case 37 MPa, were easier to separate from the RCA when compared to stronger parent concretes.

Table 3– Water absorption and density of coarse RCA influenced by parent concrete [48]

20mm sized aggregate obtained from parent concrete of strength	Water absorption (% weight in 24 hours)	Particle Density (kg/m ³)
37 MPa	3.65	2520
50 MPa	4.1	2510
58 MPa	4.86	2480
Fresh crushed granite	0.3	2800

4. PROPERTIES OF RAC

The amount of RCA included and its properties, such as porosity have been observed to influence the fresh properties, especially the workability of the RAC. The porosity of the RCA, the RCA content and the adhered cement mortar quality have a large influence on the hardened properties of RAC such as compressive strength, elastic modulus and shrinkage.

4.1 Fresh properties of RAC - Workability

RAC has a reduced workability compared to conventional concrete from natural aggregates. This is largely due to the porosity of the cement mortar adhered to the RCA causing it to rapidly absorb the free water from the mixture [49, 52]. The water absorption capacity of the RCA would depend on the moisture content in the RCA at the instance of mixing. The RCA's moisture content during the time of mixing is determined between the differences in mass at the situation of mixing and dry state. Similar to natural aggregates, RCA at oven-dry and air dry state are known to absorb more mixing water than at a saturated state; moreover the absorption increases with the increased content of RCA [53]. Therefore, to reduce their water absorption capacity and moreover maintain constant water/cement ratio, the RCA is pre-wetted or pre-saturated before its inclusion in the concrete mix [54]. In this case, adjustments to the amount of water added to the mix is based on the amount of RCA and the difference between the RCA's absorption value and moisture content during mixing.

Exteberria et al. investigated the workability of RAC while substituting the coarse natural aggregates of size 4/10 mm, 10/16 mm and 16/25 mm entirely with RCA of the same size fractions [54]. Aiming to achieve the required workability for RAC and reducing the water absorption capacity of the coarse RCA, they pre-saturated the RCA until it had reached 80% of its absorption capacity. The RCA was wetted with a sprinkler and stored under a plastic sheet for 24 hours to maintain the high humidity level. In this manner they were able to receive the desired slump value of 8-10 cm while maintaining the effective water/cement ratio. However the additive content was increased to 2% for RAC in place of the 1.28% for the reference conventional concrete.

Rogers, Fridh et al., prepared two sets of self-compacted RAC samples with a water/cement ratio of 0.5 with coarse and fine RCA sourced from both railway sleepers (S) and crushed hollow-core slabs (HCS) [9]. The authors concluded that the workability of the RAC was affected most by the fine RCA sized 0-4 mm. They attributed this to the fine RCA's large specific surface area and its larger share in the total aggregate volume.

4.2 Hardened properties of RAC

Compressive Strength

Due to the porosity and lowered density of the RCA, it is speculated that the compressive strength of RAC would decrease with increased replacement percentage of RCA. Chakradhara Rao, Bhattacharyya et al. [55] by means of a literature review and experimental investigation reported that there was no significant reduction in the compressive strength up to a coarse RCA replacement of 25%. The authors however did not communicate how significant the reduction was.

Hansen and Narud conducted an investigation to determine the influence of the water/cement ratios of the RCA's parent concrete on the compressive strength of the RAC [1]. They prepared nine different combinations of high, medium and low strength RAC using RCA derived from parent concretes of high, medium and low strength; with same mixed proportions and curing conditions. They observed that the compressive strength of high-strength RAC produced from RCA of a lower-strength parent concrete was 39% lower than the compressive strength of the same RAC produced from high-strength parent concrete.

In this manner, they deduced that the compressive strength of RAC depended not only on its water/cement ratio but also on the strength of the RCA's parent concrete namely its water/cement ratio. This relationship between the compressive strength of the RAC and the RCA's parent concrete is influenced by the porosity of the RCA's interfacial transition zone which in turn depends on the compressive strength of the parent concrete [45].

Li investigated the 28 day compressive strength for RACs of six different water/cement ratios relating to low, medium and high strength concrete [56]. These RACs were prepared at 30, 50, 70 and 100% RCA replacement ratios. His results, shown in Figure 3, indicate a steady decline of compressive strength with the increasing water/cement ratio for the 30, 70 and 100% replacements of RCA. However at 50% replacement of RCA, the largest compressive strength of about 37 MPa is recorded at 0.47 water/cement ratio; and the lowest value of 28 MPa at 0.35 when compared to 30,70 and 100% replacements at the same water/cement ratios. Poon, Shui et al. [53] have also observed different behavior for the 28 day compressive strength for RAC at 50% replacement of RCA. They noticed the compression strength to have reduced to 40 MPa at 50% from 44 MPa at 20% replacement and further increased to 45 MPa at 100% replacement. The factors affecting the behavior of RAC at 50% RCA replacement have to be further investigated.

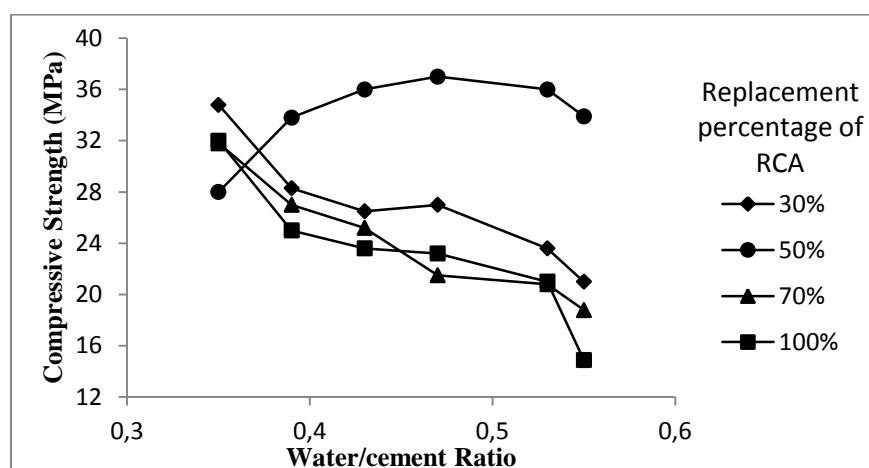


Figure 3– Relation between water/cement ratios, RCA replacement percentages and the compressive strength of RAC (adapted from Li [56]).

Elastic Modulus

The elastic modulus of RAC is always lower than that of conventional concrete due to the low elasticity modulus of the adhered mortar in the RCA [1]. Implying that as the RCA content increases, the elastic modulus of the RAC would decrease.

Xiao investigated the relation between the elastic modulus of the RAC and the RCA content by finding the elastic modulus at different RCA replacement percentages [57]. He expressed these results in terms of a relative elastic modulus defined as the ratio between the elastic modulus of the RAC and the reference concrete produced using natural aggregates. Figure 4 shows that when RCA substitutes 30% natural aggregates by mass in RAC, the elastic modulus of the RAC is 40% lesser than the reference concrete. The elastic modulus of RAC is seen to be nearly constant at RCA replacement percentages higher than 30%.

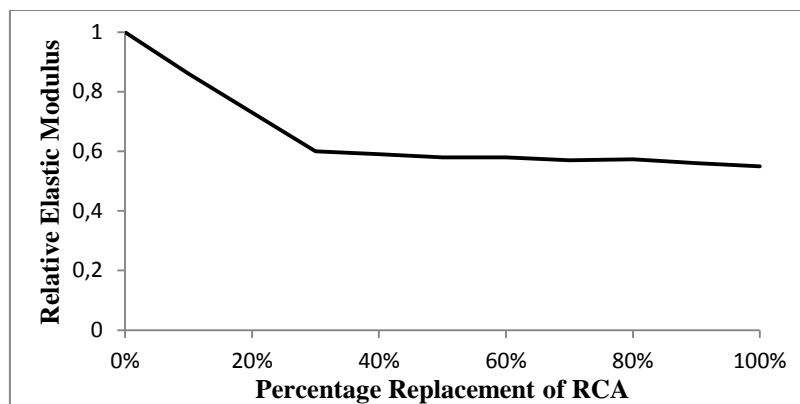


Figure 4– The elastic modulus of RAC as a function of RCA content (adapted from Xiao, Poon et al. [57]).

Drying Shrinkage

The drying shrinkage observed in RAC is higher than in conventional concrete made of natural aggregates. Researchers attribute this to the increase in cementitious material due to the old mortar adhered to RCA [15, 57] and the lower restraining capacity of the RCA when compared to natural aggregates [49].

Limbachiya, Leelawat et al., investigated the effect of the water/cement ratio and RCA content on the drying shrinkage of the RAC [15]. Test samples of high-performance RAC of design strength 60 and 70 MPa were prepared for each coarse RCA replacement of 30, 50 and 100%. From the drying shrinkage results which are shown in Figure 5 it can be inferred that:

- 70 MPa RAC and reference concrete have higher shrinkage values when compared to their 60 MPa counterparts.
- It is also seen that on replacing natural aggregates entirely with RCA, the 60 MPa has a higher shrinkage increase of 9.3% from its reference concrete compared to the 70 MPa that has increased by 6.3%.

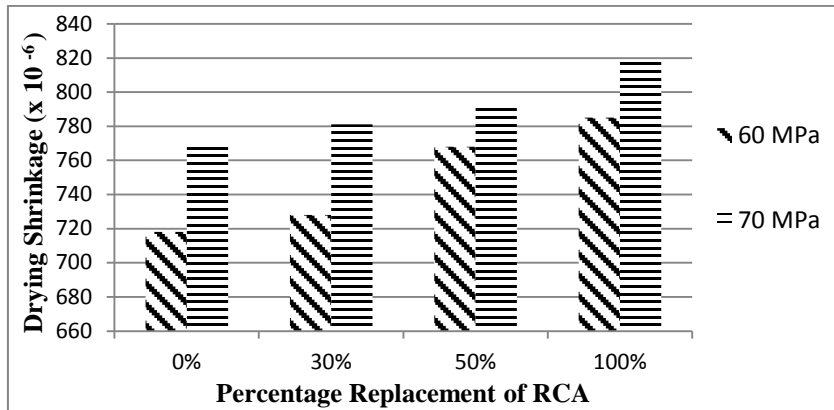


Figure 5– Drying shrinkage of RAC for different RCA content and RAC water/cement ratio (diagram based on information acquired from Limbachiya, Leelawat et al. [15]).

The results of the test for drying shrinkage performed by Rogers, Fridh et al. [9] for the 100% replacement of the coarse 8-16 mm RCA at 224 days showed that the RAC(S) had increased drying shrinkage from the reference concrete by 20%. The strain value for the RAC(HCS) was larger than the reference concrete by 12%. Given that the percentage replacement of RCA and water/cement ratio is the same for both RAC groups; it could be reasonable to assume that the difference in the drying shrinkage values could be due to larger adhered mortar content in the RAC(S).

4.3 Durability of RAC

The durability aspects are critical to investigate for RAC so as to enable its use in structural applications and for different exposure conditions. The durability of the RAC is influenced to a great extent by the physical properties of the included RCA such as its low density, high water absorption and low abrasion resistance [57]. Moreover it is the porosity of the RCA that makes the RAC vulnerable to the ingress and further transport of water, carbon dioxide as well as chlorides and other harmful chemicals which leads to cracking in concrete and corrosion of the reinforcement.

Freeze-Thaw Resistance

The freeze-thaw resistance of RAC is assumed low because of the porosity of the old cement mortar adhered to the RCA having higher absorption compared to natural aggregates. However, Nixon [58] reviewed the results from two separate investigations on accelerated freeze-thaw cycling and the flexural strength measurements after the period of freeze-thaw cycling of RAC. The tests concluded that resistance of RAC was similar to that of conventional concrete.

Limbachiya et al. investigated the freeze-thaw resistance of RAC consisting of RCA derived from precast rejects. The tests were performed according to the procedure described in ASTM C666, Procedure A: freezing and thawing in water [15]. RAC samples containing 5.5% entrained air were prepared with RCA percentage replacements of 20, 40, 60, 80 and 100%. The

durability factor calculated at the failure criterion for 100% RCA replacement surpassed the 90% limit thereby proving that the RAC had considerable freeze-thaw resistance.

Similarly, the Swedish researchers Rogers et al. designed their RAC samples with different RCA replacements, a water/cement ratio of 0.4 and 4.5% air-entrainment [9]. The scaling tests to identify the freeze-thaw resistance were carried in accordance with the Swedish standard SS 137244:2015. The test results were well within the threshold value of 0.1 kg/m^2 proving that the RAC was freeze-thaw resistant.

Limbachiya et al.[15] and Rogers et al.[9] concluded that RCA sourced from precast rejects produced RAC with suitable freeze-thaw resistance.

Chloride Ingress:

The ingress of chloride is damaging to the concrete as it causes corrosion of reinforcement; the risk of chloride ingress is furthered in RAC due to the porosity of RCA. Similar to conventional concrete, the chloride ingress in RAC occurs from its exposure to sea water or de-icing salts. RCA exposed to the aforementioned chloride sources before its inclusion in the RAC could also cause chloride ingress.

Xiao J., Poon et al. have reasoned that the chloride resistance of RAC is influenced by quality of the interface between the aggregate portion and adhered cement mortar in the RCA [57]. Cracks along this interface caused during the RCA production increases RAC's vulnerability for chloride ingress.

Kou and Poon conducted chloride penetrability tests according to ASTM C 1202 for their self-compacted RAC with varied percentage replacements of fine RCA of sizes less than 5 mm [52]. A total of three series of mixes containing fine RCA were prepared, with fine fly ash ($< 45\text{-}\mu\text{m}$) as part binder and rejected flyash ($> 45\text{-}\mu\text{m}$) as a filler in two series; and only rejected flyash in the third. They observed that the resistance to chloride ion penetration increased with increased fine RCA content especially for the series containing fly ash as binder. The authors attributed the resistance to chloride ion penetration to a filler effect caused by the inclusion of fine RCA fractions lesser than 0.3 mm in size.

Carbonation:

Carbonation is the reduction in alkalinity (neutralization) that occurs in concrete when CO_2 from air or water reacts with the products of hydration to produce carbonate and other products. The permeation of CO_2 in RAC can result from the porosity of the concrete, cement mortar or aggregate. RCA is very porous compared to natural aggregates and increases carbonation risk in RAC. Carbonation is highly dependent on the relative humidity in the concrete pores and diffusion of CO_2 occurs at a relative humidity between 50 and 70% [59].

The BCSJ standard of 1977 reported that the extent of carbonation in RAC increases by 65% with the inclusion of RCA that has already suffered carbonation and causes the reinforcement to rust [53]. BCSJ also recommended that the risk of corrosion can be reduced with reducing the water/cement ratio in RAC.

Katz noted the depth of carbonation of the RACs to be 1.3-2.5 times greater than the reference concrete [42]. However he noticed higher carbonation in the RACs with ordinary Portland cement compared to the ones with white Portland cement.

5. CONCLUSIONS

- Statistics relating to concrete waste recycling published by the Swedish Environmental Protection Agency estimates only the quantities of mineral waste fractions including concrete waste collected and subsequently the percentage recycled. However, a more timely and precise reporting of concrete waste from prefabrication industries could help create a continuous supply of RCA. Creating in this way, a market potential for RCA and subsequently RAC suitable for high-utility applications.
- The continuous and intermitted supply of concrete waste for recycling is challenged by the large transportation distances. Transportation distances could be minimized by the establishment of intermediate storage facilities and waste exchange between industrial clusters.
- Regulatory instruments such as selective demolition and source-sorting when applied to demolished concrete waste could help produce RCA of consistent quality suitable for RAC in high-utility applications. Additionally, these instruments reduce the costs arising from contaminant separation and thereby optimize the production cost of RCA.
- The adhered cement mortar content in RCA is central in determining the mechanical properties and durability aspects of RAC. Also, the adhered cement mortar in RCA derived from high strength parent concrete potentially contains more un-hydrated cement whose effect on the RAC's properties could be interesting to investigate.
- The compressive strength of RAC does not change significantly up till an RCA replacement of 25%. The compressive strength of the RCA's parent concrete has an influence on the RAC's compressive strength. Studies have shown that RACs of low water/cement ratio could show compressive strengths higher than their target strength with RCA derived from high-strength parent concrete.

REFERENCES

1. Hansen, T.C., *Recycled aggregates and recycled aggregate concrete second state-of-the-art report developments 1945–1985*. Materials and Structures, 1986. **19**(3): p. 201-246.
2. Va'zquez, E., *Recycling in Spain: Overview of CDW*, in *Progress of Recycling in the Built Environment, Final Report of the RILEM Technical Committee 217-PRE*, E. Va'zquez, Editor. 2013, RILEM. p. 145-165.
3. Mueller, A., *Recycling in Germany: Overview Regarding CDW in Germany*, in *Progress of Recycling in the Built Environment, Final Report of the RILEM Technical Committee 217-PRE*, E. Va'zquez, Editor. 2013, RILEM. p. 106-114.
4. SMED, *Avfall i Sverige 2014*, Naturvårdsverket, Editor. 2016, Naturvårdsverket: Stockholm.
5. Swedish Concrete Association, *Hållbart byggande med betong, Part 3- Vägledning för miljöcertifiering enligt BREEAM* Swedish Concrete Association, Editor. 2009.

6. Swedish Concrete Association, *Hållbart byggande med betong, Part 3- Vägledning för miljöcertifiering enligt LEED*, in *LEED Reference Guide for Green Building Design and Construction* Swedish Concrete Association, Editor. 2009.
7. Marinković, S.B., et al., *23 - Life-cycle assessment (LCA) of concrete with recycled aggregates (RAs) A2 - Pacheco-Torgal, F*, in *Handbook of Recycled Concrete and Demolition Waste*. 2013, Woodhead Publishing. p. 569-604.
8. Coelho, A. and J. De Brito, *Economic viability analysis of a construction and demolition waste recycling plant in Portugal - Part I: Location, materials, technology and economic analysis*. Journal of Cleaner Production, 2013. **39**: p. 338-352.
9. Rogers, P., et al., *High quality reclaimed concrete aggregates for new concrete*, in *Återvunnenbetong som ballast i ny betong*. 2016, SBUF.
10. Coelho, A. and J. De Brito, *9 - Preparation of concrete aggregates from construction and demolition waste (CDW)*, in *Handbook of Recycled Concrete and Demolition Waste*. 2013, Woodhead Publishing. p. 210-245.
11. Nixon, P.J., *Recycled concrete as an aggregate for concrete—a review*. Materials and structures, 1978. **11**(5): p. 371-378.
12. Mulder, E., T.P.R. de Jong, and L. Feenstra, *Closed Cycle Construction: An integrated process for the separation and reuse of C&D waste*. Waste Management, 2007. **27**(10): p. 1408-1415.
13. Vegas, I., et al., *Upgrading the quality of mixed recycled aggregates from construction and demolition waste by using near-infrared sorting technology*. Construction and Building Materials, 2015. **75**: p. 121-128.
14. Akbarnezhad, A. and K.C.G. Ong, *10 - Separation processes to improve the quality of recycled concrete aggregates (RCA) A2 - Pacheco-Torgal, F*, in *Handbook of Recycled Concrete and Demolition Waste*, V.W.Y. Tam, et al., Editors. 2013, Woodhead Publishing. p. 246-269.
15. Limbachiya, M.C., T. Leelawat, and R.K. Dhir, *Use of recycled concrete aggregate in high-strength concrete*. Materials and Structures, 2000. **33**(9): p. 574.
16. Akbarnezhad, A., et al., *Microwave-assisted beneficiation of recycled concrete aggregates*. Construction and Building Materials, 2011. **25**(8): p. 3469-3479.
17. Lotfi, S., et al., *Mechanical recycling of EOL concrete into high-grade aggregates*. Resources, Conservation and Recycling, 2014. **87**: p. 117-125.
18. Martins, I., et al., *Use of Fine Fraction*, in *Progress of Recycling in the Built Environment, Final Report of the RILEM Technical Committee 217-PRE*, E. Va'zquez, Editor. 2013, RILEM. p. 195-228.
19. 165-SRM, R.T., *Sweden*, in *Sustainable Raw Materials - Construction and Demolition Waste - State-of-the-Art Report of RILEM TC 165-SRM*, C.F. Hendriks and H.S. Pietersen, Editors. 2000, RILEM Publications SARL. p. 146-147.
20. Association, S.W.M., *Sorteringsanläggningen – en förädlingsanläggning*, RVF, Editor. 2006.
21. Kynningsrud Prefab AB, *Byggvarudeklaration BVD 3*, in *Sandwichvägg EN 14992*. 2010, Kretsloppsrådet: Sweden.
22. Swerock AB, *Byggvarudeklaration BVD 3*, in *Fabriksbetong*. 2008, Kretsloppsrådet: Sweden.
23. Nunes, K.R.A., et al., *Evaluation of investments in recycling centres for construction and demolition wastes in Brazilian municipalities*. Waste Management, 2007. **27**(11): p. 1531-1540.
24. Palm, D., et al., *Analys av lämpliga åtgärder för att öka återvändning och återvinning av bygg- och rivningsavfall 2015*, Naturvårdsverket Bromma, Sweden.

25. Christian Fischer, M.L. and D.L. McKinnon, *Overview of the use of landfill taxes in Europe* Eionet, Editor. 2012, European Environment Agency.
26. S.M.E.D., *Avfall i Sverige 2012*, Naturvårdsverket, Editor. 2014, Naturvårdsverket: Stockholm.
27. Agency), E.E.E., *Effectiveness of environmental taxes and charges for managing sand, gravel and rock extraction in selected EU countries*. 2008: Copenhagen.
28. Norden, N.C.o.M., *ENCORT-CDW :Evaluation of the European recovery target for construction and demolition waste*. 2014, Norden Copenhagen.
29. Coelho, A. and J. De Brito, *7 - Conventional demolition versus deconstruction techniques in managing construction and demolition waste (CDW)*, in *Handbook of Recycled Concrete and Demolition Waste*. 2013, Woodhead Publishing. p. 141-185.
30. Vanderley, J. and A. Sergio, *Recycling in Brazil: An overview of the present situation of CDW in managing and recycling*, in *Progress of Recycling in the Built Environment, Final Report of the RILEM Technical Committee 217-PRE*, E. Va'zquez, Editor. 2013, RILEM.
31. Federation, T.S.C., *Resource and waste guidelines during construction and demolition*, in *Kretsloppsrådet's guidelines, updated*. 2015, Sveriges Byggindustrier.
32. Silva, R.V., J. De Brito, and R.K. Dhir, *Properties and composition of recycled aggregates from construction and demolition waste suitable for concrete production*. *Construction and Building Materials*, 2014. **65**: p. 201-217.
33. 165-SRM, R.T., *Demolition and processing methods and techniques*, in *Sustainable Raw Materials - Construction and Demolition Waste - State-of-the-Art Report of RILEM TC 165-SRM*, C.F. Hendriks and H.S. Pietersen, Editors. 2000, RILEM Publications SARL. p. 20-46.
34. Ioannis Bakas, et al., *Assessment of initiatives to prevent waste from building and construction sectors*. 2011, Nordic Council of Ministers: Denmark.
35. Roussat, N., C. Dujet, and J. Méhu, *Choosing a sustainable demolition waste management strategy using multicriteria decision analysis*. *Waste Management*, 2009. **29**(1): p. 12-20.
36. Coelho, A. and J. de Brito, *Influence of construction and demolition waste management on the environmental impact of buildings*. *Waste Management*, 2012. **32**(3): p. 532-541.
37. Marinković, S., et al., *Comparative environmental assessment of natural and recycled aggregate concrete*. *Waste Management*, 2010. **30**(11): p. 2255-2264.
38. Martín-Morales, M., et al., *11 - Quality control of recycled aggregates (RAs) from construction and demolition waste (CDW) A2 - Pacheco-Torgal, F*, in *Handbook of Recycled Concrete and Demolition Waste*, V.W.Y. Tam, et al., Editors. 2013, Woodhead Publishing. p. 270-303.
39. Angulo, S.C. and A. Mueller, *Determination of construction and demolition recycled aggregates composition, in considering their heterogeneity*. *Materials and Structures*, 2009. **42**(6): p. 739-748.
40. Oikonomou, N.D., *Recycled concrete aggregates*. *Cement and Concrete Composites*, 2005. **27**(2): p. 315-318.
41. Pedro, D., J. Brito, and L. Evangelista, *Performance of concrete made with aggregates recycled from precasting industry waste: influence of the crushing process*. *Materials and Structures*, 2014. **48**(12): p. 3965-3978.
42. Katz, A., *Properties of concrete made with recycled aggregate from partially hydrated old concrete*. *Cement and Concrete Research*, 2003. **33**(5): p. 703-711.
43. RILEM TC 121-DRG, *Specifications for concrete with recycled aggregates*. *Materials and Structures*, 1994. **27**(173): p. 557-559.
44. Gonçalves, P. and J. de Brito, *Recycled aggregate concrete (RAC)–comparative analysis of existing specifications*. *Magazine of Concrete Research*, 2010. **62**(5): p. 339-346.

45. Poon, C.S., Z.H. Shui, and L. Lam, *Effect of microstructure of ITZ on compressive strength of concrete prepared with recycled aggregates*. Construction and Building Materials, 2004. **18**(6): p. 461-468.
46. de Juan, M.S. and P.A. Gutiérrez, *Study on the influence of attached mortar content on the properties of recycled concrete aggregate*. Construction and Building Materials, 2009. **23**(2): p. 872-877.
47. Hansen, T.C. and H. Narud, *Strength of recycled concrete made from crushed concrete coarse aggregate*. Concrete International- design and construction, 1983. **Volume 5**(No. 1): p. 79-83.
48. Padmini, A.K., K. Ramamurthy, and M.S. Mathews, *Influence of parent concrete on the properties of recycled aggregate concrete*. Construction and Building Materials, 2009. **23**(2): p. 829-836.
49. Agrela, F., P. Alaejos, and J.M.S. De, *12- Properties of concrete with recycled aggregates*, in *Handbook of Recycled Concrete and Demolition Waste*. 2013, Woodhead Publishing. p. 304-329.
50. Marmash, B.E., *The properties of recycled precast concrete hollow core slabs for use as replacement aggregate in concrete*. 2011.
51. Torben, C.H. and N. Henrik, *Strength of Recycled Concrete Made From Crushed Concrete Coarse Aggregate*. Concrete International, 1983. **5**(01).
52. Kou, S.C. and C.S. Poon, *Properties of self-compacting concrete prepared with coarse and fine recycled concrete aggregates*. Cement and Concrete Composites, 2009. **31**(9): p. 622-627.
53. Poon, C.S., et al., *Influence of moisture states of natural and recycled aggregates on the slump and compressive strength of concrete*. Cement and Concrete Research, 2004. **34**(1): p. 31-36.
54. Etxeberria, M., et al., *Influence of amount of recycled coarse aggregates and production process on properties of recycled aggregate concrete*. Cement and Concrete Research, 2007. **37**(5): p. 735-742.
55. Chakradhara Rao, M., S.K. Bhattacharyya, and S.V. Barai, *Influence of field recycled coarse aggregate on properties of concrete*. Materials and Structures, 2011. **44**(1): p. 205-220.
56. Li, J., *Study on mechanical behavior of recycled aggregate concrete* 2004, Tongji University.
57. Xiao, J., et al., *Recycling in China: An overview of study of recycled aggregate concrete*, in *Progress of Recycling in the Built Environment, Final Report of the RILEM Technical Committee 217-PRE*, E. Va'zquez, Editor. 2013, RILEM.
58. Nixon, P.J., *Recycled concrete as an aggregate for concrete—a review*. Matériaux et Construction, 1978. **11**(5): p. 371.
59. Pacheco Torgal, F., et al., *An overview on concrete carbonation in the context of eco-efficient construction: Evaluation, use of SCMs and/or RAC*. Construction and Building Materials, 2012. **36**: p. 141-150.

Research Council & Editorial Board of Nordic Concrete Research

Dr. Marianne Tange Hasholt, Chairman of the Research Council

Danish Concrete Association	Dr. Marianne Tange Hasholt Associate professor Technical University of Denmark Department of Civil Engineering Tel: +45 25 17 02 matah@byg.dtu.dk	Mrs. Gitte Normann Munch-Petersen Teknologisk Institut Kongsvang Allé 29 DK - 8000 Aarhus Mobile: +45 72 20 32 45 gnmp@teknologisk.dk
Finnish Concrete Association	Professor Jouni Punkki Aalto University, Dept of Civil Engineering P.O.Box 12100 FI-00076 Aalto, Finland tel. +358 50 322 4155 jouni.punkki@aalto.fi	Prof. Dr. Jukka Lahdensivu Tampere University of Technology P.O.Box 527 FI-33101 Tampere Mobile: +358 40 0733852 jukka.lahdensivu@tut.fi
Icelandic Concrete Association	Dr. Jón E. Wallevik Innovation Center Iceland IS - 112 Keldnaholti Tel: +354 522 9362 Mobile: +354 Fax: +354 522 9111 jon.w@nmi.is	Prof. Dr. Olafur H. Wallevik Innovation Center Iceland IS - 112 Keldnaholti Tel: +354 522 9000 Mobile: +354 wallevik@ru.is
Norwegian Concrete Association	Dr. Terje F. Rønning Heidelberg Cement NE / Cement Product development & Implementation P.O.Box 38 N - 3991 Brevik Tel.: +47 3557 2000 Mobile: +47 915 76 046 terje.ronning@heidelbergcement.com	Prof. Dr. Mette R. Geiker Department of Engineering NTNU N - 7034 Trondheim Tel: +47 7359 4529 Mobile: +47 4045 1218 mette.geiker@ntnu.no
Swedish Concrete Association	Tekn. Dr. Peter Utgenannt CBI Swedish Cement and Concrete Research Institute P.O. Box 857 SE - 501 15 Borås Tel: +46 105 166 870 Mobile: +46 706 452 008 Peter.utgenannt@cbi.se	Tekn. Dr. Mårten Janz ÅF, International Division Hallenborgs gata Box 585 SE-201 25 Malmö Tel: +46 10 505 7334 Mobile: + 46 70 293 6338 marten.janz@afconsult.com
Editor	Prof. Johan Silfwerbrand KTH Royal Institute of Technology Dept. of Civil & Architectural Engrg. Brinellvägen 23 SE-100 44 Stockholm Tel: +46 8 790 8033 Mobile: +46 70 726 4005 jsilfwer@kth.se	

June 1st, 2017

ISBN: 978-82-8208-055-2 ISSN: 0800-6377
Printed by Helli - Visuell kommunikasjon, Oslo